https://doi.org/10.15388/vu.thesis.854
https://orcid.org/0000-0002-6090-3063

VILNIUS UNIVERSITY
CENTRE OF PHYSICAL SCIENCES AND TECHNOLOGY

Laura Lukavičiūtė-Navickienė

Synthesis of Calcium Hydroxyapatite of Different Morphology, Comparison of Properties and Application in Cosmetics

DOCTORAL DISSERTATION

Natural Sciences,
Chemistry (N 003)

VILNIUS 2025

The dissertation was prepared between 2021 and 2025 at Vilnius University.

Academic Supervisors:
Assoc. Prof. Dr. Edita Garškaitė (Vilnius University, Natural Sciences, Chemistry – N 003) (From 2021-10-01 to 2022-05-31).
Prof. Habil. Dr. Aivaras Kareiva (Vilnius University, Natural Sciences, Chemistry – N 003) (From 2022-06-01 to 2025-09-30).
Academic Consultant:
Assoc. Prof. Dr. Rūta Gancevičienė (Vilnius University, Medical and Health Sciences, Medicine – M 001).

This doctoral dissertation will be defended in a public meeting of the Dissertation Defence Panel:

Chairman – **Assoc. Prof. Dr. Tatjana Kochanė** (Vilnius University, Natural Sciences, Chemistry – N 003).

Members:
Habil. Dr. Agnieszka Gladysz-Plaska (Maria Curie-Sklodowska University in Lublin, Natural Sciences, Chemistry – N 003),
Prof. Dr. Ligita Jančorienė (Vilnius University, Medical and Health Sciences, Medicine – M 001),
Prof. Dr. Rasa Pauliukaitė (Centre of Physical Sciences and Technology, Natural Sciences, Chemistry – N 003),
Prof. Habil. Dr. Arūnas Ramanavičius (Vilnius University, Natural Sciences, Chemistry – N 003).

The dissertation shall be defended at a public meeting of the Dissertation Defence Panel at 16:00 hour on 9 December 2025 in Inorganic Chemistry auditorium 141 of the Institute of Chemistry, Faculty of Chemistry and Geoscience, Vilnius University.

Address: Naugarduko Street 24, LT-03225 Vilnius, Lithuania
Tel. +370 5 219 3105; e-mail: info@chgf.vu.lt

The text of this dissertation can be accessed at the libraries of Vilnius University and Center for Physical Sciences and Technology, as well as on the website of Vilnius University:
www.vu.lt/lt/naujienos/ivykiu-kalendorius

https://doi.org/10.15388/vu.thesis.854
https://orcid.org/0000-0002-6090-3063

VILNIAUS UNIVERSITETAS
FIZINIŲ IR TECHNOLOGIJOS MOKSLŲ CENTRAS

Laura Lukavičiūtė-Navickienė

Skirtingos morfologijos kalcio hidroksiapatito sintezė, savybių palyginimas ir naudojimas kosmetikoje

DAKTARO DISERTACIJA

Gamtos mokslai,
Chemija (N 003)

VILNIUS 2025

Disertacija rengta 2021–2025 metais Vilniaus universitete.

Moksliniai vadovai:
Doc. dr. Edita Garškaitė (Vilniaus universitetas, gamtos mokslai, chemija – N 003) (Nuo 2021-10-01 iki 2022-05-31).
Prof. habil. dr. Aivaras Kareiva (Vilniaus universitetas, gamtos mokslai, chemija – N 003) (Nuo 2022-06-01 iki 2025-09-30).
Mokslinė konsultantė:
Doc. dr. Rūta Gancevičienė (Vilniaus universitetas, medicinos ir sveikatos mokslai, medicina – M 001).

Gynimo taryba:
Pirmininkė – doc. dr. Tatjana Kochanė (Vilniaus universitetas, gamtos mokslai, chemija – N 003).

Nariai:
habil. dr. Agnieszka Gladysz-Plaska (Maria Curie-Sklodowska universitetas Liubline, gamtos mokslai, chemija – N 003),
prof. dr. Ligita Jančorienė (Vilniaus universitetas, medicinos ir sveikatos mokslai, medicina – M 001),
prof. dr. Rasa Pauliukaitė (Fizinių ir technologijos mokslų centras, gamtos mokslai, chemija – N 003),
prof. habil. dr. Arūnas Ramanavičius (Vilniaus universitetas, gamtos mokslai, chemija – N 003).

Disertacija ginama viešame Gynimo tarybos posėdyje 2025 m. gruodžio mėn. 9 d. 16 val. Chemijos ir geomokslų fakulteto Chemijos instituto Neorganinės chemijos auditorijoje (141).
Adresas: Naugarduko g. 24, LT-03225, Vilnius, Lietuva. Tel. +370 5 219 3105; el. paštas info@chgf.vu.lt

Disertaciją galima peržiūrėti Vilniaus universiteto ir Fizinių ir technologijos mokslų centro bibliotekose ir VU interneto svetainėje adresu:
https://www.vu.lt/naujienos/ivykiu-kalendorius

LIST OF ABBREVIATIONS

ACP - amorphous calcium phosphate.
ANOVA - analysis of variance.
ATCC - American Tissue and Cell Culture.
BCP - biphasic calcium phosphate.
BG - bioactive glass.
BMZ - basement membrane zone.
CaPs - calcium phosphates.
CDHA - calcium deficient hydroxyapatite.
CHA - calcium hydroxyapatite.
CN - coordination number.
DMEM - Dulbecco's Modified Eagle's Medium High Glucose.
DMSO - dimethyl sulfoxide.
EDX - energy Dispersive X-ray.
EU - European Union.
FDA - Food and Drug Administration.
FE-SEM - field-emission scanning electron microscope.
FTIR - Fourier transform infrared spectroscopy.
hMBC - human bone marrow cells.
ICP - Inductively Coupled Plasma.
ICP-OES - Inductively Coupled Plasma Optical Emission Spectrometry.
IEC - International Electrotechnical Commission.
ISO - the International Organization for Standardization.
MHM - mesoporous hydroxyapatite microspheres.
MTT - 3-[4,5-dimethylthiazol-2-yl]-2,5 diphenyl tetrazolium bromide.
NMF - natural moisturizing factor.
O/W - oil in water.
PTFE - polytetrafluoroethylene.
SBF - simulated body fluid.
SC - stratum corneum.
SCCS - Scientific Committee on Consumer Safety.
SEM - scanning electron microscope.
SNOM - scanning near-field optical microscope
SPF - sun protection factor.
TEWL - transepidermal water loss.
TRIS - tris(hydroxymethyl)aminomethane ($C_4H_{11}NO_3$).
UVA - ultraviolet A rays.
UVB - ultraviolet B rays.

W/O - water in oil.
XRD - X-ray diffraction.
α-TCP - α-tricalcium phosphate.
β -TCP - β -tricalcium phosphate.

CONTENTS

INTRODUCTION

Calcium hydroxyapatite ($Ca_{10}(PO_4)_6(OH)_2$; CHA) is a widely recognized biomaterial. Its extensive use in the biomedical field is attributed to its chemical similarity to human hard tissue: CHA is the main mineral component of teeth and bones, responsible for their strength and hardness [1]. Synthetic CHA exhibits remarkable osteoconductivity, biocompatibility, chemical stability and non-toxicity [2-7]. These advantageous and versatile characteristics make it suitable for a wide range of medical uses, including bone repair and regeneration [8], orthopaedic bone fillers [9], protein adsorption [10], and drug delivery [11]. CHA materials are safe, well-tolerated, and compatible with biological systems [12].

Interest in the use of calcium phosphates (CaPs) in cosmetics is growing, and has been particularly evident in recent decades [13, 14]. Indeed, the excellent properties of CHA that made them a versatile material in medicine can also be useful in the cosmetics field [15, 16]. First and foremost, the excellent biosafety of CHA allows one to substitute cosmetic ingredients raising health concerns with safer alternatives. The properties of CHA permits one to design materials that can fulfil different functions requested by the cosmetics industry. The main applications of CHA as a cosmetic ingredient reported in the scientific literature are in oral care, skin care, hair care, and deodorants [13]. It was even recently demonstrated that the CHA composite dressing offers a promising wound dressing for acute wound treatment and skin protection [17].

The quality of synthetic biomaterials, including CHA is highly dependent on the overall characteristics and features of the synthesised powders. Such attributes include density, purity, phase composition, crystallinity, particle size, particle-size distribution, particle morphology, and specific surface area [6, 7, 18-25]. Thus, all mentioned properties of bioceramics are highly sensitive to the processing conditions, which are very much responsible for the crystallinity, crystal shape, crystal size, crystal size distribution and phase purity of the resulting powders.

The aim of this PhD thesis was to review the cationic substitution effects in calcium hydroxyapatite on its bioproperties, to synthesise cation-substituted calcium hydroxyapatite coatings and bulk samples and evaluate antibacterial properties of obtained samples with possible application in cosmetics. To achieve this goal, the main tasks were formulated:

To review the cationic substitution effects in calcium hydroxyapatite on its bioproperties.

To investigate cationic substitution effects on morphological properties of $Ca_{10}(PO_4)_6(OH)_2$.

To develop low-temperature synthesis method for antibacterial calcium hydroxyapatite coatings.

To investigate the antibacterial properties of cation-substituted CHA and skin creams containing them.

The novelty and originality of PhD thesis.

For the first time, it was shown that different cationic substitution (in the presence of smaller and larger ions) has significant effects on morphological properties of calcium hydroxyapatite. A crystalline calcium hydroxyapatite coatings were successfully synthesised from $CaCO_3$ coatings by a dissolution-precipitation method at low temperature of 80 ºC in aqueous media. This method was used for the synthesis of partially Cu^{2+} and Zn^{2+} ion-substituted calcium hydroxyapatite coatings. After incubation for 24 h of these coatings, zones of inhibition were detected in the presence of a colony of *B. subtilis* bacteria. It was found, that metal-substituted CHA bulk samples exhibited effective antimicrobial properties. The addition of zinc enhanced antimicrobial efficacy but diminished biocompatibility, while copper maintained both high antimicrobial activity and biocompatibility, making it an ideal choice for developing cosmetic materials. Dermal creams containing CHA with copper and iron ions also proved to be potent antimicrobial products with good cell viability.

Statements for defence:

- Different cationic substitution has significant effects on morphology of calcium hydroxyapatite.
- Dissolution-precipitation method at low temperature of 80 ºC in aqueous media can be used for the synthesis of partially Cu^{2+} and Zn^{2+} ion-substituted calcium hydroxyapatite antibacterial coatings.
- Metal-substituted calcium hydroxyapatite samples demonstrate promising antimicrobial potential for medical and materials science applications.
- The discovery of antimicrobial products with good cell viability highlights the importance of optimizing the balance between antimicrobial activity and biocompatibility in metal-substituted calcium hydroxyapatites.

1. LITERATURE REVIEW

1.1. CALCIUM HYDROXYAPATITE ($Ca_{10}(PO_4)_6(OH)_2$)

1.1.1. General characteristics

Calcium hydroxyapatite (CHA) is a calcium phosphate mineral with the formula $Ca_{10}(PO_4)_6(OH)_2$, crystallizing in the apatite structure (hexagonal, space group $P6_3/m$) [25] and an ideal Ca/P ratio of 1.67 [14] (see Fig. 1).

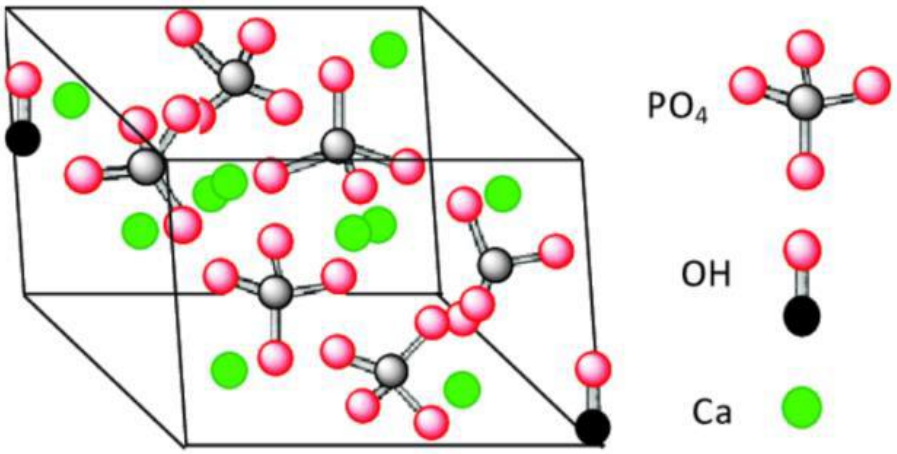

Fig. 1. The crystal structure of calcium hydroxyapatite [25].

It is the most thermodynamically stable calcium phosphate phase under physiological conditions and constitutes the principal inorganic component of vertebrate bone and tooth enamel [14]. Stoichiometric CHA is highly crystalline and exhibits very low solubility in neutral or basic aqueous environments, dissolving mainly only under acidic pH [26].

In contrast, biological apatite (bone mineral) is typically a non-stoichiometric, carbonated form of CHA with nanoscale crystallites and various ionic substitutions (e.g. Na^+, Mg^{2+}, Sr^{2+}, CO_3^{2-}) incorporated into the lattice [27]. A wide range of synthesis routes – including precipitation, sol–gel processing, hydrothermal crystallization, and high-temperature solid-state reactions – have been developed to produce hydroxyapatite with controlled phase purity, particle size, morphology, and crystallinity [28]. This tunability in composition and structure allows researchers to tailor CHA materials for specific applications while maintaining its characteristic stability and apatite phase behaviour.

1.1.2. A widely recognized biomaterial

Owing to its close similarity to bone mineral, CHA is widely regarded as a leading biomaterial in medicine, valued for its outstanding biocompatibility, bioactivity (ability to bond with host bone), and osteoconductivity (support of new bone growth) without inducing toxicity or immune rejection [29]. Clinically, CHA -based bioceramics are utilized in orthopedics and dentistry as bone graft substitutes, porous scaffolds, and implant coatings – for example, bulk hydroxyapatite granules and cements fill bone defects, and CHA coatings on titanium implants promote firm osseointegration [30]. Hydroxyapatite is also exploited as a vehicle for drug delivery, taking advantage of its adsorption capacity and pH-sensitive solubility to carry and release therapeutics in acidic environments (such as in osteoporotic lesions, inflammatory sites, or tumour tissues) [14].

Beyond traditional medical uses, CHA has found emerging roles in consumer health and cosmetic products. For instance, nano-hydroxyapatite is added to toothpastes as a remineralizing agent to restore enamel and reduce sensitivity, and it is being explored in skincare and sunscreen formulations as a safe, bioactive ingredient [14]. A notable example in aesthetic medicine is an FDA-approved dermal filler composed of CHA microspheres in a biocompatible gel matrix, which is injected to restore soft-tissue volume and simultaneously stimulates new collagen production *in vivo* [31]. These developments underscore the significance of hydroxyapatite in contemporary materials science and regenerative medicine, where its bioactive and osteoconductive properties are used for improved orthopedic implants, dental care technologies, targeted drug delivery systems, and innovative cosmetic therapies.

1.2. CHARACTERISTICS OF HUMAN SKIN

Human skin is composed of three layers, each with distinct cellular makeup and functions. The epidermis is the outermost layer, consisting of stratified squamous epithelium that is predominantly made of keratinocytes and is typically 0.05–0.1 mm (thicker on palms/soles) [32, 33]. As an avascular layer, the epidermis receives nutrients by diffusion from the underlying dermis and serves as the first barrier against environmental factors. Beneath it lies the dermis, a thicker (1–2 mm on average) fibrous connective tissue layer rich in collagen and elastin fibers, which provides tensile strength and elasticity to the skin. The deepest layer is the hypodermis (subcutis), composed mainly of adipose tissue and loose connective tissue, which cushions underlying

structures, insulates the body, and allows the skin to move freely over muscles and bones [32]. These layers work together to protect the body, regulate temperature, and provide sensory information.

Key cellular components of the skin include:

Keratinocytes: The main cells of the epidermis (~95% of epidermal cells), which originate in the basal layer and undergo differentiation as they migrate outward. Keratinocytes produce keratin proteins and lipids, forming the structural scaffold of the epidermis and ultimately creating the cornified layers that constitute the physical barrier.

Melanocytes: Pigment-producing cells located in the basal layer of the epidermis (typically a ratio of ~1 melanocyte per 10 basal keratinocytes). Melanocytes synthesise melanin and transfer it to keratinocytes, contributing to skin colour and protecting deeper tissues from ultraviolet (UV) radiation damage [34].

Langerhans cells: Dendritic immune cells found mainly in the suprabasal epidermis. They serve as antigen-presenting cells, capturing foreign substances that penetrate the skin and migrating to lymph nodes to activate T-cells, thus playing a sentinel role in cutaneous immune defence [35].

Fibroblasts: The primary cell type of the dermis responsible for producing and remodelling the extracellular matrix. Fibroblasts secrete collagen (especially types I and III) and elastin fibers, as well as ground substance components like hyaluronic acid and fibronectin, thereby maintaining the dermal structure and the skin's mechanical resilience. A healthy dermal fibroblast population is crucial for wound healing and for supporting the epidermis above [36].

At the interface of the epidermis and dermis is the basement membrane zone (BMZ), a specialized thin extracellular matrix that cements the two layers together. Extracellular matrix molecules on both sides of the basement membrane create a "sticky" interface that tightly joins the epidermis and dermis [37]. Nutrients and oxygen diffuse from dermal capillaries across this interface to sustain the avascular epidermis. With aging, the basement membrane flattens and becomes less undulating, reducing the surface area of contact between epidermis and dermis and weakening their attachment. Despite this, in healthy skin the BMZ effectively compartmentalizes the layers and is critical for resisting shearing forces and facilitating tissue repair after injury [32].

The outermost portion of the epidermis, the *stratum corneum* (SC), is the principal barrier layer of skin. It consists of 15–30 layers of flattened, dead keratinocytes (called corneocytes) embedded in an extracellular lipid (ceramides, cholesterol, and free fatty acids) matrix – an arrangement often

likened to a “brick-and-mortar” structure. This unique architecture makes the SC a formidable barrier to transepidermal water loss (TEWL) and of external chemicals or microbes. The SC’s dry, slightly acidic environment and continuous turnover further contribute to its protective function [33]. A critical feature of the SC is the presence of natural moisturizing factor (NMF) within the corneocytes, which aids in maintaining skin hydration. NMF is a mixture of low molecular weight, water-attracting substances generated by the breakdown of the filament-aggregating protein filaggrin during the terminal differentiation of keratinocytes. Key components of NMF include free amino acids (especially serine, glycine, alanine), pyrrolidone carboxylic acid, urocanic acid, lactic acid, urea, and various electrolytes (e.g., sodium, potassium, calcium, phosphate). These hygroscopic molecules are responsible for binding water within the corneocytes [38]. An increase in TEWL indicates a compromised barrier that is allowing excessive water to escape and potentially irritants to enter [39]. Occlusive moisturizers that restore lipids and “seal” the skin surface can reduce TEWL and improve hydration by reinforcing the SC’s barrier function. Another component of the skin’s barrier is the skin microbiome – the community of commensal microorganisms (bacteria, fungi, and viruses) residing on the skin surface [40, 41].

The surface of the skin is characterized by a mildly acidic pH (approximately 4.5–5.5 in healthy adults), often referred to as the acid mantle. This pH gradient – acidic at the SC surface and gradually less acidic in deeper layers – is critically important for enzymatic and barrier functions. Notably, lipid-processing enzymes such as β-glucocerebrosidase and acidic sphingomyelinase act in the outer epidermis to convert precursors into ceramides and other lipids that form the permeability barrier; these enzymes are activated at pH ~5 and are inhibited if the pH becomes neutral or alkaline [42, 43].

Skin appendages contribute to the biochemical environment of the skin. One of these appendages are sebaceous glands. Human sebum is a complex mixture of lipids: roughly 50–60% triglycerides (and their hydrolysed free fatty acids), ~25% wax esters, ~10–15% squalene, and smaller proportions of cholesterol and cholesterol esters. Uniquely, squalene and wax esters are found almost exclusively in sebum and not elsewhere in the body’s lipids [44]. Hormonal influences (e.g., androgens) strongly regulate sebaceous gland activity, which is why skin oiliness and acne are prominent in adolescence [45].

Sweat is produced by two types of sweat glands: eccrine and apocrine. Eccrine sweat glands are distributed widely across the skin and secrete a dilute salt solution primarily for thermoregulation. Eccrine sweat is ~99% water and

~1% solutes. The solutes include sodium and chloride (giving sweat its saltiness), potassium, small amounts of calcium and magnesium, as well as metabolic waste products like lactate, urea, ammonia, and amino acids. This composition is akin to a very dilute plasma [46]. Evaporation of eccrine sweat from the skin surface dissipates heat and is crucial for cooling the body during overheating or exercise. Besides thermoregulation, eccrine sweating has ancillary roles [47].

The skin, despite its barrier nature, is an accessible route for delivering certain drugs or therapeutic agents topically or transdermally. Penetration of substances through the skin primarily occurs via three pathways across SC: intercellular, transcellular, and appendageal routes. In the intercellular route, molecules traverse by diffusing through the continuous lipid matrix between the corneocytes (i.e., around the cells rather than through them). This pathway creates a tortuous path through the "mortar" of the SC and is generally considered the dominant route for most neutral, lipophilic compounds. In the transcellular route, molecules actually pass through the corneocytes – entering and exiting through the cell membranes and crossing the keratin-filled cytoplasm in a serial fashion. Because corneocyte interiors are hydrophilic (rich in keratin and water) this route tends to favour small, relatively hydrophilic molecules that can diffuse through cell membranes, or conversely very polar molecules that might hop through aqueous regions, but it is a much less common pathway than intercellular for most drugs. The third pathway is the appendageal route (transappendageal), which exploits skin appendages – primarily hair follicles and sweat ducts – as conduits to bypass the SC barrier [48]. Appendages penetrate through the epidermis into the dermis, so substances can travel down these shunts, at least partway, effectively circumventing the densely packed corneocyte layers. Hair follicles in particular have been shown to act as reservoirs for topically applied nanoparticles and drugs, releasing them gradually into surrounding skin. Although appendages occupy only ~0.1% of the skin's surface area, they can contribute disproportionately to penetration for certain formulations, especially in the early time after application or for larger, hydrophilic agents that struggle to cross intact SC [49]. In practice, all three pathways may operate in parallel to some extent, but the intercellular lipid pathway is most significant for the majority of drugs and chemicals. This path permits diffusion of small hydrophobic molecules (typically under ~500 Da) through the lipid bilayers between corneocytes [50]. The follicular pathway is especially relevant for particulate systems (like microspheres, lipid nanoparticles) and has been leveraged in targeted delivery (e.g., delivering drugs to hair follicles

for local action in acne or using follicular uptake for transdermal immunization) [51].

Several factors influence skin penetration of topically applied compounds. Schematical presentation of possible drug penetration routes across human skin is depicted in Fig. 2.

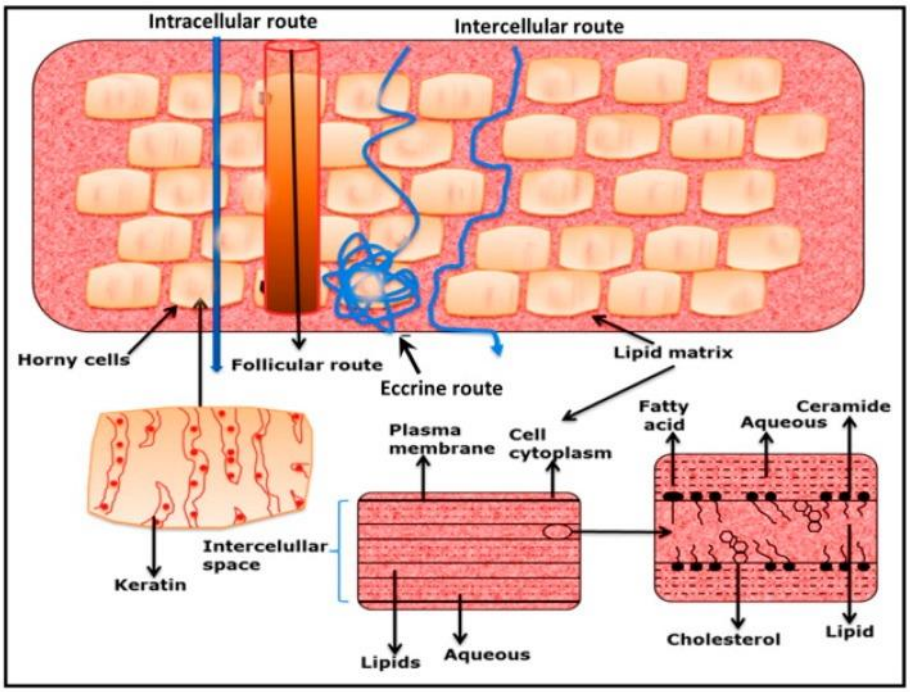

Fig. 2. Possible drug penetration routes across human skin [53].

A key factor is molecular size (molecular weight): smaller molecules penetrate more readily. Empirically, very few compounds with molecular weight above ~500 Da penetrate the intact skin in significant amounts – this observation is often called the "500 Dalton rule" [53]. Compounds larger than this threshold (such as proteins, peptides, or polymers) have difficulty diffusing through the tight lipid/protein mesh of the SC. Another crucial factor is lipophilicity [54].

Skin exposure to inorganic (mineral-based) compounds is common – examples include zinc, iron, magnesium, copper and other [55]. Numerous studies on topical mineral-based formulations, such as zinc oxide and titanium dioxide, demonstrate minimal skin penetration and excellent dermal tolerability, with particles typically remaining confined to the outermost skin layers and follicular openings [56]. Even at the nanoscale (where particle size is <100 nm), ZnO and TiO_2 have been found to stay confined to the SC, with

minimal if any passage beyond it. As a result, they rarely cause irritation or toxicity; their primary interaction with skin is to sit on the surface and reflect/scatter UV light (in the case of sunscreens) [57,58]. They are also chemically unreactive in the context of skin (zinc oxide is actually mildly antiseptic and used in diaper creams to soothe irritation). Titanium dioxide and iron oxides in cosmetic pigments similarly are largely inert and remain on the skin surface [55]. The skin's tolerance for these substances is high, and allergic responses are exceedingly rare because these minerals are not sensitizing (they do not typically bind to proteins or activate immune cells in a way that causes allergy) [59].

However, exposure to certain inorganic compounds can disrupt the skin's homeostasis, leading to irritation or damage. For instance, hard water, which contains elevated calcium and magnesium carbonate, can have a mild effect on skin: as it dries, it can leave behind mineral residues that increase skin pH slightly and lead to dryness or exacerbate eczema in sensitive individuals, but these effects are generally subtle [60]. Inorganic heavy metal salts (such as nickel or chromate) are a special case – while they do not penetrate deeply, they can act as haptens and induce allergic contact dermatitis in susceptible people. For instance, nickel ions from jewellery can filter into sweat and penetrate the upper skin, triggering immune recognition and eczema. This is an immunologic interaction rather than a toxic one and depends on individual sensitivity [59].

Regarding calcium and hydroxyapatite – these specific minerals have particular relevance to skin biology and biomedical applications. Calcium ions (Ca^{2+}) are not only tolerated by the skin but are crucial for epidermal function. The epidermis maintains a calcium gradient, with low Ca^{2+} in the basal layer and high Ca^{2+} in the upper granular layer, which signals keratinocytes to differentiate and form the barrier. If calcium is removed (e.g., by chelators), skin differentiation is impaired; conversely, providing calcium (in a balanced way) can aid in barrier recovery after injury [61]. Topical products containing calcium (like calcium pantothenate or calcium in wound dressings) are generally well-tolerated. CHA is the mineral form of calcium phosphate that makes up bone and teeth. It has become a material of interest in dermatology and cosmetics. Medical-grade CHA is used in dermal fillers (a product which is CHA microspheres in a gel carrier) to restore volume and stimulate collagen in the skin. The reason CHA can be used in this way is its excellent biocompatibility – the body recognizes it as a natural substance (it's analogous to bone mineral) and thus it typically does not incite a significant foreign body or allergic reaction. When CHA is injected or implanted in the skin, it stays where placed (being insoluble) and gradually integrates or resorbs over years,

while promoting new collagen formation in the surrounding tissue [62]. Topically, CHA has even been explored as a sunscreen ingredient (as it can scatter UV light) and as a component in wound dressings [63]. Studies show that CHA is non-toxic and does not trigger adverse inflammation in skin tissue [14]. In wound healing applications, CHA can assist by providing a scaffold for cell migration and by modulating the wound microenvironment (it has been noted to help reduce excess inflammation and promote tissue regeneration). Thus, the interactions of Ca, phosphate, and hydroxyapatite with skin are generally positive or neutral – they are tolerated well, and in some cases even leverage normal skin physiology (as with Ca^{2+} signalling or CHA bioactivity) [64].

In summary, the skin's response to inorganic compounds depends on the specific chemical nature of those compounds. Insoluble, inert minerals (like oxides, elemental metals, hydroxyapatite) mostly remain on the skin surface or within appendages and do not penetrate or react, resulting in good tolerance. Soluble salts that are close to physiological pH (e.g., NaCl, calcium sulfate) are innocuous in the concentrations commonly encountered. Issues arise with reactive or extreme-pH compounds – these can erode the barrier or cause irritant reactions. The skin's robust barrier means that, aside from local irritation or allergy, systemic absorption of inorganic compounds is usually negligible. This is advantageous for using mineral-based substances in topical products (sunscreens, medicated creams, dressings) because they can exert local effect without systemic toxicity. Even novel uses of minerals, such as nanoparticle carriers or mineral-based biomaterials for skin repair, have so far shown a high degree of compatibility with human skin [64].

1.3. SKIN PROTECTION CREAMS

Moisturizers are topical formulations intended to increase skin hydration and improve the skin's barrier function [65]. In practice, moisturizers/emollients are complex mixtures of substances (lipids, humectants, etc.) designed to make the epidermis softer, more pliable, and less prone to dryness [66]. Occlusives and humectants are two key classes of moisturizing ingredients: occlusives form a hydrophobic film over the skin to reduce TEWL, whereas humectants attract water into the SC to increase its water content [67]. Common occlusive agents include petrolatum, lanolin, mineral oil, and silicones, while typical humectants include alpha-hydroxy acids, glycerol, urea, and hyaluronic acid [66].

Barrier creams (also called protective creams) are formulations meant to maintain or enhance the skin's physical barrier. They create a protective layer

on the surface that shields the skin from external irritants (chemicals, moisture, allergens) and prevents excessive drying [68]. Such products are often used in occupational settings or in conditions like diaper dermatitis and incontinence-associated dermatitis, to guard against irritants (urine, feces, harsh substances) by forming a persistent film that resists wash-off [69]. Barrier creams can be formulated as creams, ointments, or pastes, and many contain a combination of occlusive and humectant ingredients to both shield and hydrate the skin [68]. In contrast to standard moisturizers, a barrier cream's primary function is prophylactic protection – for example, to reduce irritant contact dermatitis in workers by blocking chemical penetration [70].

In the European Union (EU), most skin creams for hydration or protection are regulated as cosmetic products. The EU Cosmetic Regulation (EC No. 1223/2009) defines a cosmetic as "any substance or mixture intended to be placed in contact with the external parts of the human body… with a view exclusively or mainly to cleaning them, perfuming them, changing their appearance, protecting them, keeping them in good condition, or correcting body odours" [71]. Such products do not primarily claim to treat or prevent disease. Products like ordinary moisturizers and barrier creams fall under this cosmetic category as long as they are marketed for maintaining skin in good condition (e.g. preventing dryness or mild irritation) and not for curing a medical condition [72]. In the EU, some high-end "barrier repair" creams are even classified as Class IIa medical devices when they act primarily by physical means and are marketed for managing dermatological conditions like atopic dermatitis [71, 72]. Thus, the same type of product (a moisturizing cream) can be either a cosmetic, a medicinal product, or a medical device depending on its composition, intended use, and claims.

A primary function of skin protection creams is to reduce TEWL and reinforce the SC barrier [66]. Occlusive ingredients in these creams deposit a thin hydrophobic film over the SC that slows the evaporation of water from the skin.

Skin protectant creams can mitigate inflammation through multiple pathways. Firstly, by repairing the physical barrier and maintaining hydration, they reduce the penetration of irritants and allergens that trigger cutaneous inflammation [73]. Dry, cracked skin allows entry of microbes and irritants, which leads to activation of immune cells and release of pro-inflammatory cytokines [67]. Many modern therapeutic moisturizers contain added anti-inflammatory or immunomodulatory ingredients. These can include botanical anti-inflammatories like liquorice, chamomile, comfrey, oatmeal, and cannabinoids among others [74]. Such additives actively downregulate

cutaneous inflammation by interfering with the production of inflammatory mediators.

Oxidative stress from UV light and pollution is a major cause of skin damage, leading to lipid peroxidation, DNA damage, and inflammation in the skin. Skin protection creams often include antioxidants to counter these harmful free radicals. Vitamins are common choices: vitamin E (α-tocopherol) and vitamin C (ascorbic acid) are well-established topical antioxidants that, when absorbed into the SC, help neutralize reactive oxygen species generated by UV exposure. These antioxidants can protect cellular membranes and collagen from oxidative damage, thereby preventing or slowing the process of photoaging [75]. However, because ascorbic acid and tocopherol can be unstable when exposed to light and air, more stable derivatives (like magnesium ascorbyl phosphate for vitamin C or tocopheryl acetate for vitamin E) are often used in formulations. Once in the skin, these derivatives are converted to their active forms and contribute to the skin's redox balance [76]. In addition to vitamins, many creams incorporate botanical antioxidants (e.g. polyphenols from green tea, resveratrol, coenzyme Q10) intended to bolster the skin's defence against environmental stress. By reducing oxidative stress, antioxidant-rich creams help attenuate inflammation (since oxidative stress can trigger inflammatory pathways) and protect the structural proteins of the skin [77]. Overall, this antioxidant defence mechanism complements the physical barrier protection, especially in day creams that function as both moisturizers and environmental shields.

An intact skin barrier is also a critical defence against pathogens. Skin protection creams contribute to antimicrobial defence in a few ways [73]. Research has shown that some occlusive moisturizers can induce the skin's innate immune protection [78]. Additionally, some barrier creams and ointments include antiseptic agents or metal compounds to provide direct antibacterial action [79]. By keeping microbial counts low and maintaining skin integrity, protective creams help prevent infection and secondary inflammation that could be caused by microbial overgrowth.

Many skin protection creams, especially daytime moisturizers, incorporate sunscreen agents to guard against UV radiation. Chemical UV filters are organic compounds that absorb high-energy UV photons and dissipate the energy as heat; examples include avobenzone, octinoxate, oxybenzone, and octocrylene (among many others) [80]. Each chemical filter has a specific spectrum of UV absorption, so formulations often combine multiple filters to achieve broad-spectrum coverage (UVB and UVA protection). Physical UV filters are inorganic mineral pigments – primarily zinc oxide and titanium dioxide – that act by reflecting and scattering UV radiation away from the skin

(and to a lesser extent, absorbing it) [80]. These minerals are micronized in creams to appear transparent on skin while still providing a UV shield. Physical filters tend to be photostable and are less likely to cause irritation, making them suitable for sensitive skin and children [81]. By including such UV filters, a protection cream can significantly reduce UV penetration into the epidermis. The benefits are well-documented: daily use of a broad-spectrum sun protection factor (SPF) moisturizer has been shown to prevent UV-induced collagen degradation and signs of photoaging. It also lowers the formation of sunburn cells and mutations in the skin [82]. In essence, UV filters in these creams serve as an "external barrier" against a major environmental aggressor, complementing the creams' role in maintaining the skin's internal barrier and health.

Hyaluronic acid is another potent humectant that can hold many times its weight in water; as a large polymer, it mainly moisturizes the surface of the skin and gives a transient plumping effect to fine lines [83]. Urea is a natural moisturizing factor component with dual actions: at low concentrations (≈10%), urea is strongly hygroscopic (binding water into the SC) and it also has keratolytic properties that help exfoliate dry, scaly skin. By gently disrupting corneocyte adhesions, urea allows the outer dry cells to shed, which improves skin smoothness and facilitates penetration of other moisturizing ingredients. Importantly, urea has been shown to improve barrier function and reduce TEWL in xerotic skin – it signals keratinocytes to produce lipids and antimicrobial peptides, thus strengthening the barrier [84]. Furthermore, glycerin not only hydrates but also contributes to barrier repair; studies indicate that glycerol can accelerate recovery of skin elasticity and enhance the effectiveness of the skin's own lipid synthesis when used regularly [65].

Topical antioxidants (vitamin C, vitamin E, niacinamide) are included in many skin creams to protect the skin from oxidative damage caused by UV light and pollution [75, 76].

Niacinamide has antioxidant properties and has been shown to significantly reduce oxidative stress and UV-induced damage in keratinocytes by enhancing DNA repair enzymes. It also improves epidermal barrier function by stimulating ceramide production and has documented anti-inflammatory effects, which can help reduce redness and blotchiness [85].

Trace bioactive minerals (calcium, magnesium, zinc, iron, copper, manganese) are increasingly recognized for their roles in skin physiology, and some dermatological products aim to deliver these minerals to the skin [79]. Ca^{2+} is crucial for regulating keratinocyte differentiation; there is a natural calcium gradient in the epidermis (low in basal layers, high in the *stratum granulosum*) that signals cells to mature and form the SC. A proper Ca^{2+} level

in the epidermis is needed for the formation of lamellar bodies and lipid secretion, so maintaining Ca^{2+} can promote barrier function. However, too much calcium in the outer skin can actually impede desquamation, which is why some barrier repair formulations adjust the balance of calcium and magnesium (Mg^{2+}) [86]. Magnesium is another ion involved in barrier homeostasis – an optimal Ca/Mg ratio has been shown to accelerate barrier recovery in damaged skin, partly by modulating epidermal inflammation. Studies indicate that increasing magnesium (relative to calcium) in a topical application can benefit conditions like atopic dermatitis by reducing inflammatory signalling and improving lipid synthesis, thereby optimally repairing the skin barrier [87]. Zinc is a trace element with numerous skin roles: it is a cofactor for over 100 enzymes, including DNA/RNA polymerases and matrix metalloproteinases, and is vital for cell proliferation and wound healing. Zinc also stabilizes cell membranes and can regulate immune responses; topically, zinc oxide or zinc salts have been used to speed up healing of ulcers, reduce inflammation in acne and dermatitis and as a physical UV filter [88]. Iron is essential for collagen synthesis (as a cofactor for prolyl and lysyl hydroxylase enzymes) and for catalase, the key enzyme that breaks down hydrogen peroxide in cells. While iron is usually supplied via blood, some topical formulations include iron-rich thermal spring water or ferrous ions to potentially support these processes *in situ* – though iron must be carefully balanced, as excess iron can catalyse free radical formation [79]. Copper is another critical cofactor: it's needed for lysyl oxidase, the enzyme that cross-links collagen and elastin, meaning copper is directly tied to the strength and elasticity of the dermis. Copper peptides in anti-aging creams promote collagen synthesis and angiogenesis. Moreover, copper has potent antimicrobial properties; metallic copper or copper compounds can kill bacteria and fungi on contact (the term "oligodynamic effect" describes this), and copper-based creams have been used as adjuncts in wound care for their biocidal effect [89]. Another microelement manganese is required for the mitochondrial form of superoxide dismutase and also plays a role in collagen formation (it is a cofactor for glycosyltransferases involved in forming the extracellular matrix) and wound healing [79]. In practical terms, mineral-rich thermal waters (containing magnesium, calcium, etc.) have been used in dermatology to treat sensitive skin and eczema – studies suggest they can improve the skin barrier and reduce inflammation, possibly due to these minerals' effects on keratinocytes and immune cells [79].

Skin protection creams are typically formulated as emulsions, with the choice of emulsion type influencing their properties [90]. Formulators must carefully adjust pH, viscosity, and rheology to optimize stability and skin

compatibility. Skin's natural surface pH is mildly acidic (~4.5–5.5), which is critical for barrier function and microbiome balance [43]. Thus, creams are typically buffered in the 5–6 range to maintain the acid mantle and avoid disrupting SC integrity. An alkaline product can increase skin irritation and TEWL, especially in atopic or sensitive skin [91]. Viscosity and flow behaviour determine a cream's spreadability and staying power on the skin [90].

Modern skin protection formulations often include penetration enhancers and advanced delivery systems to improve efficacy. These technologies facilitate the transport of active compounds (such as antioxidants, vitamins, or anti-irritants) into the epidermis or ensure they remain on the surface as needed. Such vesicles have been shown to increase the retention of actives in the skin and enhance their permeation to deeper layers [92]. Nanoemulsions and microemulsions are another strategy: these colloidal emulsions with droplet sizes in the 10–100 nm range are thermodynamically stable and often transparent [93]. Microemulsions can improve drug stability, increase dermal permeability, and provide sustained release of actives [94]. Their surfactant-rich structures fluidize SC lipids, effectively reducing the barrier resistance and enhancing ingredient uptake [93]. Additionally, polymeric nanoparticles (e.g., solid lipid nanoparticles, nanostructured lipid carriers) may be used to protect sensitive ingredients from degradation and release them gradually. These nanocarriers can adhere to the skin surface or penetrate via hair follicles, increasing local bioavailability of actives [92]. In all cases, the inclusion of such delivery systems must be balanced with safety and regulatory considerations, but when well-designed, they can significantly boost the protective and restorative performance of skin creams.

Individual skin types require tailored protection cream formulations to address their specific physiological needs and tolerances. Formulations for sensitive or reactive skin are kept as simple and inert as possible to minimize irritation triggers. Products in this category are typically free of fragrances, colorants, and common contact allergens [95]. By eliminating unnecessary additives and using mild emulsifiers, sensitive skin creams maintain the skin's integrity and comfort.

Dry or xerotic skin lacks sufficient lipids and natural moisturizing factors, so protective cream formulations often contain a combination of humectants and occlusives to restore moisture balance [65]. For severely dry or atopic skin, water-in-oil emulsions or ointment-like textures (with a higher oil phase) are commonly used, as they provide longer-lasting occlusion and protection in harsh conditions [96].

For oily skin, the challenge is to protect the skin without excess oil or clogging pores. Thus, creams for oily or acne-prone individuals are formulated to be lightweight, non-comedogenic, and oil-controlling. Oil-in-water emulsions with a high water content (and lower oil percentage) or gel-based vehicles are preferred to avoid a heavy feel [73, 97].

Atopic skin has a compromised barrier (with reduced ceramides and increased TEWL) and a high sensitivity to irritants [98]. These creams are typically highly occlusive and lipid-rich, often in a water in oil (W/O) emulsion or ointment base, to compensate for the defective barrier and prevent allergen entry [99] .

Cutting-edge skin protection creams are incorporating bio-derived materials and potent bioactives to enhance skin repair and defence. Biopolymers sourced from nature (such as collagen, elastin, chitosan, alginate, and silk fibroin) are increasingly used as they are biocompatible and can impart functional benefits [100].

Robust evaluation methods are essential to substantiate the efficacy of skin protection creams, encompassing both laboratory (*in vitro*) tests and clinical (*in vivo*) assessments [101]. Skin surface pH measurements are one of the tools – a protective cream aimed at restoring the acid mantle should maintain or slightly lower the skin pH towards the optimal ~5.0, and this can be verified with flat surface electrodes [102]. When antimicrobial efficacy is claimed (for example, a cream for healthcare workers that "reduces bacteria on the skin"), microbiological assays are performed. And newer techniques like microplate laser nephelometry and luminometric quantification of bacterial adenosine triphosphate are also available [103]. Over days or weeks, instrumental measurements (TEWL, corneometry, erythema via chromameter) track the rate of barrier recovery [104]. Additionally, long-term clinical trials might be done for specific use-cases: for example, in occupational settings, workers could use the product over several weeks and dermatologists would evaluate incidence and severity of contact dermatitis versus a control group [105]. Underpinning both in vitro and in vivo efficacy testing are regulatory guidelines and requirements, particularly strict in the EU (and by extension Lithuania) [106].

1.4. CALCIUM HYDROXYAPATITE IN CREAMS.

CHA is an inorganic calcium phosphate and represents the most thermodynamically stable CaP phase under physiological conditions [107]. It can be prepared in a wide range of particle sizes and morphologies – from nano- to micro-scale – including near-spherical nanoparticles, rod-like or

needle-like nanocrystals, and plate-like microcrystals [108]. The ability to tailor CHA size and shape via controlled synthesis is well-documented; varying synthesis parameters (e.g. precursors, pH, temperature) allows control over crystal habit and dispersity [108]. These morphological features directly influence its surface characteristics: smaller or needle-shaped particles yield higher specific surface areas and more reactive surface sites than bulk CHA [30]. Additionally, CHA can be engineered with mesoporosity or even hollow microspherical structures to further increase surface area and payload capacity [30, 109], which is advantageous for topical delivery of actives.

CHA's surface area and porosity are thus tunable, and they impact its interactions in creams. Nanoscale CHA typically exhibits a high Brunauer–Emmett–Teller surface area due to its fine size [110]. For instance, reducing CHA to the nanometer scale increases its surface-to-volume ratio and often its adsorption capacity and reactivity [30]. Porous or agglomerated forms of CHA can adsorb significant amounts of oils or active compounds within their pores. In contrast, densely sintered or larger crystalline CHA has lower surface area and is less interactive. The porosity can be introduced through templating or precipitation methods [29], yielding CHA particles capable of trapping lipophilic substances – a feature useful in creams for absorbing sebum or carrying active ingredients. In all cases, CHA remains a rigid particulate filler, so its high surface area contributes to its functionality (e.g. adsorptive mattifying effect) without swelling or dissolving in the cream matrix.

The crystallinity of CHA significantly affects its solubility and stability in different media. Stoichiometric, well-crystallized CHA is sparingly soluble in water at neutral pH and is stable in alkaline conditions [111]. It only dissolves significantly under acidic conditions (e.g. pH < ~6), where protonation of phosphate groups leads to mineral dissolution [14]. Poorly crystalline or calcium-deficient CHA – often approaching amorphous calcium phosphate (ACP) – is more soluble and can release calcium and phosphate ions more readily [112]. Indeed, intentional ionic substitutions (e.g. with monovalent or divalent cations) or reduced crystallinity can increase CHA's solubility [27]. In topical emulsions, this means a highly crystalline CHA will remain largely intact on the skin surface, whereas a less crystalline form might gradually dissolve, potentially supplying Ca^{2+} locally.

Surface charge and zeta potential: CHA particles carry surface charges that depend on surface chemistry and pH. In aqueous dispersions at physiological or slightly acidic pH (such as skin pH ~5.5), CHA typically acquires a net negative surface charge due to deprotonation of surface phosphate and hydroxyl groups. Measured zeta potential values for CHA nanoparticles are usually negative (e.g. on the order of –10 to –30 mV at neutral pH) [113]. This

negative zeta potential confers colloidal stability by electrostatic repulsion, meaning CHA particles resist agglomeration in water-based media above their isoelectric point (which for CHA is around pH 7–8) [113]. The most stable dispersion conditions for CHA are reported at pH >5, where sufficient surface charge keeps the particles apart [113]. In a cream, this translates to CHA remaining well-dispersed in the aqueous phase (especially if the formulation pH is slightly acidic or neutral).

A key advantage of CHA as a topical ingredient is its excellent biocompatibility. CHA is inherently non-toxic, non-immunogenic, and biocompatible, being the same mineral phase found in human bone and teeth [106]. When synthesised to mimic biological CHA (including similar crystallinity and ion substitutions), it exhibits superior bioactivity without causing irritation [106]. In dermatological applications, CHA has shown high dermal tolerance – it does not sensitize the skin or provoke adverse reactions in tested formulations [14]. Studies highlight that CHA is safe even if nano-sized, as it tends to remain in the SC and does not significantly penetrate living tissue [14]. In cream matrices, CHA is physically and chemically stable: it does not decompose over time, and its presence can even improve formulation stability. For example, recent developments include the use of CHA nanoparticles as solid emulsifiers in Pickering emulsions (particle-stabilized emulsions) [114]. In one patent, CHA nanoparticles served to stabilize an oil-in-water (O/W) emulsion in place of traditional surfactants [114], demonstrating that CHA can integrate into a cream's structure and maintain a stable dispersion of oil and water. Moreover, CHA can form hybrid complexes with polymers (as some patents combine CHA with biopolymers) to enhance compatibility and rheology in creams [115, 116]. Taken together, the inertness and safety profile of CHA make it a stable filler that does not undermine the cream's integrity; instead, it can confer beneficial stability and extend the functional shelf-life of topical formulations.

Topically applied CHA in creams can influence the skin through multiple pathways, both physical and biochemical. One primary mode of action is barrier reinforcement by supplementation of the SC. The SC is principal barrier against environmental insults and TEWL [33]. The skin normally maintains a calcium ion gradient across the epidermis (low Ca^{2+} in basal layers, high in the upper epidermis) that is crucial for keratinocyte differentiation and barrier homeostasis [61]. By slowly releasing Ca^{2+} in the vicinity of the SC (especially in acidic environment in skin wounds), CHA could influence this calcium gradient. Calcium ions are well-known to trigger keratinocyte differentiation and the formation of lamellar lipids and corneodesmosomes essential for barrier function [61]. Thus, a controlled

release of calcium from CHA might promote the natural maturation of the epidermis and strengthen the barrier from within. It should be noted, however, that the skin's calcium balance is finely tuned; any effect of topical CHA on the calcium gradient would be localized and gradual. Studies in skin biology indicate that an optimal calcium level in the SC is required for orderly differentiation, while an abrupt change can modulate barrier repair mechanisms[61]. In practical terms, CHA in a cream provides a reservoir of calcium ions at the interface of the SC: as these ions leach out, they may subtly enhance keratinocyte cohesion and differentiation in the upper layers, contributing to improved barrier resilience and skin homeostasis over time [117].

Another important mechanism of CHA in skin applications is its role in sebum absorption and oil control, contributing to a matte effect on the skin. Due to its high surface area and affinity for lipids, finely powdered CHA can adsorb sebum from the skin surface [14]. Excess sebum (skin oil) often leads to a shiny appearance and can clog pores; CHA helps mitigate this by binding fatty acids onto its surface. By soaking up oils, CHA-containing creams leave a dry, non-greasy finish (the "mattifying" effect). This not only improves the cosmetic appearance but also has secondary benefits: makeup applied over an CHA-enhanced cream may last longer and resist smudging [14]. By controlling sebum, CHA also indirectly prevents the growth of lipophilic bacteria (such as *Cutibacterium acnes*) that contribute to acne, as those microbes thrive on excess oil.

CHA's interaction with the skin's microflora and its potential antibacterial properties constitute another mechanism of action. In its pure form, CHA is not a strong antimicrobial agent; it is considered biocompatible and generally inert toward human cells and common skin flora [14]. However, CHA can influence microflora indirectly. By reducing sebum and altering the microenvironment (as noted above), CHA makes the skin surface less hospitable to bacteria and yeasts that feed on lipids or thrive in moist, oily conditions. For example, by adsorbing fatty acids, CHA may help prevent the formation of malodour, which arises when skin microbes metabolize sebum components [14]. Furthermore, there is emerging evidence that nanoscale CaP particles (including CHA) have intrinsic antibacterial effects under certain conditions [118]. A recent study compared ACP and crystalline CHA nanoparticles and found both could inhibit a range of bacteria, though ACP was more potent against Gram-positive strains. The proposed mechanisms include the gradual release of high local concentrations of calcium and phosphate ions which can stress bacterial cells, as well as the particles' high adsorptive surface which may disrupt bacterial membranes or biofilms. That

said, the antimicrobial power of undoped CHA is modest [118]. To enhance this, manufacturers often dope or functionalize CHA with antimicrobial ions or combine CHA with known antimicrobials (e.g. chitosan, silver, zinc) to create synergistic effects [14].

CHA may also exert anti-aging effects in the skin, largely via indirect stimulation of dermal components such as collagen. While topical CHA primarily stays in the superficial layers, any dissolved calcium or interaction at the cellular level can influence signals in the epidermis and dermis. Calcium is a known regulator of epidermal proliferation and differentiation, and optimal calcium levels can encourage a healthy turnover of keratinocytes (important for a youthful complexion) [60]. More directly, research from the field of aesthetic dermatology has shown that CHA can stimulate collagen synthesis when introduced into the dermis via injection. Injectable micron-sized CHA (as used in dermal fillers) has been documented to promote the production of collagen types I and III, as well as elastin, leading to clinically observable improvements in skin firmness and elasticity [64].

In creams and topical formulations, CHA can serve not only as an inert filler but as a functional ingredient or even an active agent conferring specific benefits. One major role is as a carrier system for active substances. Owing to its high surface area and ability to bind a variety of molecules, CHA can be used to deliver active ingredients such as vitamins, antioxidants, or peptides in a stable form. Several studies and patents have exploited CHA as a micro/nanoscopic carrier to enhance the delivery of actives to the skin [14, 26]. Moreover, CHA's surface chemistry allows for modifications (e.g. coating with lipids or surfactants or even metallic ions such as copper or zinc) to tune the release rate of the attached actives [14]. This expands CHA's role from a passive additive to an active participant in the cream's therapeutic or cosmetic efficacy.

Another established role of CHA in topical products is as a UV-reflecting and light-scattering agent. Mineral sunblocks traditionally rely on TiO_2 and ZnO to scatter and absorb harmful UV radiation; however, CHA has been proposed as a safer alternative inorganic UV filter. Recent research has demonstrated that well-engineered CHA provides broad-spectrum UV protection, and interest in CaP-based sunscreens is growing [14]. One study noted that CHA has a strong UV absorption band below ~247 nm and can attenuate wavelengths up to ~340 nm. By itself, this covers UVB and some UVA, and importantly, CHA is non-photocatalytic (unlike TiO_2 which can generate free radicals under UV). This means CHA does not induce oxidative stress on the skin upon UV exposure – a significant safety advantage [14].

Beyond serving as a carrier and optical agent, CHA can be an active functional ingredient through ion substitution and doping. The crystal lattice of hydroxyapatite is quite flexible and can accommodate various foreign ions [27]. By substituting or incorporating certain metal ions into CHA, one can create a multifunctional ingredient. A prominent example is antimicrobial doping: CHA doped with silver (Ag^{+}), zinc (Zn^{2+}), copper (Cu^{2+}), or other metal ions gains the antibacterial properties of those ions while retaining the scaffold of CHA [14, 119]. Ag-doped CHA, for instance, has been shown to significantly inhibit bacterial growth; silver ions released from the CHA lattice can disrupt bacterial cell membranes and metabolic enzymes. Similarly, Zn^{2+}-substituted CHA brings the well-known antimicrobial and soothing effects of zinc (commonly used in calamine and diaper rash creams) into the CHA particle [88]. These doped CHA particles can continuously release trace amounts of antimicrobial metal ions on the skin, helping to control bacterial proliferation (useful for acne-prone or sensitive skin) and even combat odour-causing bacteria. Copper-doped CHA adds the antifungal and collagen-promoting aspects of Cu – copper ions can stimulate angiogenesis and skin healing in addition to antimicrobial effects, which could be beneficial in wound-healing creams [89]. Iron (Fe^{3+}) and manganese (Mn^{2+}) dopants have also been explored: for example, Fe-doped CHA in a chitosan film was found to have excellent UV-blocking ability and antibacterial activity, showing potential as an active wound dressing that protects against infection and UV damage simultaneously [62]. Manganese and iron substitutions can also broaden CHA's absorbance into the UVA range, meaning Fe/Mn-doped CHA could serve as improved sunscreens with additional biological activity. However, for therapeutic or high-performance applications, doped CHA offers a tunable platform: one can design an CHA-based ingredient that not only acts as a filler but also delivers active metal ions (antibacterial, anti-inflammatory, etc.) in a controlled fashion. For instance, an CHA incorporating Zn^{2+} and Mg^{2+} might simultaneously calm irritation (zinc's effect), boost epidermal repair (magnesium affects the migration and adhesion of human skin fibroblasts), and strengthen the skin barrier (via calcium from CHA itself) [117, 120]. This versatility underscores CHA's role as more than just an inert powder – it is a multifunctional active that could be customized for specific dermatological outcomes.

Formulating creams with CHA requires careful consideration of its dispersion in different emulsion types. The mineral is stable at typical emulsion processing temperatures (70–80 °C) and can withstand the heat of emulsification without degradation [108]. Furthermore, studies on Pickering emulsions (stabilized by solid particles) demonstrate that unmodified

hydroxyapatite nanoparticles can stabilize either O/W or W/O emulsions under the right conditions (e.g. high particle concentration, optimal oil/water ratio, and sufficient mixing energy) [114].

Another key consideration is the compatibility of CHA with common excipients, including emulsifiers, thickeners, and preservatives. Because CHA particles have charged surfaces (bearing Ca^{2+} and PO_4^{3-} sites), they can interact with ionic emulsifiers or polymers [30]. On the other hand, preservatives that are acid-based (e.g. sorbic or benzoic acid) can locally lower pH and might dissolve CHA on contact, so buffer systems are useful to stabilize pH. In general, CHA is reported to be stable in the neutral pH range and has very low solubility at physiological pH, which helps it coexist with most ingredients without dissolving or precipitating [30].

Physical stability issues like aggregation, sedimentation, or phase separation are central concerns when formulating CHA creams. Aggregation of CHA particles is driven by their high surface energy and tendency to clump. The use of dispersants (e.g. polyols, polysorbates) or milling techniques can break apart agglomerates and should be employed during manufacturing. Indeed, continuous high-shear mixing after emulsification is advised until the batch cools to setting, to prevent any CHA clusters from settling out [121]. If CHA particles migrate (settle) and concentrate in one region of the container, they can bring along some water or oil, potentially inducing phase separation or a break in the emulsion. High-density sediment at the bottom of a jar, for instance, might be observed as a clear serum layer on top – an undesirable outcome. It has been noted that maintaining a slightly alkaline pH (around pH 8–10) improves the dispersion stability of hydroxyapatite suspensions, likely by imparting sufficient surface charge to repel particles electrostatically. However, in a cosmetic cream a pH that high may not be skin-friendly, so a compromise pH ~7 is typically chosen [121].

CHA is generally regarded as a biocompatible and well-tolerated material, owing to its presence in human bone and teeth. *In vitro* and *in vivo* studies largely support its safety in dermal applications, although certain factors (like particle size and shape) can influence biological responses. Cell culture experiments indicate that hydroxyapatite nanoparticles have low intrinsic cytotoxicity [4]. However, at extremely high concentrations or with very small (<50 nm) particles, some adverse effects can occur [64]. In animal models of wound healing, CHA has even been associated with anti-inflammatory benefits, helping to modulate the healing response [64] – an encouraging sign that it does not provoke adverse inflammation. Overall, the material's long history of use as a bone graft and even as an injectable dermal filler supports its favourable tolerability profile in contact with tissues. By extension, the

topical application of CHA – where the particles predominantly remain in the superficial layers of the SC – is expected to pose minimal risk, provided the formulation is free of irritant impurities [64].

While CHA is not yet a mainstream ingredient in skincare, preliminary trials and analogies from other uses suggest it is safe for human skin. In animal studies, topical CHA has been applied to wounds or burns to evaluate its regenerative effects, and these studies report enhanced healing with no delay or toxicity in the skin. In particular, in vivo study using rats models found that collagen matrices containing hydroxyapatite supported tissue repair without adverse effects, indicating good biocompatibility in skin tissue repair contexts [64]. No systemic absorption of calcium or phosphate occurs from topical CHA – the particles remain on or in the upper skin layers and eventually slough off with normal epidermal turnover. Notably, penetration studies on analogous mineral oxides (like zinc oxide and titanium dioxide used in sunscreens) have shown that insoluble mineral particles do not traverse beyond the SC into systemic circulation [13].

In the EU, CHA is permitted as a cosmetic ingredient, subject to general safety requirements under the EU Cosmetics Regulation (EC) No. 1223/2009. It is typically listed as "Hydroxyapatite" in ingredient lists. The EU's Scientific Committee on Consumer Safety (SCCS) recently reviewed nano-hydroxyapatite for cosmetic use. For dermal (leave-on) products, the SCCS noted that the material was safe at the maximum concentrations reported by industry (which were around 5% in skincare formulations) [122]. Notably, these safety endorsements apply to hydroxyapatite of defined particle shapes: the SCCS specified that at least 95% of particles should have an aspect ratio < 3 (roughly equiaxed) and no more than 4–5% of particles with higher aspect ratios, to avoid needle-like forms [122]. The Committee expressed concern about needle-shaped hydroxyapatite nanoparticles, which could potentially penetrate cell membranes or exhibit asbestos-like toxicity if inhaled. Consequently, manufacturers are advised to avoid using CHA in a needle/rod form or to thoroughly assess its genotoxic potential if such shapes are present. Hydroxyapatite is not classified as a UV filter or preservative in the EU, so it doesn't have a specific maximum concentration limit in cosmetics beyond the general safety principle (unlike ZnO or TiO_2 which have explicit limits for UV filtering purposes) [122].

For the trace elements Zn, Cu, Fe, and Mn that may be present as dopants or impurities in CHA, regulatory considerations also apply. These metals are not prohibited in cosmetics *per se*, but their usage is controlled by safety assessments. Zinc in the form of zinc oxide is actually an allowed UV filter in EU cosmetics up to 25% (non-nano form), and both nano and bulk ZnO are

deemed non-toxic on skin due to negligible absorption [123]. If Zn is introduced via Zn-doped hydroxyapatite, the formulation should ensure that any released Zn^{2+} ions remain low (well under levels causing irritation or systemic exposure). Copper and manganese ions are sometimes used in skincare (for instance, copper peptides for skin repair, or manganese in trace as an antioxidant cofactor), and are generally permitted at the low concentrations typical for cosmetic use. There are no specific EU annex restrictions on Cu or Mn compounds in leave-on cosmetics (aside from colorants like manganese violet which is allowed as a pigment) [41]. Therefore, a CHA doped with Cu^{2+} or Mn^{2+} would be acceptable as long as it passes the product safety assessment – the assessor would consider if any Cu or Mn could leach out and whether that level is safe. Iron is commonly present in cosmetics as iron oxides (pigments) which are approved colorants [44], and trace iron in CHA (or Fe-doped CHA) is not problematic in itself. The presence of these metals must also be communicated in the ingredient listing if they impart a significant function or coloration (for example, a doping that gives hydroxyapatite a colour might need CI pigment labelling). In Lithuania, cosmetics regulation is fully harmonized with EU law, so the same rules apply: CHA and its metal-doped variants must be safe for human health, and products require a safety assessment dossier. As a final regulatory note, there is ongoing surveillance of nanomaterials in cosmetics. Hydroxyapatite (nano) being on the SCCS radar means future regulations could impose explicit concentration or shape limits if new evidence emerges.

Although CHA is a relatively novel ingredient in topical skincare, there are a few commercial and experimental formulations that have incorporated CHA. One example in mainstream cosmetics, hydroxyapatite has appeared in certain makeup products. Some high-end foundation and concealer formulas include micro-scale hydroxyapatite as a filler to scatter light and blur skin imperfections.

Several patents by cosmetic companies describe the use of CHA in topical formulations, suggesting a growing interest in this ingredient. L'Oréal, for example, filed a patent for a cosmetic method to smooth wrinkles around the eyes using a composition containing hydroxyapatite [124]. The patent discusses that applying a cream with CHA particles can help fill in fine lines and tighten the periocular skin, thereby reducing the appearance of wrinkles and under-eye bags. Another patent (WO 1996/41611) by *Mansouri et al*. describes ceramic hydroxyapatite microcarrier particles (1–10 μm, spherical) used in skin care compositions to deliver active ingredients to the epidermis [125]. In that formulation, CHA serves as a vehicle: actives like herbal extracts, vitamins, or antimicrobials adsorb onto the porous CHA particles,

which are then delivered onto the skin via a cream or lotion. The hydroxyapatite not only shuttles these actives in a targeted way but also forms a temporary "shield" on the skin that helps retain moisture (an interesting concept of a mineral-based moisturizing barrier).

Researchers have been investigating CHA in topical delivery systems as well. A notable example is the development of a vitamin C hydroxyapatite nanocomposite gel – *Sliem et al.* created a nanocomposite where ascorbic acid (a potent but unstable antioxidant) was immobilized onto nano-hydroxyapatite particles within a carboxymethyl cellulose gel [126]. This experimental formulation showed greatly improved photo-stability and thermal stability of vitamin C, meaning the CHA protected the vitamin from degradation. When tested, this CHA-based nanocarrier not only preserved the active ingredient but also was found to be safe on skin cells, with no cytotoxicity observed up to 50 μg/mL and excellent biocompatibility [126]. Another academic example is the use of CHA in wound healing ointments or dressings: studies have combined hydroxyapatite with polymers like chitosan to make hydrogel creams that can be applied on burns or chronic wounds. These composite creams aim to harness CHA's ability to stimulate tissue regeneration; for instance, CHA/chitosan gels have shown synergistic effects in promoting collagen synthesis and angiogenesis in injured skin [64]. While these are not commercial products yet, they demonstrate the experimental use of CHA in semi-solid topical formulations for skin repair.

Additionally, CHA has been compared to other calcium-based compounds in lab studies. One study examined a cream containing calcium carbonate vs. one with calcium hydroxyapatite for treating skin dryness, and it was noted that the CHA cream had a more sustained moisturizing effect (presumably because CHA is less soluble and remained as a reservoir of calcium on the skin). These comparative explorations suggest that CHA may offer advantages over simpler minerals in topical use, combining the desirable inert properties of an earth mineral with a degree of biofunctionality.

Looking ahead, CHA holds exciting potential for innovative skincare and dermatological applications. One promising avenue is the integration of CHA into advanced delivery systems, such as nanoparticles and other biocompatible carriers. Given CHA's ability to bind and stabilize various molecules, it could serve as a nano-reservoir for active ingredients in future creams. More realistically, CHA may find uses in specialty dermocosmetics like anti-pollution creams (where CHA could bind heavy metals or pollutants on the skin surface due to its adsorptive capacity) or in antimicrobial creams (CHA doped with silver or copper could slowly release those ions for anti-bacterial effect on acne-prone skin). The dopability of hydroxyapatite is well-

known in biomaterials research – ions like Zn^{2+}, Cu^{2+}, Ag^{+}, Sr^{2+} can be substituted into the CHA lattice to impart specific biological effects. In a future personalized skincare context, one could customize a CHA-based cream: e.g., Zn-doped CHA for someone with oily, acne-prone skin (providing zinc's anti-inflammatory benefit) or Sr-doped CHA for someone with sensitive skin (strontium is known to soothe irritation). These doped variants would retain CHA's overall biocompatibility while tailoring the trace ionic milieu to the skin's needs – a very fine-tuned approach to skincare. As research progresses, it is clear that CHA is not just a passive "mineral filler" but a versatile platform. Its use in cosmetics is still in early stages, but given the positive safety profile and multifunctionality, we expect to see calcium hydroxyapatite feature prominently in next-generation dermocosmetic products that aim to blur the line between cosmetic and therapeutic. In summary, CHA's future applications could range from being a carrier for advanced actives, a post-treatment skin rejuvenator, to a component of smart, bio-interactive creams that adapt to and heal the skin – fulfilling the promise of truly functional skincare rooted in biomaterial science.

2. EXPERIMENTAL

2.1. SYNTHETIC PROCEDURES

2.1.1. Synthesis of bulk calcium hydroxyapatite

Calcium nitrate tetrahydrate ($Ca(NO_3)_2 \cdot 4H_2O$, ≥99%, Roth) and diammonium hydrogen phosphate ($(NH_4)_2HPO_4$, ≥98%, Roth) were utilized as precursors for the synthesis of pristine ACP. Iron nitrate nonahydrate ($Fe(NO_3)_3 \cdot 9H_2O$, ≥98%, Roth), copper nitrate trihydrate ($Cu(NO_3)_2 \cdot 3H_2O$, ≥99.5%, Roth) and zinc nitrate hexahydrate ($Zn(NO_3)_2 \cdot 6H_2O$, ≥99.5%, Roth) were used for the synthesis of Fe-, Cu-, and Zn-substituted calcium hydroxyapatite samples, respectively. Magnesium nitrate hexahydrate ($Mg(NO_3)_2 \cdot 6H_2O$, ≥98%, Roth), manganese nitrate tetrahydrate ($Mn(NO_3)_2 \cdot 4H_2O$, ≥98%, Roth), strontium nitrate ($Sr(NO_3)_2$, ≥98%, Roth), and barium nitrate ($Ba(NO_3)_2$, ≥99 %, Roth) were used for the synthesis of Mg-, Mn-, Sr- and Ba-substituted calcium hydroxyapatite samples, respectively. Wet precipitation synthesis was applied, and Ca to P ratio was kept as 1.5:1, for the synthesis of ACP. Firstly, 1 M Ca^{2+} nitrate solution was prepared by dissolving metal salt in deionized water. The pH of 0.5 M $(NH_4)_2HPO_4$ solution was adjusted to 10 by adding concentrated ammonia solution (NH_4OH, 25%) under a constant mixing. After mixing of $Ca(NO_3)_2$ and $(NH_4)_2HPO_4$ and aging for 10 min, the obtained precipitates were washed with deionized water and isopropanol and dried in an oven at 50 °C overnight. Finally, the obtained ACP was ground in an agate mortar and annealed in a furnace at 700 °C for 5 h (air atmosphere, heating rate of 5 °C/min) in order to induce the crystallization of tricalcium phosphate (α-TCP).

The synthesis of CHA, Fe:CHA, Cu:CHA, Zn:CHA, Mg:CHA, Mn:CHA, Sr:CHA and Ba:CHA samples was performed *via* a phase transformation of α-TCP in an aqueous solution. The synthesised α-TCP was used as a precursor for the hydrothermal synthesis of doped and un-doped CHA samples. The α-TCP powders (0.3 g) were placed in 90 ml PTFE liner to which aqueous solutions of various metal salts with different concentrations (20 ml) were added. The vessels were sealed in stainless steel reactors, transferred to a pre-heated oven and maintained at 200 °C for 3 h. Subsequently, the vessels were cooled down to room temperature. The samples were filtered, washed with ethanol and acetone, and dried at 50 °C overnight.

2.1.2. Synthesis of calcium hydroxyapatite coatings

The synthesis of the CHA porous layers was carried out on Ti (Thermo Scientific; 1.0 mm thick, 99.2%; CAS 7440-32-6) wafers, which were laser cut (1x1 cm) in the open access mechanics centre. The titanium wafers were mechanically abraded to remove the oxide film formed in the air and surface scratches. The titanium plates were mechanically abraded with sandpaper of different grit sizes (1000-2500 grit). The plates were scrubbed for 1 min on each side. The plates were then chemically treated by soaking for 30 minutes at 70°C in a solution of 96% 5 ml H_2SO_4 and 7% 0.35 ml HCl. After soaking, the plates were washed in an ultrasonic bath with distilled water and ethanol for 5 minutes. The cleaned plates were dried overnight at room temperature. The prepared plates were used for the synthesis of $CaCO_3$ and CHA.

For the preparation of the solution, 11.807 g of $Ca(NO_3)_2{\cdot}4H_2O$ was weighed and dissolved in 100 ml of ethanol (99.8%). Concentration was 0.5 mol/l. The solution was subjected to magnetic stirring at a temperature of 30°C until complete dissolution was confirmed. The submerged plates were then placed in a furnace, manufactured by Nabertherm, for heat treatment. A CO_2-rich environment within the furnace was established by positioning ceramic plates coated with activated carbon adjacent to the submerged plates. The furnace was programmed to elevate its internal temperature from an initial 20°C to 550°C at a rate of 3°C/min. Upon reaching 550°C, this temperature was maintained for a duration of 5 h. During the reaction, $Ca(NO_3)_2$ was thermally decomposed into CaO, followed by a reaction of the CaO with the CO_2 to form calcite. Before removal from the furnace, the furnace was cooled by lowering the temperature to 20°C at a rate of 3°C /min.

For the synthesis of CHA, a solution was prepared by weighing 0.14 g of Na_2HPO_4 and 0.6057 g of TRIS ($C_4H_{11}NO_3$) buffer. The weighed materials were dissolved in 100 ml of distilled water. The solution was stirred on a magnetic stirrer until dissolved and maintained at 30°C. The pH of the solution was alkaline (approximately 9-10). After the dissolution of the materials, the solution was poured onto $CaCO_3$-synthesised plates and soaked for 7 days at 80°C. After removal from the solution, the samples were washed with distilled water, dried and used for further analysis. The formation of CHA follows this reaction:

$$10\ CaCO_3 + 6\ Na_2HPO_4 + 2\ H_2O = Ca_{10}(PO_4)_6(OH)_2 + 8\ NaHCO_3 + 2\ Na_2CO_3$$

In order to introduce Cu^{2+} ions, a mixture of $Ca(NO_3)_2$ and $Cu(NO_3)_2$ was prepared at a concentration of 0.5 mol/l. 5.9036 g of $Ca(NO_3)_2{\cdot}4H_2O$ and

5.814 g of $Cu(NO_3)_2 \cdot 2.5H_2O$ (Sigma-Aldrich) were weighed. The substances were dissolved in 100 ml of ethanol. After the solution has been prepared, the chemically and mechanically treated titanium plates were dropped into the solution in a porcelain dish to submerge. This was then heated in an oven under a CO_2 atmosphere in a previously mentioned manner. After the heating procedure, the plates were dipped into a solution of 0.14 g Na_2HPO_4 + 0.6057 g TRIS buffer (dissolved in distilled water) and soaked for one week at 80°C. A similar procedure was repeated for the introduction of Zn^{2+} ions (weighed 7.4365 g $Zn(NO_3)_2 \cdot 6\ H_2O$; Chempur). To successfully alloy Zn^{2+} ions, the synthesis was also carried out by direct dropping of already synthesised CHA onto titanium plates into $Zn(NO_3)_2 \cdot 6H_2O$ solution. 7.4365 g of the material was weighed and dissolved in 100 ml of distilled water. A further modification of the Zn-CHA synthesis was also performed. First, $CaCO_3$ was synthesised according to the methodology described for the synthesis of $CaCO_3$ on Ti substrates, then Ti plates containing the synthesised calcium carbonate were dipped into a solution of 0.14 g Na_2HPO_4 + 0.6057 g TRIS buffer + 7.4365 g $Zn(NO_3)_2 \cdot 6\ H_2O$, which was prepared by dis-solving these materials in distilled water.

2.1.3. Preparation of creams

For the preparation of creams, the following reagents and their concentrations (%) were used: synthesized CHA, Fe:CHA, Cu:CHA, and Zn:CHA samples (0.1%), isopropyl myristate (8%) (Sigma-Aldrich, ≥ 90%), stearic acid (1.5%) (Sigma-Aldrich, ≥ 98%), petrolatum Vaseline® (0.5%) (Sigma-Aldrich, ≥ 98%), sunflower oil (1%) (Sigma-Aldrich), eumulgin B25 (1.5%) (Sigma-Aldrich, ≥ 98%), cetyl alcohol (4%) (Sigma-Aldrich, ≥ 99.5%), betaine (2%) (Sigma-Aldrich, ≥ 98%), glycerol (20%) (Sigma-Aldrich, 99%), phenoxyethanol (1%) (Sigma-Aldrich, ≥ 99%), ethanol (2%) (Vilniaus degtine, 92%), and deionized water (58.4%). The oil phase was melted in a separate beaker with slow stirring and heating of the fat phase raw materials up to 75–80 °C. The aqueous phase raw materials were also mixed and heated to 75-80 °C. Both phases, after the ingredients have been evenly mixed and reached a uniform temperature in the range of 75-80 °C, were combined by pouring the oily phase into the aqueous phase. After joining, homogenization was performed at 2000-3000 rpm for 2 min, maintaining the same temperature. The mixture was cooled to 35°C while stirring and the temperature-sensitive ingredients were added. The phases were combined by homogenization for 2 min using 2000-3000 rpm.

2.2. CHARACTERIZATION

A Rigaku MiniFlex II diffractometer emitting Ni-filtered Cu Kα radiation and working in Bragg-Brentano (θ/2θ) geometry was applied to collect powder X-ray diffraction data. During the data collection, 2θ angle was changed from 10 to 60°, step width of 0.01° and scanning speed of 5°/min were applied. Raman spectra were recorded at room temperature using a combined Raman and scanning near-field optical microscope (SNOM) WiTec Alpha 300 R (Germany) with a 532 nm excitation laser source (power 40.9 mW). Infrared (FTIR) spectra were recorded using a Bruker ALPHA ATR spectrometer in the range of 4000−400 cm^{-1}. A Hitachi SU-70 field-emission scanning electron microscope (FE-SEM) was used to study the surface morphology of the samples. For the elemental analysis, the samples were dissolved in 5% nitric acid (HNO_3, Rotipuran® Supra 69%, Carl Roth) and diluted to appropriate volume. Calibration solutions were prepared by an appropriate dilution of the stock standard solutions (single-element ICP standards 1000 mg/L, Carl Roth). Perkin Elmer Optima 7000 DV ICP-OES spectrometer was used for the determination of elemental composition of the samples.

The stability of the synthesised cosmetic products was evaluated by applying centrifugal force to the dispersion system. The centrifugation stability test was performed by weighing an equal amount of each sample into centrifuge tubes, which were placed in the centrifuge drum and subjected to a centrifugal force of 3000 rpm for 5 min. After the test, phase separation was assessed visually.

The determination of CHA, Fe:CHA, Cu:CHA, and Zn:CHA cream samples' cytotoxicity toward osteoblasts (U2-OS line) was performed using normative method (ISO 10993: Biological evaluation of medical devices; Part 5: Tests for in vitro cytotoxicity; Part 12: Biological evaluation of medical devices, sample preparation and reference materials (ISO 10993–5:2009 and ISO/IEC 17025:2005). The conditioned medium was obtained by 24-hour/37 °C incubation of 200 mg of sample in 1 ml of reference medium for osteoblast culturing (the Dulbecco's Modified Eagle's Medium High Glucose [DMEM] supplemented with 10% of fetal bovine serum). The same sample weight of creams was introduced to the medium and emulsified using 1% DMSO. The osteoblasts were cultivated with conditioned medium for 24 hours. The normative Neutral Red method was performed to assess the osteoblasts' viability. The growth control were osteoblasts cultured in non-conditioned DMEM medium. 70% ethanol was applied for the positive control for cell death. The test was repeated six times. Statistical analysis was performed using GraphPad Prism 10.0 software. The normality of distribution was

verified using Shapiro–Wilk's test. To evaluate statistical significance, the ANOVA test with post hoc Dunnett's multiple comparison (0.05) was performed.

Substances for experiments' usability control: gentamycin sulphate (Sigma-Aldrich), fluconazole (Pfizer Chemicals) as antibacterial and antifungal agents, respectively, and 70% ethanol as substance of proven cytotoxicity toward eukaryotic cells. American Tissue and Cell Culture (ATCC) reference cell line applied: osteoblasts U2-OS (Sigma-Aldrich). ATCC reference microbial cells applied: bacteria *Staphylococcus aureus* 6538 (Merck) and *Pseudomonas aeruginosa* 27853 (Merck); fungus: *Candida albicans* 10231 (Sigma-Aldrich).

Evaluation of the antibacterial properties of synthesised coatings on Ti substrates were tested using the inhibition zone method in the presence of Gram-negative *Escherichia coli* and Gram-positive *Bacillus subtilis* bacteria. Microbiological tests were conducted after 24 hours of incubation at 37°C.

3. RESULTS AND DISCUSSION

3.1. OVERVIEW OF CATIONIC SUBSTITUTION EFFECTS IN CALCIUM HYDROXYAPATITE ON BIOPROPERTIES

It is clear that metal-modified phosphates have improved the antibacterial and antifungal properties of bioceramics. We reached this conclusion in our recently published review article. A special improvement of bioproperties is observed when silver, copper, iron and zinc ions are introduced instead of calcium into the structure of CHA. The influence of silver ions has been studied very thoroughly. It was shown that a minor amount of silver dopant cannot alter the microstructure, stability, and crystallinity of the CHA structure in an implant and has a significant effect on the new bone formation and bone remodelling processes [127].

However, there is still a lack of excellent technological solutions for obtaining a good quality of copper, iron and zinc ions-substituted CHA. Previous studies indicated that Fe can have an inhibitory effect on osteoblast mineralisation in vitro. CHA samples substituted for Fe^{3+} were synthesised by different synthesis methods and characterised [128, 129]. CHA samples substituted for Fe were also tested for their biocompatibility, antibacterial property, drug release capability, cell adhesion and division on human osteosarcoma cells (MG-63) [130, 131]. The drug release profile was tested for one of the most effective and widely used drugs methotrexate for the treatment of various cancers and rheumatoid arthritis. More sustained and controlled drug release has been observed with increased iron concentration in CHA. Furthermore, antibiotic-loaded iron-substituted CDHA is highly suitable for clinical orthopaedic applications and for theranostics [132]. CHA, when substituted with iron, showed UV protection properties and was used to make sunscreen creams [133]. The superparamagnetic properties of microspheres can enable smart mechanisms for the on-demand release of therapeutic factors in situ by low alternated magnetic signals. Recently, magnetic BG (45S5) based scaffolds covered with Fe loaded CHA nanoparticles were obtained and their cytotoxicity was investigated [134]. Overall, the results obtained suggested that magnetic Fe-CHA coatings seem to enhance the biological performance of 45S5 BG based scaffolds.

The biomedical properties of these Cu-substituted different phosphates were also investigated. Copper-substituted BCP ceramic showed biocompatibility with bone marrow cells [135]. The good adherence with Cu-doped BCP samples is highlighted in Fig. 3.

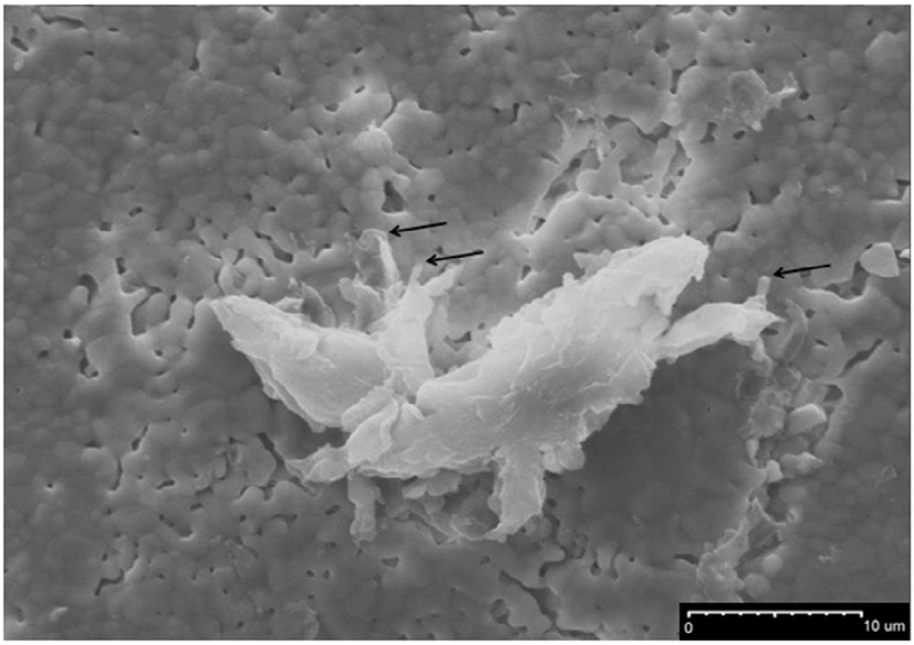

Fig. 3. Bone marrow adherent cell (black arrows) after 8 days of culture on a Cu-doped biphasic calcium phosphate ceramic disk [135].

Novel copper-doped mesoporous hydroxyapatite microspheres (Cu-MHMs) were successfully synthesised by using a microwave-assisted hydrothermal method using creatine phosphate as the organic phosphorus source [136]. Cu-MHMs consisting of CHA nanorods/nanosheets as building blocks exhibited a hollow mesoporous structure and a high specific surface area, which made them promising for drug delivery and for the application in repairing massive bone defects. Copper-containing phosphate coatings on different bone implants were also fabricated and investigated [137, 138]. *In vitro* characterisation on bioactivity and biocompatibility of copper-doped hydroxyapatite coatings deposited on the Ti6Al4V alloy with increasing copper content was evaluated under simulated body fluid (SBF) and cytotoxicity tests [138]. The cytotoxicity evaluation using MTT assays showed that the 3 mol% Cu-CHA coating was not toxic under in vitro characterizations.

Numerous investigations have highlighted that zinc-containing phosphate compositions are also innovative as biomaterials to fill bone cavities, can be a matrix for cells and have an antibacterial effect that supports regeneration of damaged tissue [139]. ZnO-doped CHA samples showed increased bone mineral formation [140]. Zinc-based degradable biomaterials have recently appeared due to their biocompatibility, biodegradability, and pro-regeneration

properties [141, 142]. For bioimplants, however, phosphate-based ceramic materials have been investigated and used. CHA doped with Zn showed non-toxic characteristics with enhanced MG-63 cell proliferation activity. The results suggested that 1 mol% Zn-CHA scaffolds may have enormous potential in bone repair and regeneration. Zinc-doped CHA showed the desired strength, bioactivity, and degradation to suit a variety of implant applications [143]. In conclusion, Zn-doped CHA enhanced the radiation effect on breast cancer cells [144]. CHA samples doped with Zn were also designed for dental applications, osteogenic differentiation of hMBC, and functionalisation of different implant alloys [145–147].

Thus, the breakthrough on further metal-substitution studies in CHA is necessary for surgeons to have dental implants, knee, or hip implants with excellent biocompatibility on hand. Scientists have to turn to this area of research again, because so far we only know about the sufficiently effective biological effects of these metal ions and about the possibility of using phosphates containing them in the treatment of dental canals or osteoporosis. The recent results suggested that the variation in surface morphological structure of metal-substituted CHA could be effective tool in hindering bacterial growth. This insight may contribute to the development of antibacterial scaffolds. Thus, different cationic and structural modifications of CHA could be useful for providing antibacterial activity to various biomaterials.

3.2. TAILORING CALCIUM HYDROXYAPATITE MORPHOLOGY VIA SUBSTITUTION EFFECTS OF DIVALENT/TRIVALENT CATIONS

In this part, the hydrothermal synthesis method to produce CHA of controlled morphology without the use of organic additives was developed. The influence of smaller (Mg^{2+}, Mn^{2+}) and larger (Sr^{2+}, Ba^{2+}) ions on the hydrolysis of α-TCP and crystal growth of CHA particles was investigated.

3.2.1. Investigation of calcium hydroxyapatite formation in the presence of smaller (Mg^{2+}, Mn^{2+}) and larger (Sr^{2+}, and Ba^{2+}) ions

Four series of hydrothermal syntheses with varying amounts of Mg^{2+}, Mn^{2+}, Sr^{2+}, and Ba^{2+} ions were carried out to investigate the influence of foreign ions on the hydrolysis process of α-TCP. The ionic radii (CN = 6) of the foreign ions applied in this study increase in the following order: Mg^{2+} (0.72 Å) < Mn^{2+} (0.83 Å) < Sr^{2+} (1.18 Å) < Ba^{2+} (1.35 Å) [148]. Fig. 4 shows the representative powder XRD patterns of the samples prepared under different

synthetic conditions in the presence of divalent cations. At lower temperature (120 °C), the smaller cations had the highest impact on the hydrolysis process of α-TCP. Even at concentration as low as 0.1 mol %, the presence of Mg^{2+} ions induced the formation of small amount of β-TCP secondary phase. This effect became more evident with increasing Mg concentrations, and 5 mol% of Mg^{2+} hindered the hydrolysis process completely, and only starting α-TCP could be identified in the XRD pattern of Mg-5-120. The inhibitory effect of Mg on the CHA crystal growth and its preference for the β-TCP structure has been reported previously. Unlike in the case of Mg^{2+}, the lowest Mn^{2+} concentration (0.1 mol%) did not induce the formation of β-TCP; however, the presence of β-TCP became evident in the sample Mn-0.5-120. Higher concentrations of Mn^{2+} ions (1, 5, and 10 mol% of Mn^{2+}) completely inhibited the hydrolysis of α-TCP. That is, even if the lowest Mg concentration (0.1 mol%) was enough to cause the formation of some β-TCP along with the major CHA phase, higher concentrations of Mn had a more prominent effect on the α-TCP hydrolysis, and a lower concentration of Mn^{2+} than Mg^{2+} is sufficient to completely hinder the process of CHA formation under the hydrothermal treatment at 120 °C.

Sr^{2+} ions had the lowest effect on the hydrolysis of α-TCP: single-phase CHA was obtained with even 1 mol% of this cation present in the synthesis mixture; however, higher concentrations of Sr retarded the hydrolysis process and induced the formation of β-TCP.

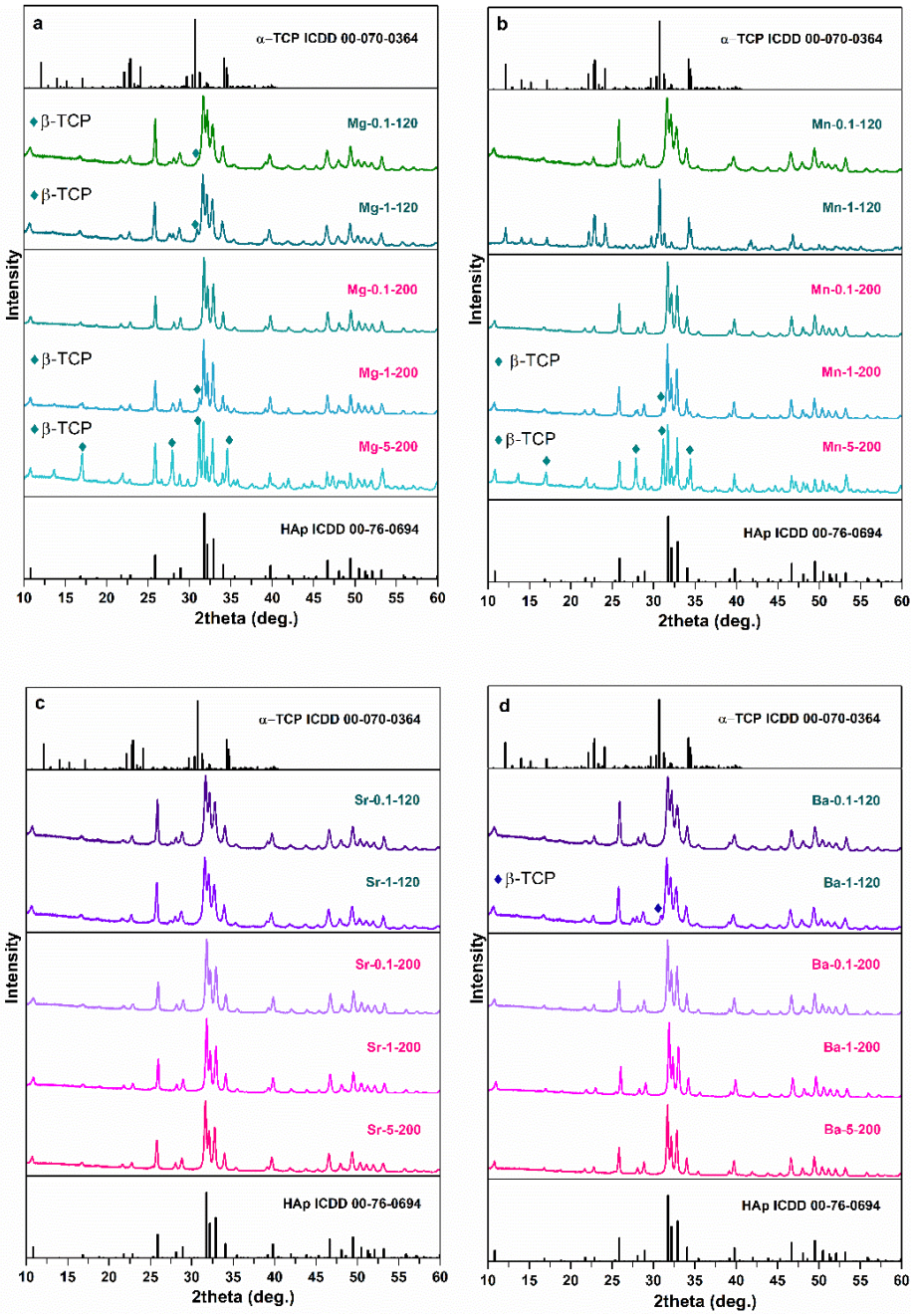

Fig. 4. XRD patterns of the samples after hydrothermal treatment at 120 °C for 3 h and at 200 °C for 5 h. Varying concentrations of smaller and larger ions were used as additives: (a) Mg-x-120 and Mg-x-200; (b) Mn-x-120 and Mn-x-200; (c) Sr-x-120 and Sr-x-200; and (d) Ba-x-120 and Ba-x-200.

Finally, the Ba^{2+} ions had an inferior effect: concentration of 0.5 mol% resulted in the formation of some β-TCP while 5 mol% of Ba^{2+} prevented the hydrolysis process completely.

The obtained results indicate that the formation of β-TCP in an aqueous medium can be promoted by the presence of foreign ions. Increased temperature and time of the synthesis resulted in an increased crystallinity of the final products which is seen from sharp diffraction peaks. Interestingly, it appeared that Ba^{2+} had similar impact as Mg^{2+} under milder conditions, but higher temperature and longer process revealed significant differences between the effect of these cations.

Several distinct bands at around 940–1180 cm^{-1} and around 500–660 cm^{-1} were observed in all FTIR spectra of the synthesised samples. Bands centred at ca. 1023 and 1090 cm^{-1} are assigned to asymmetric P–O stretching vibrations (ν_3), while the band with a peak at 960 cm^{-1} corresponds to symmetric P–O stretching vibrations (ν_1) of CHA [149]. The results of FTIR spectroscopy are in a good agreement with the results of the XRD analysis.

Elemental analysis of the final products was performed by means of ICP-OES in order to determine if the foreign ions from the solution transfer to the obtained powders during the hydrolysis reaction and to estimate the incorporation level of these ions as compared to the initial M-to-Ca ratios. ICP-OES analysis revealed that only a limited amount of foreign ions was incorporated into the final products. It is obvious that for smaller ions (Mg^{2+} and Mn^{2+}), the discrepancies between the initial and final (in obtained powders) molar ratios were less significant as compared to those of Sr^{2+} and Ba^{2+}. The actual percentage of Mg^{2+} and Mn^{2+} ions was in good agreement with the initial ratios of cations in the reaction mixture up to 5 mol%, which indicates that during the hydrolysis of α-TCP these ions are transferred to the synthesis products. An increasing concentration of these ions in the reaction solution only slightly increased their content in the obtained powders. In the case of Sr^{2+}, appreciably higher discrepancies were observed, which indicates that after the reaction a significant amount of Sr^{2+} ions remained in the solution. For instance, the reaction performed with 5 mol% resulted in the product containing only about a half of this amount. Of all the metals studied, Ba^{2+} ions were characterized by the lowest ability to incorporate into the obtained product. The difference between the initial ratios of cations and the actual molar ratio varied in the range from 34% to 84% being higher for samples with high initial concentration of Ba^{2+}. Whereas Ba^{2+} can partially substitute Ca^{2+} in CHA, only small quantities of Ba^{2+} can be introduced into the CHA structure in an aqueous solution. This is due to the large radius of

this ion. Hence, a limited amount of Ba^{2+} detected in the final product is not surprising.

Morphology of the prepared powder particles was examined by scanning electron microscopy. Figs. 5 and 6 show the SEM images of higher magnification with details of the selected samples. Differences in morphology depending on the synthesis conditions could be seen in the SEM images of the samples. Hydrothermal treatment at 120 °C with 0.1 mol% of various cations resulted in the formation of plate-like crystals. When higher concentrations of metal ions are introduced into the reaction mixture, the formation of both plate-like and hexagonal rod-like particles occurred. In some cases, self-assembly of the rods into flower-like structures was observed. Under the hydrothermal treatment at 200 °C, the formation of the rod-like together with plate-like crystals occurs even when lowest investigated concentration (0.1 mol%) of metal ions is introduced to the reaction mixture. Increasing metal concentrations go hand in hand with an increased fraction of rod-like particles.

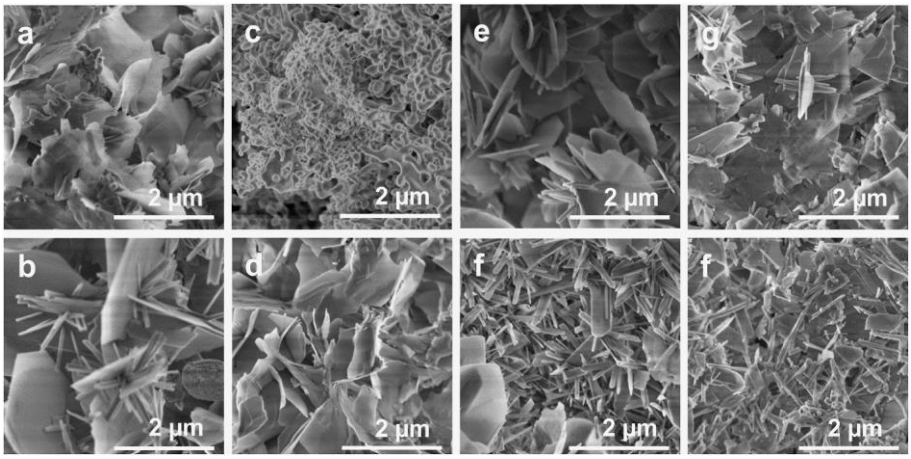

Fig. 5. SEM images of the samples after hydrothermal treatment at 120 °C for 3 h: (a) Mg-0.1-120; (b) Mg-1-120; (c) Mn-0.1-120; (d) Mn-1-120; (e) Sr-1-120; (f) Sr-5- 120; (g) Ba-0.1-120; (h) Ba-1-120.

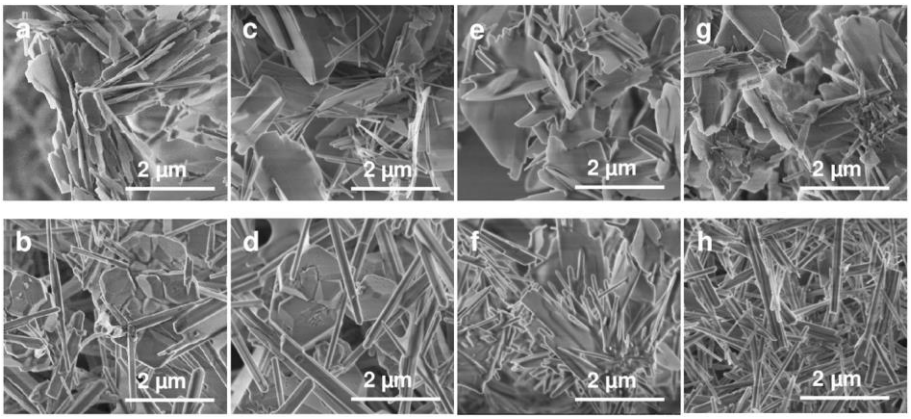

Fig. 6. SEM images of the samples after hydrothermal treatment at 200 °C for 5 h: (a) Mg-0.1-200); (b) Mg-5-200; (c) Mn-0.1-200; (d) Mn-5-200; (e) Sr-0.1-200; (f) Sr-5-200; (g) Ba-0.1-200; (h) Ba-5-200.

The sample prepared with 5 mol% of Ba^{2+} consisted of hexagonal rod-like particles only. Taking into account the most prominent influence of Ba^{2+} ions on the formation of rod-like CHA crystals, an additional series of experiments with varying Ba^{2+} concentrations (1, 2, 3, and 4 mol%) were performed at 200 °C. The samples prepared with 1 and 2 mol% of Ba^{2+} still contained some plate-like structures (see Fig. 7).

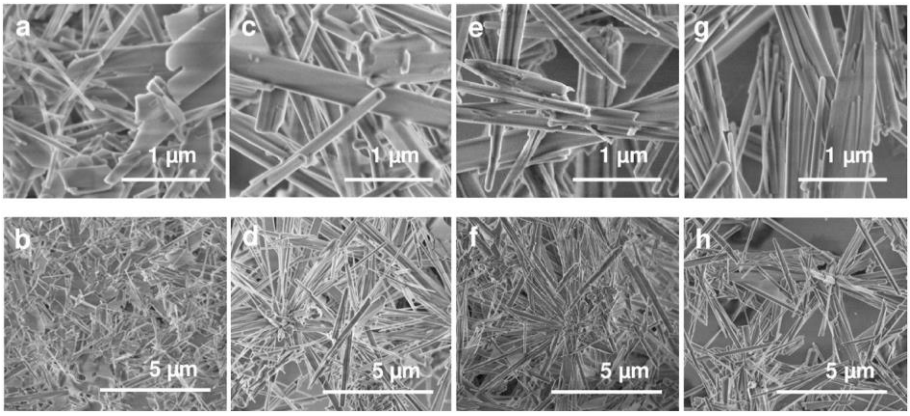

Fig. 7. SEM images of the samples after hydrothermal treatment at 200 °C for 5 h: a), b) α-TCP-Ba (1 mol%); c), d) α-TCP-Ba (2 mol%); e), f) α-TCP-Ba (3 mol%); g), h) α-TCP-Ba (4 mol%).

No such structures were observed in SEM images of the sample prepared with 3 and 4 mol% of Ba^{2+}, these samples were comparable to that prepared

with 5 mol% of Ba^{2+} and consisted of rod-like particles. The average diameter and length of the rods were around 0.2 and 4 μm, respectively. The concentration of Ba^{2+} ions did not significantly affect the dimensions of the obtained CHA rods.

These results indicate clearly that the morphology of the final products depends on the conditions of the hydrothermal synthesis, but the concentration and nature of the foreign ion play a key role in this process. According to other studies, the differences in morphological features of CHA samples appear because of the varying inhibiting effect of the substituting ion, as well as due to the formation of defects and strains in the CHA lattice [150, 151].

In conclusion, by applying divalent cations as controlling agents for the hydrothermal synthesis, morphology control of doped calcium-deficient hydroxyapatite was achieved. Hydrothermal synthesis conditions (temperature, time) affected the phase purity and morphology of the final products, but the nature and concentration of the foreign ions were the main factors determining the characteristics of the products. Smaller ions (Mn^{2+} and Mg^{2+}) were found to have a stronger inhibiting effect on the hydrolysis process of α-TCP as compared to larger ions (Ba^{2+} and Sr^{2+}). Higher temperatures and longer reaction times lead to the formation of single-phase CHA in the presence of higher concentrations of the metal ions. This was especially notable in the case of Ba^{2+} and Sr^{2+}. Moreover, increased temperature and time of the hydrothermal synthesis resulted in an increased crystallinity of the final products. Samples consisting of solely plate-like (exposed *c*-planes) or rod-like (exposed *a(b)*-planes) CHA crystals were obtained by modifying the synthesis conditions.

3.2.2. Investigation of calcium hydroxyapatite formation in the presence of Fe^{3+}, Cu^{2+} and Zn^{2+} ions

CHA and metal-substituted samples Fe:CHA, Cu:CHA, and Zn:CHA were also synthesised using above developed method. Fig. 8 shows the powder XRD pattern of non-substituted CHA sample prepared by hydrothermal synthesis via a phase transformation of α-TCP in an aqueous solution. All diffraction lines are indexed confirming that monophasic CHA was obtained. The XRD patterns of metal-substituted samples (Fe:CHA, Cu:CHA and Zn:CHA) are presented in Fig. 9.

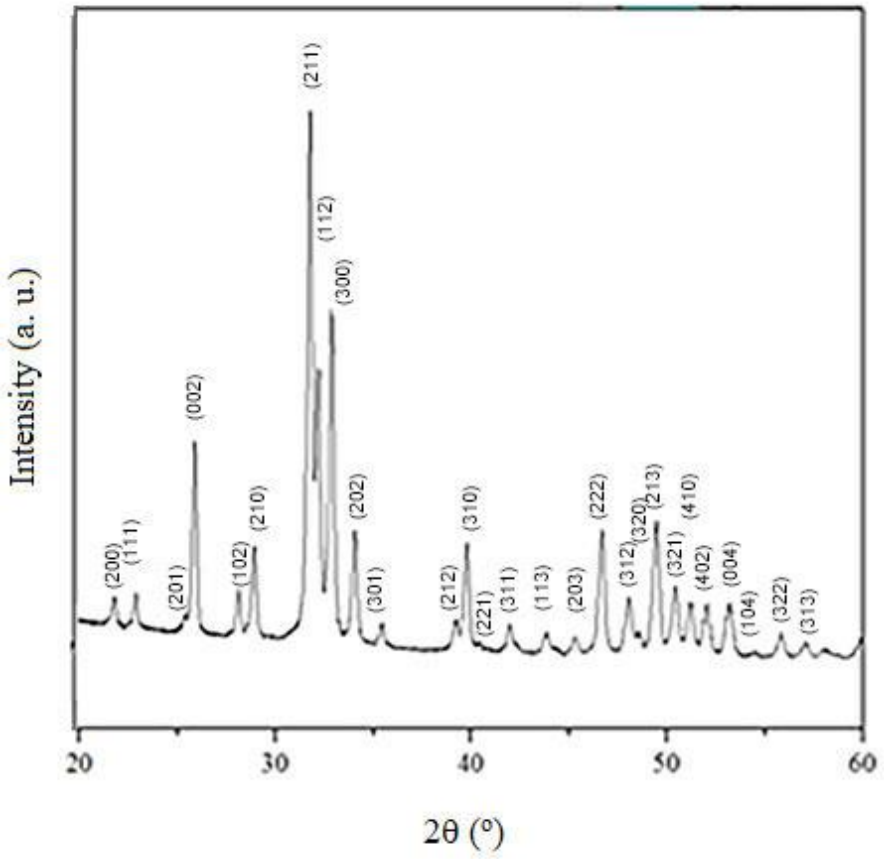

Fig. 8. XRD pattern of CHA prepared by hydrothermal synthesis *via* a phase transformation of α-TCP in an aqueous solution.

In the presence of Fe^{3+} and Cu^{2+} ions, the formation of different TCP phases (β-TCP and α-TCP) as secondary phases is evident. Unlike Fe^{3+} and Cu^{2+} ions, Zn^{2+} ions did not induce the formation of β-TCP or α-TCP.

FTIR spectra of all synthesised samples were very similar, regardless of metal substitution as shown by two representative FTIR spectra of CHA samples (Fig. 10). These FTIR results again are in a good agreement with the XRD data. The results of the elemental analysis of the synthesised specimens are summarized in Table 1. ICP-OES analysis revealed that only small amounts of Fe^{3+} and Cu^{2+} ions were incorporated into the final products. It is evident that Zn^{2+} ions almost completely substituted Ca^{2+} ions in the CHA structure.

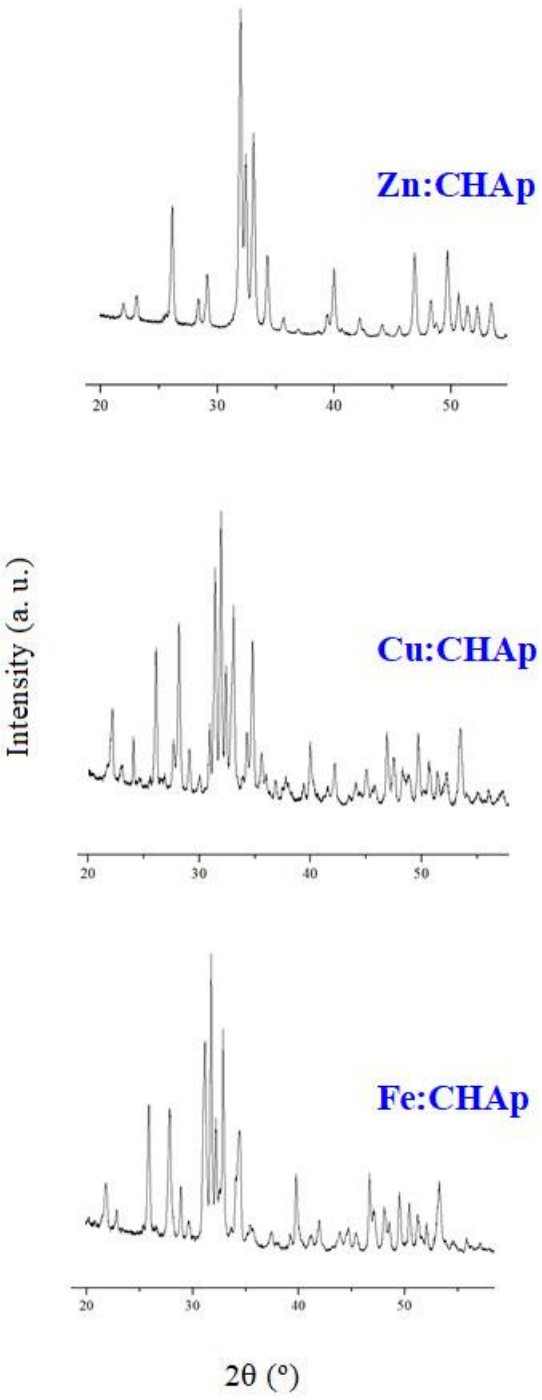

Fig. 9. XRD patterns of Fe:CHA, Cu:CHA, and Zn:CHA samples.

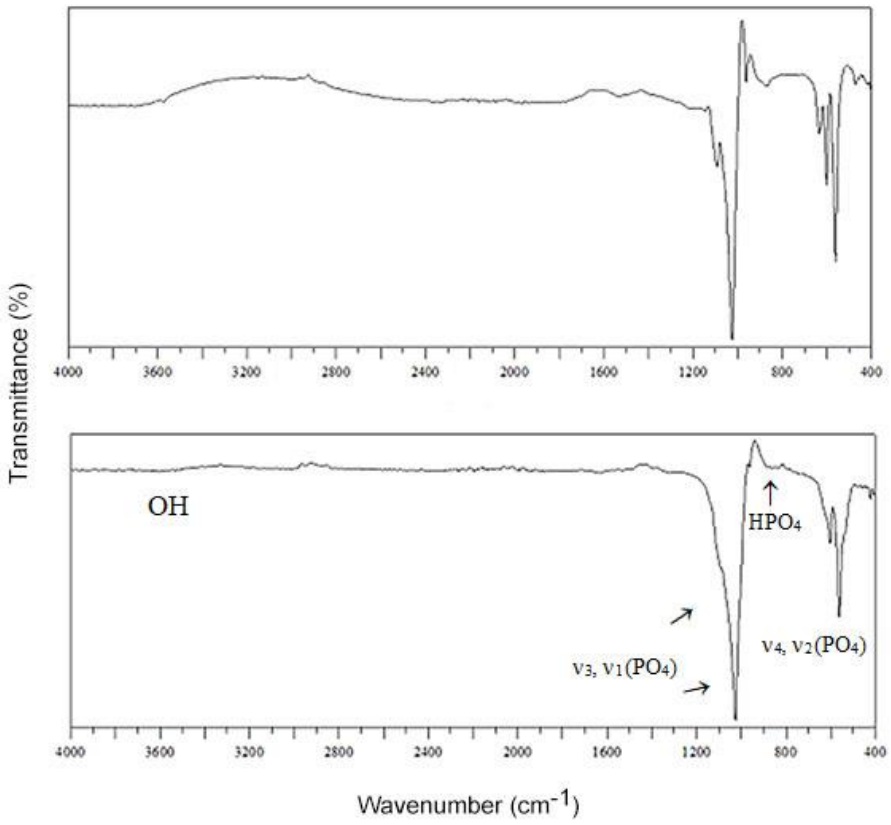

Fig. 10. FTIR spectra of Cu:CHA (bottom) and Zn:CHA (top) samples.

Table 1. Metal concentrations determined by the ICP-OES analysis of the samples obtained at 200 °C for 5 h (standard deviations in parentheses).

Sample	Theoretical amount foreign metal, mol%	Determined amount, mol%			
		Ca^{2+}	Fe^{3+}	Cu^{2+}	Zn^{2+}
CHA	0	99.75(2)	-	-	-
Fe:CHA	10	90.51(1)	8.44(2)	-	-
Cu:CHA	10	91.02(3)	-	8.70(1)	-
Zn:CHA	10	89.67(2)	-	-	10.03(2)

The surface morphology of the synthesised samples was investigated by SEM. Fig. 11 displays the SEM images of CHA, Fe:CHA, Cu:CHA, and Zn:CHA samples.

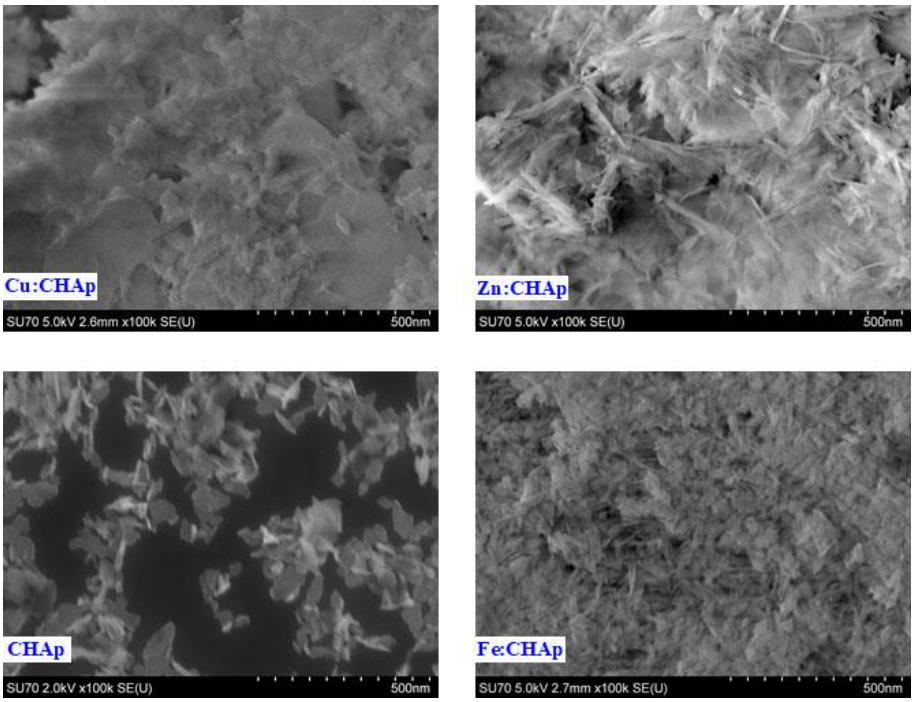

Fig. 11. SEM micrographs of the CHA, Fe:CHA, Cu:CHA, and Zn:CHA samples obtained by hydrothermal synthesis.

The images reveal small morphological differences depending on the type of substituent. Hydrothermal treatment of non-substituted α-TCP at 200 °C resulted in the formation of differently oriented and slightly agglomerated plate-like crystals of CHA. The individual particles were approximately 50 nm in size. When metal ions were introduced into the reaction mixture, the formation of plate-like particles with additional shapes and a higher degree of agglomeration occurred. The Fe^{3+}-containing sample consisted of plate-like and needle-shaped particles of similar size (~50 nm). The sample with 10 mol% Cu^{2+} featured large plate-like structures with smaller particles evenly distributed on the plate surfaces. In the case of Zn^{2+}-substituted CHA, the powder comprised both plate-like and fibrous particles, ranging in size from 50 to 100 nm.

Finally, by applying Fe^{3+}, Cu^{2+} and Zn^{2+} cations as controlling agents for the hydrothermal synthesis, the morphology control of CHA was achieved. Notably, it highlights the phase purity of CHA and Zn:CHA (in the presence of Fe^{3+} and Cu^{2+} ions, the α- and β-TCP phases have formed). The synthesised nanosized CHA, Fe:CHA, Cu:CHA, and Zn:CHA samples were used as

additives in the preparation of skin creams. These results will be discussed in the next part of the dissertation.

3.3. LOW-TEMPERATURE SYNTHESIS OF CALCIUM HYDROXYAPATITE COATINGS

In the present part of PhD thesis, the low-temperature synthesis of substituted calcium hydroxyapatite with copper and zinc ions on titanium substrates was performed. XRD analysis, FTIR and Raman spectroscopies, and SEM were employed to evaluate the phase composition, surface functional groups, crystallinity, and morphology of the coatings. Antibacterial properties of the coatings were tested using the inhibition zone method.

3.3.1. Synthesis and characterization of calcium hydroxyapatite coatings

The synthesis of the CHA porous layers was carried out on Ti wafers. The prepared plates initially were used for the synthesis of $CaCO_3$ coatings. Crystalline calcium hydroxyapatite was then synthesised from these $CaCO_3$ coatings through the dissolution-precipitation method at low temperature (80 ^oC). The phase composition of the coatings was determined by XRD. The XRD patterns showed that a layer of $CaCO_3$ was formed on the Ti substrate. At $2\theta = 29.4°$, the most intense peak characteristic of calcite ($CaCO_3$) was visible. The data were in a good agreement with literature [152]. As was already mentioned, CHA was then synthesised from these $CaCO_3$ coatings through the dissolution-precipitation method. The XRD results clearly showed the formation of CHA with characteristic reflections in the 31-32.5° 2θ angle range (see Fig. 12).

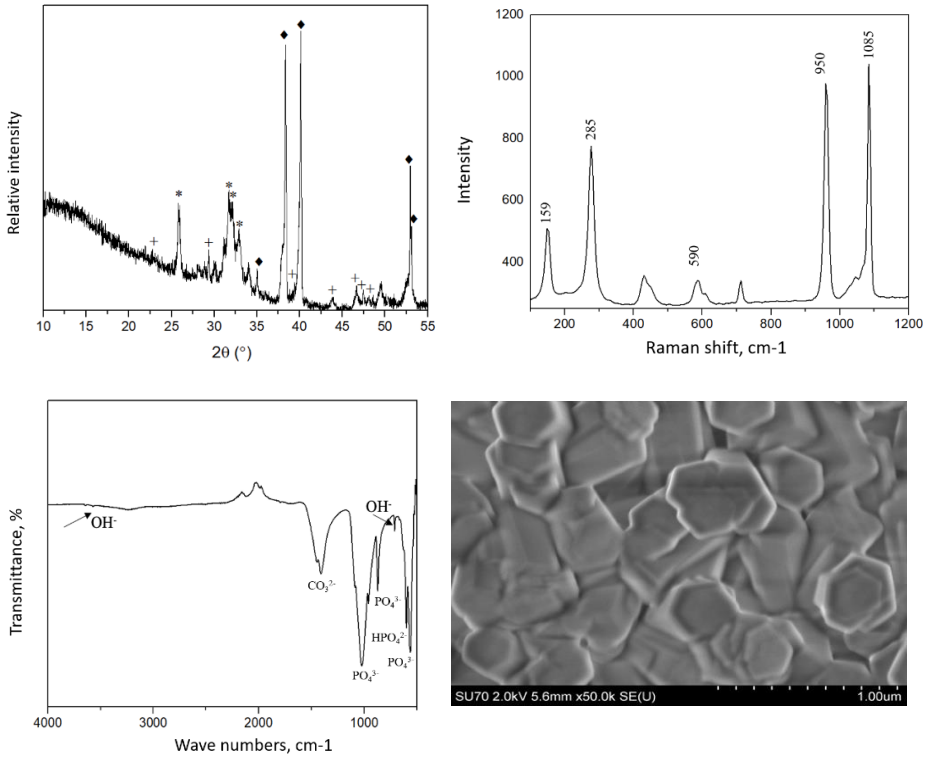

Fig. 12. XRD pattern (top, left), Raman spectrum (top, right), FTIR spectrum (bottom, left) and SEM micrograph (bottom, right) of a calcium hydroxyapatite coating on a Ti substrate. Diffraction reflections: * - HAP [PDF: 96-431-7044]; ♦ - Ti [PDF: 96-901-6191]; + $CaCO_3$ [PDF: 96-154-7348].

The peaks of $CaCO_3$ are also identified, proving that some $CaCO_3$ still remains unreacted. In addition, intense diffraction peaks of the Ti substrate are visible. Thus, it can be concluded that a layer of calcium hydroxyapatite has formed on the titanium substrate. Fig. 12 also shows Raman spectrum of CHA coating. The PO_4^{3-} peaks at 590, 950, 1085 cm^{-1} of the phosphate group oscillations belong to CHA. The peak around 285 cm^{-1} is attributed to Ca-PO_4 and Ca-OH bonds. The FTIR spectrum of the calcium hydroxyapatite layer on a Ti substrate is also depicted in Fig. 12. The FTIR spectra shown here identify absorption peaks for PO_4^{3-} (560-600 cm^{-1}, ~600 cm^{-1} and 1000-1100 cm^{-1}), OH^- (3600-3500 cm^{-1} and 630 cm^{-1}), CO_3^{2-} (1460-1530 cm^{-1}), as well as for HPO_4^{2-} (610-615 cm^{-1}) [149]. Thus, it can be concluded that the Raman and FTIR spectroscopy results obtained confirmed the X-ray diffraction data for the successful formation of $Ca_{10}(PO_4)_6(OH)_2$ coatings on the Ti substrate. The

morphological features of CHA coatings were investigated by SEM. Hexagonal CHA particles of 20 nm in size were formed at low temperature. A particular morphological feature of the synthesised CHA (Fig. 12) is that a very high degree of homogeneity and distribution of particle size is achieved.

3.3.2. Synthesis and characterization of Cu^{2+}- and Zn^{2+}-substituted calcium hydroxyapatite coatings

The phase crystallinity and purity of Cu^{2+}-substituted CHA specimens synthesised by low-temperature sol-gel and dissolution-precipitation method were also investigated by means of XRD analysis. It was determined, that during the heating of mixture of $Ca(NO_3)_2$ and $Cu(NO_3)_2$ solutions in a CO_2 atmosphere, in addition to $CaCO_3$, a copper hydroxide carbonate $Cu_2(OH)_2CO_3$ (malachite) also has formed. It is not surprising, since it is known that pure $CuCO_3$ does not form in an aqueous media under normal conditions:

$$2\ Cu(NO_3)_2 + CO_2 + 4\ NaOH \rightarrow Cu_2(OH)_2CO_3 + 4\ NaNO_3 + H_2O$$

Fig. 13 represents the XRD pattern of the CHA coating where Ca^{2+} ions are substituted by Cu^{2+} ions.

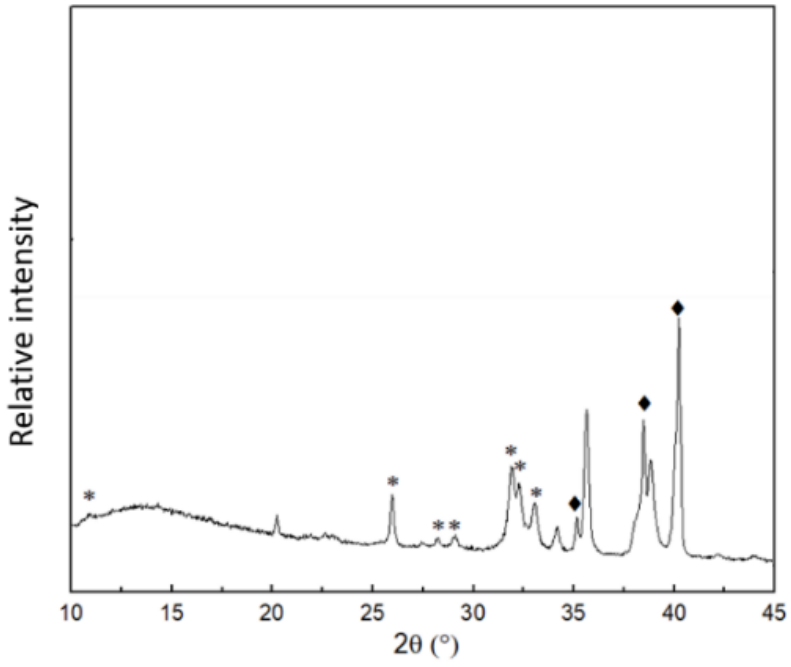

Fig. 13. XRD pattern of the Cu-CHA coating obtained on the Ti substrate. Diffraction reflections: * - CHA; ♦ - Ti.

The XRD results indicate that the low-temperature dissolution-precipitation method can be successfully used for the synthesis of partially Cu^{2+} ion-substituted CHA. Treatment of $CaCO_3$ containing a small amount of impure $Cu_2(OH)_2CO_3$ with sodium hydrogen phosphate produces copper substituted Cu-CHA:

$$10\text{-}x\ CaCO_3 + x\ Cu_2(OH)_2CO_3 + 6\ Na_2HPO_4 + 2\ H_2O =$$

$$Ca_{10-x}Cu_x(PO_4)_6(OH)_2 + x\ Cu(OH)_2 + 8\ NaHCO_3 + 2\ Na_2CO_3$$

Fig. 14 represents the Raman spectrum of a CHA coating substituted with Cu^{2+} ions.

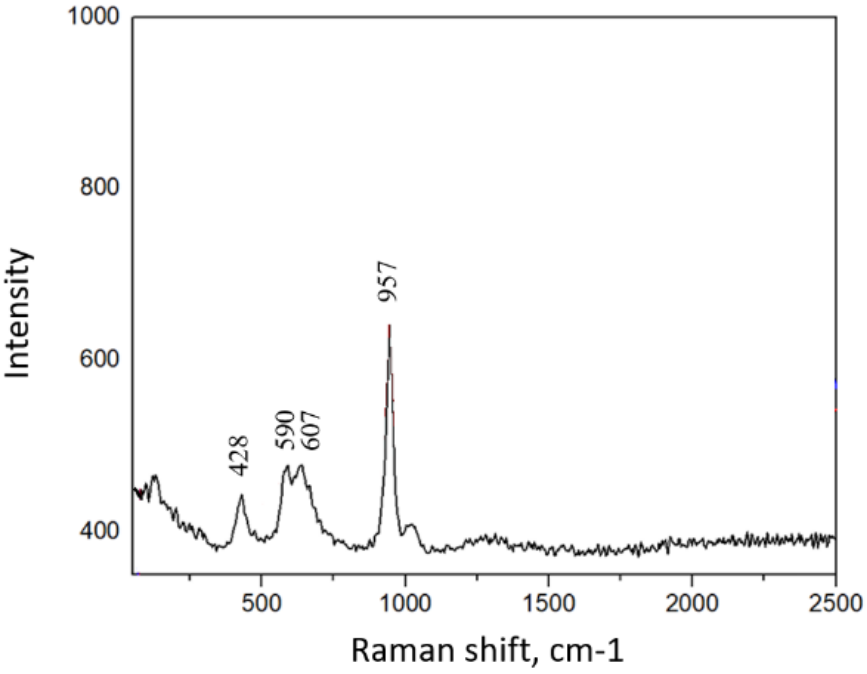

Fig. 14. Raman spectrum of the Cu-CHA coating obtained on the Ti substrate.

In this Raman spectrum, the band at 428 cm^{-1} of the phosphate group vibrations are visible, while the bands at 590, 607 cm^{-1} also belong to the PO_4^{3-} asymmetric vibrations of the CHA. The band at 957 cm^{-1} corresponds to a fully symmetric stretching of PO_4^{3-}. The sharpness of this band confirms a good crystallinity of the Cu-CHA coating [153].

However, the formation of CHA coatings substituted with Zn^{2+} ions by the above preparation method did not proceed. The results presented in the XRD pattern of the coating synthesised by the low-temperature dissolution-precipitation method (by forming mixed carbonates from a mixture of

$Zn(NO_3)_2 \cdot 6H_2O$ and $Ca(NO_3)_2 \cdot 4H_2O$ and dropping the product into Na_2HPO_4 + TRIS buffer solution) confirmed only formation of calcite which was not transformed to the Zn-CHA. Therefore, different variations of the proposed synthesis method were tested to obtain a Zn-CHA coating on Ti substrate. An attempt was made to synthesise the Zn-CHA coating by direct immersing of the already synthesised CHA coating on Ti into $Zn(NO_3)_2$ solution. The reaction was carried out under the same conditions at 80°C for one week. The XRD pattern of the resulting product is shown in Fig. 15.

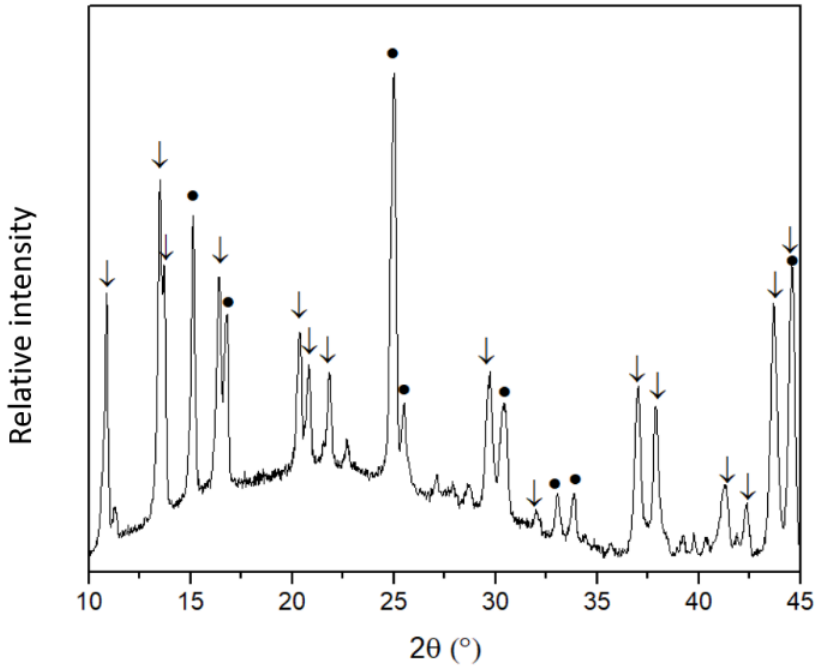

Fig. 15. XRD pattern of CHA doped with Zn^{2+} coatings synthesised by immersing the CHA coating on Ti in zinc nitrate solution. Diffraction reflections: • - TiO_2 [PDF: 96-152-8779]; ↓ - $Zn(OH)(NO_3)(H_2O)$ [PDF:96-152-9913].

Unexpectedly, the Zn-CHA did not form, and also the CHA coating dissolved, although the solubility of CHA is very low. An even more unexpected result was the formation of almost single phase zinc hydroxide nitrate monohydrate $Zn(OH)(NO_3)(H_2O)$ instead of Zn-CHA on the Ti substrate.

The SEM images clearly showed that the addition of copper to the CHA also changes the morphology of the particles. Instead of the hexagonal 20 nm particles of CHA, fibrous crystallites with a snowflake shape of about 1 μm have formed (see Fig. 16).

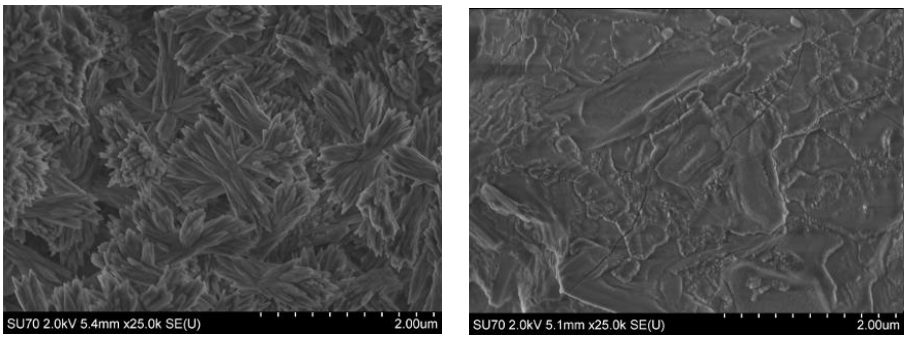

Fig. 16. SEM micrographs of Cu-CHA (left) of $Zn_3(OH)_4(NO_3)_2$ coatings (right) fabricated on Ti substrate.

The volumetric snowflake crystallites are composed of interlocking needles between 0.5 nm and 1 nm in size. The morphology of the Zn^{2+}-containing samples synthesised by forming mixed carbonates from a mixture of $Zn(NO_3)_2{\cdot}6H_2O$ and $Ca(NO_3)_2{\cdot}4H_2O$ and immersing the product into a Na_2HPO_4 + TRIS buffer solution differs considerably from that of the CHA and Cu-CHA. The representative SEM image of this sample is also shown in Fig. 16. It can be seen that homogeneous coatings with some cracks have formed. The coatings are composed of planar crystals larger than 1 μm forming a continuous coating. Few accumulations of smaller particles are also visible on the Ti surface.

Elemental analysis of the synthesised Cu and Zn containing coatings was carried out by EDX analysis. The EDX spectra of both samples are presented in Fig. 17.

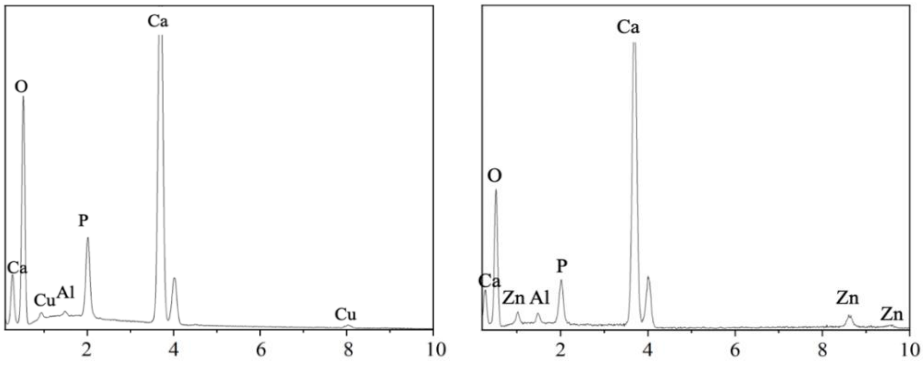

Fig. 17. EDX spectra of Cu-CHA (top) and $Zn_3(OH)_4(NO_3)_2$ coatings (bottom) fabricated on Ti substrate.

In the case of Cu-CHA coating, the Ca/P ratio of ~1.62 was found to be almost identical to the calcium/phosphorus ratio in stoichiometric CHA (1.67). The molar ratio of calcium to copper was Ca:Cu = 1:0.033, i.e. about 3.3 mol% of the calcium was likely replaced by copper. The formula for the synthesis product could be then written $Ca_{9,7}Cu_{0,3}(PO_4)_6(OH)_2$ or $Ca_{9,85}Cu_{0,15}(PO_4)_6(OH)_2$, if the reaction produced a further stoichiometric amount of copper hydroxide. From the EDX measurements of the sample with zinc, the Ca/P ratio determined was completely unreasonable as it did not correspond to any possible calcium/phosphorus ratio in known phosphates. Although calcium and phosphorus were detected in the synthesised coating, XRD analysis failed to detect calcium phosphate crystalline phases. It is likely that a significant amount of amorphous calcium carbonate and/or a very small amount of calcium hydroxyapatite remained in the coating. The EDX spectrum shows that the coating synthesised contains a significant amount of zinc.

3.3.3. Investigation of antibacterial properties

Evaluation of the antibacterial properties of synthesised coatings on Ti substrates revealed no zones of CHA inhibition in the presence of Gram-negative *Escherichia coli* and Gram-positive *Bacillus subtilis* bacteria. Subsequent microbiological tests conducted after 24 h of incubation at 37 °C demonstrated zones of inhibition in samples containing Cu-CHA when exposed to a colony of *B. subtilis* (see Fig. 18). According to existing literature [154], Gram-positive bacteria possess a negatively charged cell surface and a substantial peptidoglycan membrane, ranging from 20-80 nm in thickness. In contrast, Cu^{2+} ions are positively charged and adhere to these negatively charged surfaces, thereby inducing apoptosis in Gram-positive bacteria. Similar observations on the effects of Cu-doped titanium alloy coatings on Gram-positive bacteria have been reported in a study by Kalaivani *et al*. [155].

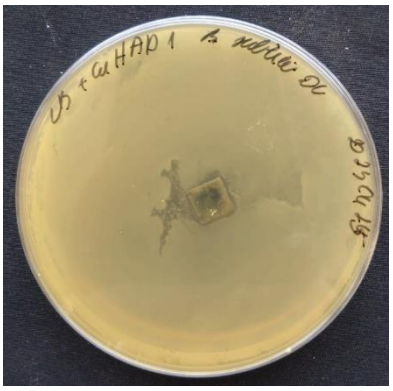

Fig. 18. Results of antibacterial performance tests of low-temperature synthesised Cu-CHA coating on Ti with *B. subtilis*. Blue arrow marks inhibition zone.

Fig. 19 illustrates the zones of inhibition associated with samples doped with Zn^{2+} ions when exposed to a *B. subtilis* colony. However, no zones of inhibition were observed in the presence of *E. coli*.

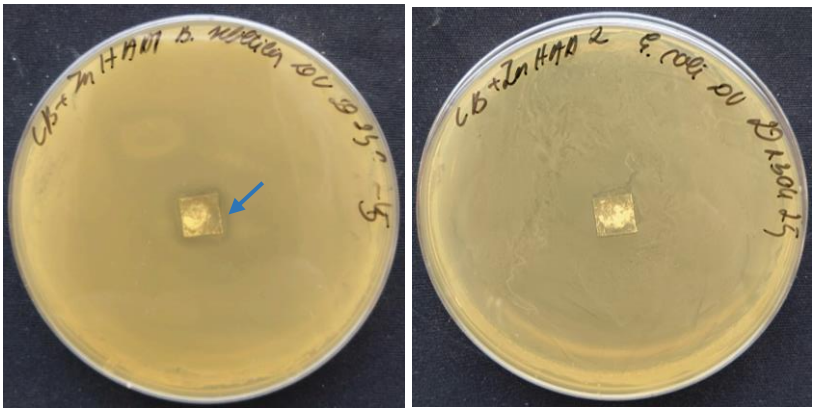

Fig. 19. Results of antibacterial performance tests of low-temperature synthesised coatings with Zn^{2+} ions on Ti with (left) *B. subtilis* and (right) *E. coli* bacteria. Blue arrow marks inhibition zone.

Inhibition zone of coating with Cu-CHA coating on Ti were 10.5 mm ± 0.5 mm average from 9 measurement, the plate with the $Zn_3(OH)_4(NO_3)_2$ coatings were 15 mm ± 1.8 mm. Several factors may explain the lack of inhibition zones in some cases with Cu^{2+} and Zn^{2+} ion coatings. One plausible explanation is that materials from coatings do not substantially diffuse into the medium; the fraction that does diffuse exhibits inhibitory effects solely against *B. subtilis*. Another possibility is the absence of direct contact between the metal ions and the bacteria. Alternatively, the concentrations of metal ions may be insufficient for inhibition.

Titanium and calcium phosphate ceramics have emerged as the gold standard in orthopaedic applications. Titanium alloys exhibit commendable mechanical strength and resistance to physiological corrosion, courtesy of an intrinsic oxide layer. Calcium phosphates, particularly CHA, offer unparalleled biocompatibility, accelerating biological responses and promoting strong bone-implant interfaces. When CHA-based ceramics are implanted, a fibrous layer is formed on the surface of the ceramics, which helps the implant to bond to the living bone. This stabilises the implant and anchors it to the surrounding tissue.

In this study, the incorporation of Zn^{2+} ions into CHA was investigated. Zinc is a critical trace element in humans, constituting approximately 3 g in the adult body. It serves both catalytic and structural roles in various biological

processes, including metabolism, cell division, and gene transcription. Zinc deficiency is detrimental, particularly affecting the immune system [156]. Zinc is found as a trace element in bone. Scientific publications have reported that zinc stimulates bone formation by activating osteoblast proliferation and differentiation. Zn-CHA also has antibacterial properties against Gram-negative and Gram-positive bacteria. CaP doped with less than 1 % zinc ions exhibits effective biological activity [156]. The Zn-CHA samples obtained by the different methods show a different distribution of zinc in the coating. The dependence of the Zn-CHA biological response on the zinc content has been investigated in various experiments. *In vitro* adhesion and proliferation studies have shown that human osteoblast cells respond better to Zn-CHA layers compared to pure CHA coatings.

Another cation included in our research was Cu^{2+}. The introduction of Cu ions into the CHA structure also provides antibacterial properties to the CHA, which reduces the risk of inflammation after implantation. Despite promising applications in orthopaedics, the literature shows that commercial success is still a long way off. This is not only due to the burden of the regulatory processes involved in bringing metal-doped materials to the health market, but also due to the difficulty in proving the effect of the element experimentally. Today's challenges are to combine in the same study all the characteristics related to the element: material studies (chemical composition, phase composition, formation, biomechanical aspects (brittleness, mechanical strength and oxidation resistance) and biological aspects (cytotoxicity, bactericidal, osteogenic and angiogenic properties) [157]. Cu is a trace element essential for numerous physiological functions, including respiration, energy production, and tissue formation. It is crucial for bone collagen maturation and osteoblast function. Key studies have substantiated the antimicrobial efficacy of Cu-doped CHA [158].

3.4. APPLICATION OF SYNTHESISED CALCIUM HYDROXYAPATITE SAMPLES IN COSMETICS

The effect of Fe^{3+}, Cu^{2+}, and Zn^{2+} substitution in CHA on the antimicrobial properties of CHA are summarized in this part of dissertation. Notably, it highlights the antimicrobial activity of Zn:CHA and Cu:CHA against *Staphylococcus aureus* and *Candida albicans*. The synthesised nanosized CHA, Fe:CHA, Cu:CHA, and Zn:CHA samples were used as additives in the preparation of skin creams. *In vitro* biological studies of the resulting skin creams demonstrated their antimicrobial activity against *Pseudomonas*

aeruginosa, and showed a reduction in osteoblasts cells viability of in the range of 20–40%.

The photographs of fabricated cream samples are presented in Fig. 20.

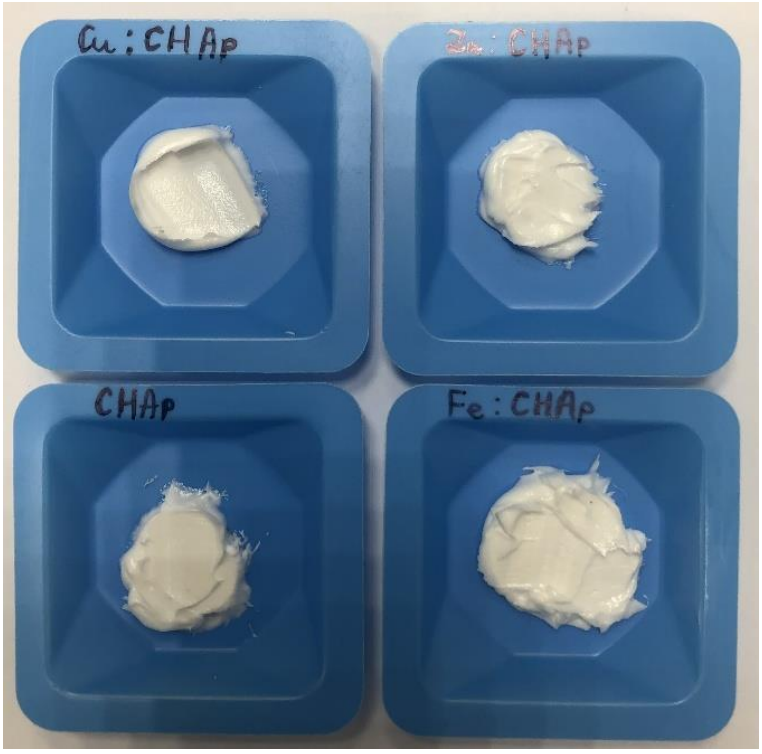

Fig. 20. The photographs of fabricated cream samples using nanosized CHA (bottom, left), Fe:CHA (bottom, right), Cu:CHA (top, left), and Zn:CHA (top, right) samples.

From these images, it is evident that the external appearance of all the creams prepared with different CHA is nearly identical. The morphology of the cream samples was also appeared almost the same across all formulations, regardless of the type of calcium hydroxyapatite used. SEM micrographs of cream samples are presented in Fig. 21. These results clearly indicate that the morphology of the cream products differs significantly from that of the hydroxyapatites.

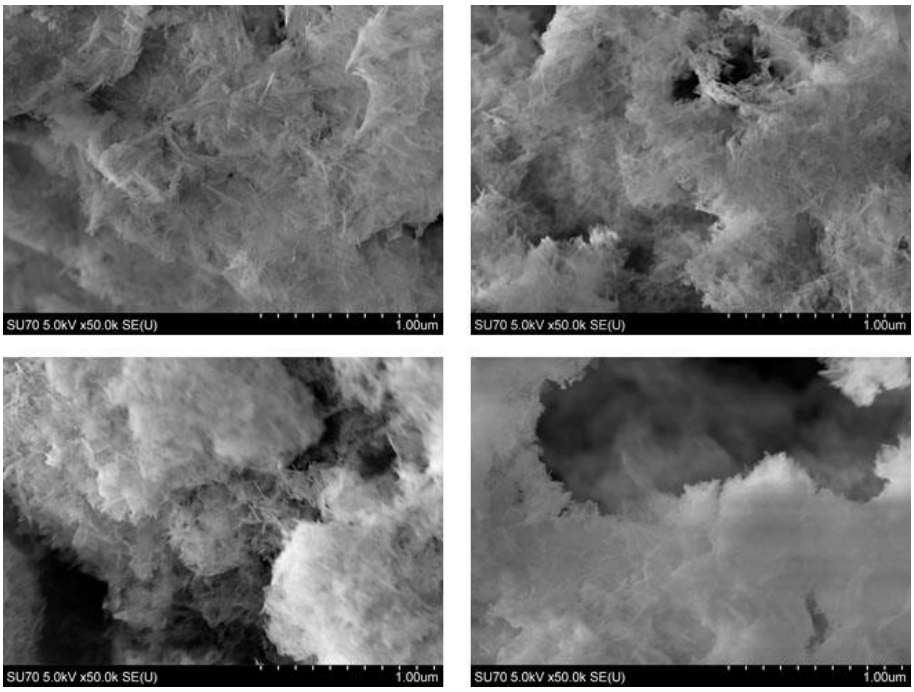

Fig. 21. The SEM micrographs of fabricated cream samples using nanosized CHA (bottom, left), Fe:CHA (bottom, right), Cu:CHA (top, left), and Zn:CHA (top, right) samples.

3.4.1.Biocompatibility assessments

The primary focus of this study was to engineer a series of hydroxyapatite-based materials by incorporating various metals (Zn, Cu, or Fe) to enhance their antimicrobial properties while maintaining biocompatibility with human cells. Biocompatibility assessments were carried out using osteoblasts. Results from osteoblast viability assays (Fig. 22) demonstrate that the unmodified CHA material did not induce cell death, confirming its biocompatibility in comparison to the untreated control (C+). Both Fe^{3+}- and Cu^{2+}-substituted CHA materials also showed no significant cell death, thus preserving their biocompatibility.

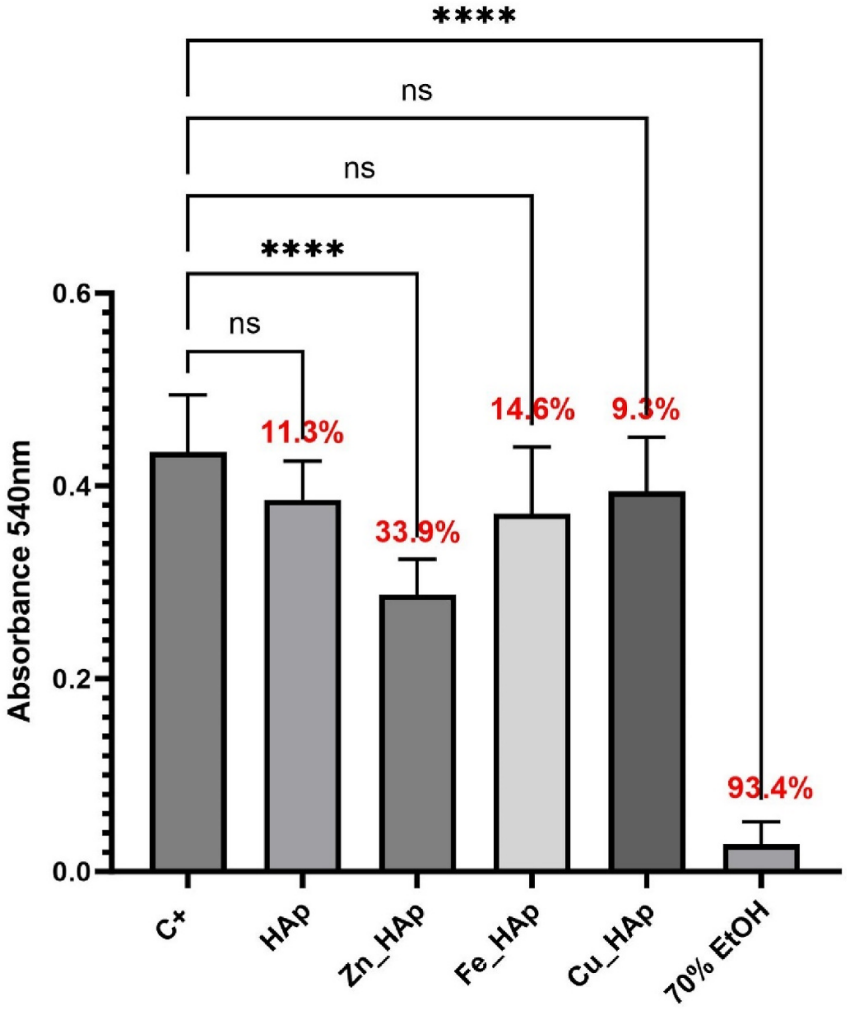

Fig. 22. The survivability/cytotoxicity of osteoblasts exposed to the provided powder samples. C+ – growth control, i.e. osteoblasts cultured in non-conditioned DMEM medium. Bars show level of cellular growth, while percentage values show cytotoxicity of the specific samples. Asterisks show statistical significance, while ns – lack of statistical significance.

In contrast, Zn-substituted CHA led to over 30 % cell death in osteoblasts, indicating potential cytotoxicity.

The analysis of the cream samples (Fig. 23) revealed a more pronounced effect on osteoblast viability.

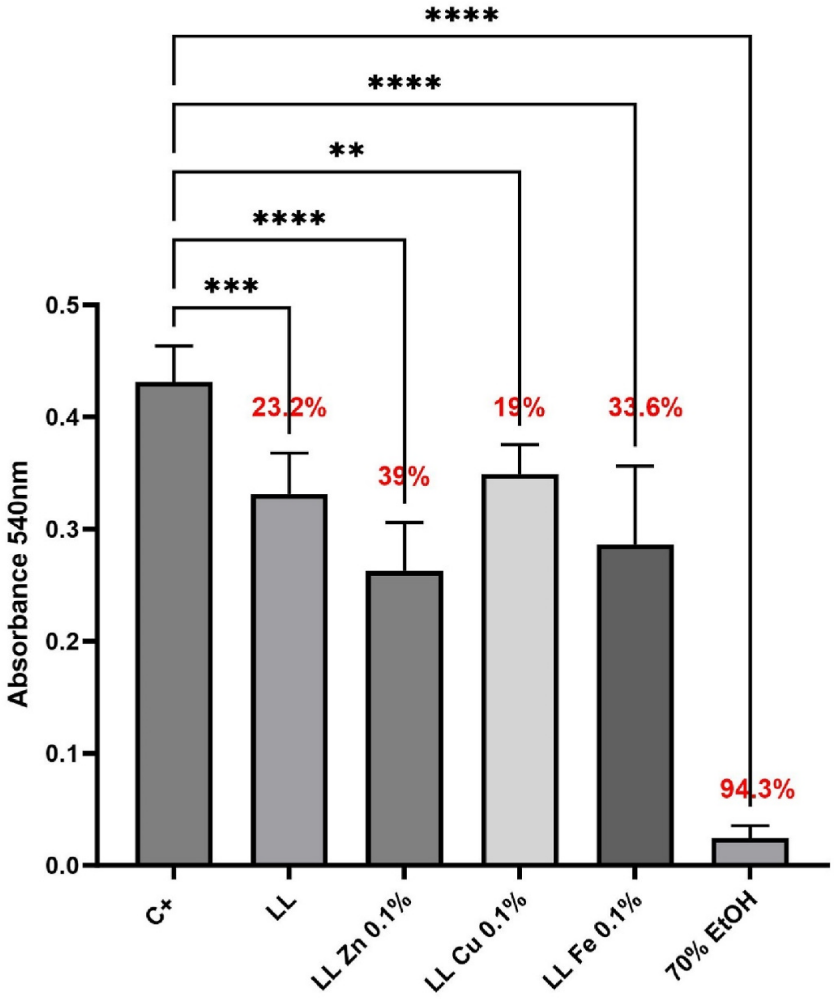

Fig. 23. The survivability/cytotoxicity of osteoblasts exposed to the provided cream samples. C+ – growth control, i.e., osteoblasts cultured in non-conditioned DMEM medium. Bars show level of cellular growth, while percentage values show cytotoxicity of the specific samples. Asterisks show statistical significance, while ns – lack of statistical significance.

The material without metal additives significantly reduced cell viability; however, toxicological standards generally consider reductions around or below 20 % to be insignificant. These findings suggest that creams containing Cu and Fe are as biocompatible as the sample without metals. In contrast, the Zn-containing cream, similar to Zn:CHA, showed potential cytotoxicity, raising concerns about its suitability for clinical or cosmetic applications.

3.4.2. Antimicrobial activity

The antimicrobial efficacy of the materials was evaluated against two bacterial strains — *Staphylococcus aureus* (Gram-positive) and *Pseudomonas aeruginosa* (Gram-negative) — as well as a yeast strain, *Candida albicans*, representing a broad spectrum of common pathogens. The flat, polystyrene surface of multi-well plate was likely less conducive to microbial growth compared to the porous hydroxyapatite surface, which may explain the more robust bacterial growth observed on the latter (see comparison of C+ and CHA in Figs. 24 and 25). Therefore, two comparisons were made to assess microbial growth reduction for each bacterial pathogen, with the control being either the polystyrene surface (C+) or hydroxyapatite.

The addition of Zn^{2+} and Cu^{2+} to CHA effectively reduced biofilm formation in Gram-positive bacteria and yeast but was less effective against Gram-negative bacteria. In contrast, metal-doped materials in creams were effective against both bacterial types, with Zn-containing samples also exhibiting antifungal properties (Figs. 24–26). These differential effects likely result from the unique cell wall structures and surface charges of the microorganisms, which influence their interactions with the metal-doped materials. A summary of the antimicrobial properties is presented in Table 2.

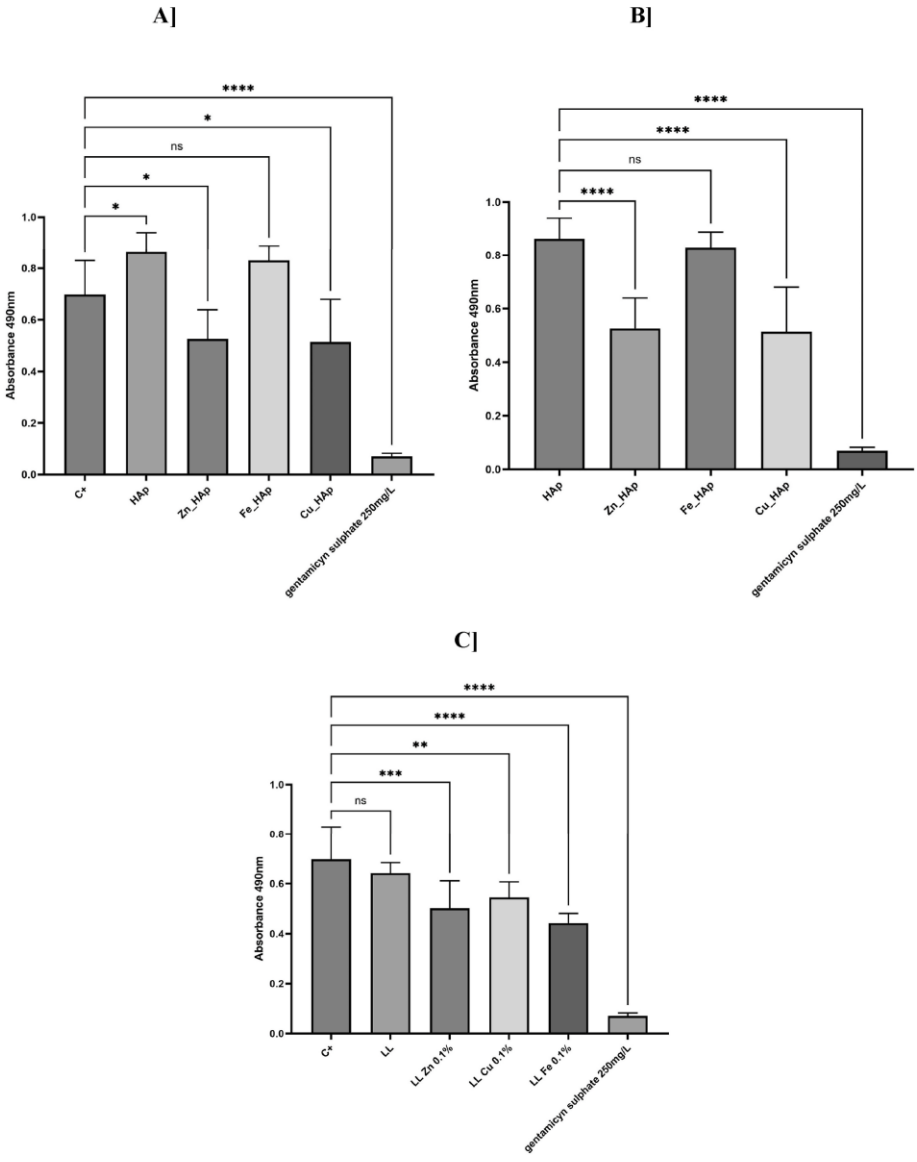

Fig. 24. Reduction of *S. aureus* growth resulting from exposure to the investigated samples: A) and B) powders; C) creams. For powders two charts were performed with different sets of positive controls (C+ or CHA). Asterisks show statistical significance, while ns – lack of statistical significance.

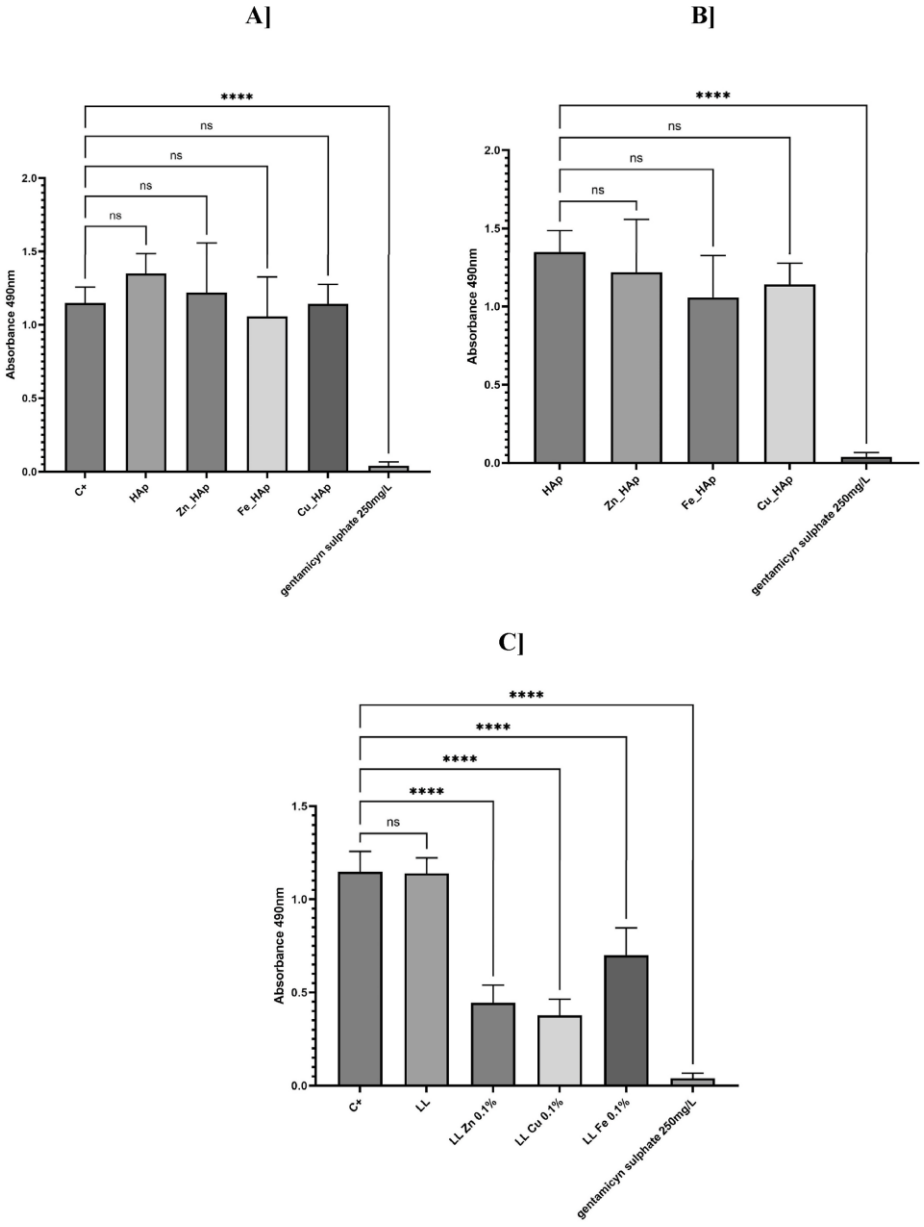

Fig. 25. Reduction of *P. aeruginosa* growth resulting from exposure to the investigated samples: A) and B) powders; C) creams. For powders two charts were performed with different sets of positive controls (C+ or CHA). Asterisks show statistical significance, while ns – lack of statistical significance.

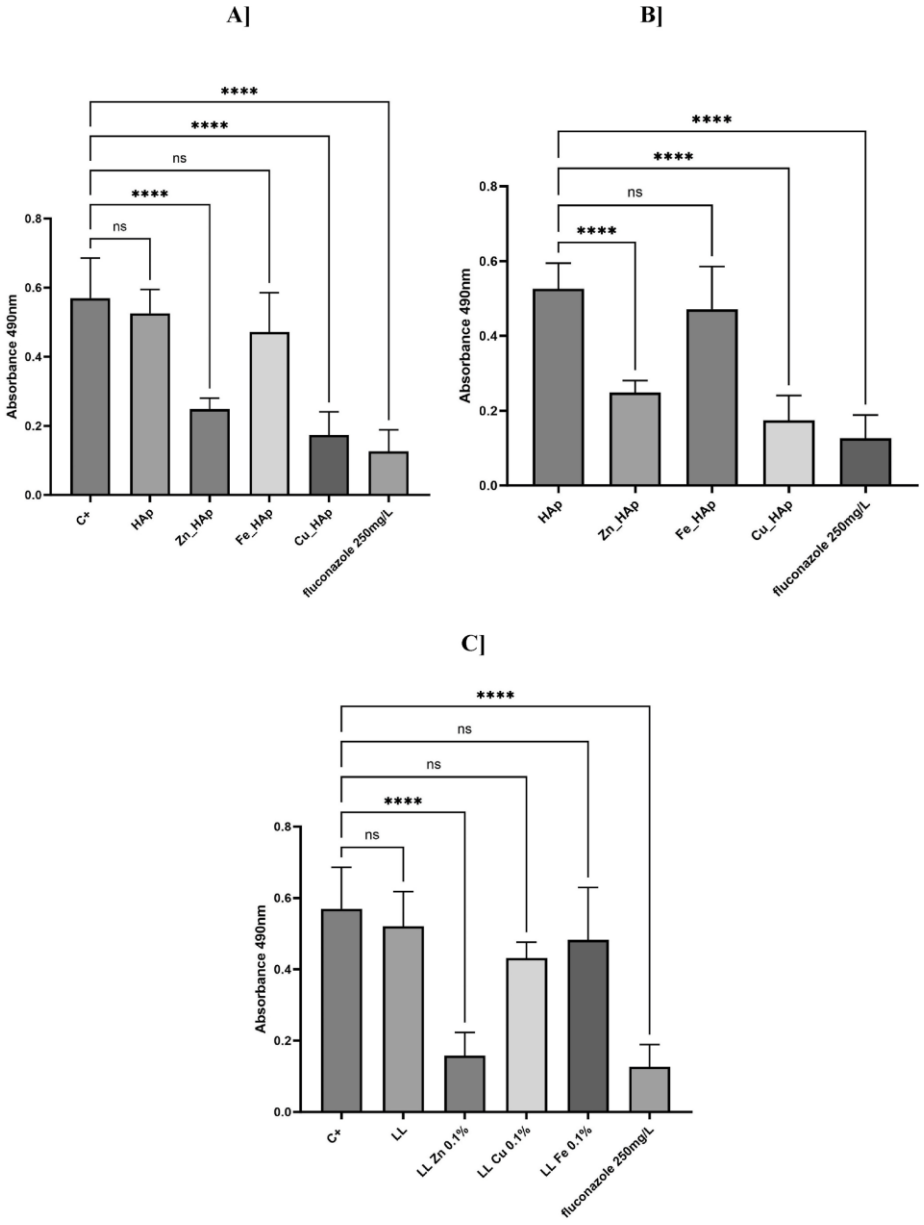

Fig. 26. Reduction of *C. albicans* growth resulting from exposure to the investigated samples: A) and B) powders; C) creams. For powders two charts were performed with different sets of controls (C+ or CHA). Asterisks show statistical significance, while ns – lack of statistical significance.

Table 2. Summarized antimicrobial properties of investigated powders and creams. "–" – lack of activity; "+" – weak activity against pathogen; "++" – stronger activity against pathogen.

Material	**Pathogen**		
	S. aureus	***P. aeruginosa***	***C. albicans***
CHA	–	–	–
Zn:CHA	+	–	++
Fe:CHA	–	–	–
Cu:CHA	+	–	++
LL	–	–	–
LL Zn	+	++	++
LL Cu	+	++	+
LL Fe	+	+	–

The incorporation of metal-doped hydroxyapatites into dermal creams has shown promising results, particularly in terms of biocompatibility and antimicrobial properties. The antimicrobial action of hydroxyapatite is primarily attributed to its high concentration of calcium ions, which induce calcium stress in bacterial cells, leading to cell death [159, 160]. This is a significant finding as it suggests a non-antibiotic approach to controlling microbial growth, which could be particularly valuable in settings where antibiotic resistance is a concern. Doping hydroxyapatite with essential metal ions such as copper, zinc, and iron enhances these antimicrobial effects. Copper, for example, exhibits potent antimicrobial properties, by disrupting bacterial cell membranes, leading to cell death. Similarly, zinc ions interfere with bacterial cell wall integrity and metabolic processes, increasing bacterial permeability and ultimately causing cell death. These metal ions play crucial roles in cellular structures such as cell membranes and DNA, and are actively involved in processes such as electron transfer and catalysis. However, excessive levels of these metals can be cytotoxic, potentially causing cellular damage or death [161]. The question of why the antimicrobial effect of Zn, Cu and Fe:CHA is enhanced when mixed with the creams is complex and difficult to answer definitively. Several factors may contribute to the increased antimicrobial effect when metal-doped materials are combined with creams. For example, improved contact between the materials could be achieved and could play a role [162]. Additionally, a synergistic effect with the cream components may also contribute to this behaviour [163]. Regarding biocompatibility, research indicates that zinc-substituted and copper-substituted hydroxyapatites are cytocompatible, likely due to the combined

effects of their microporous surface structure and the beneficial release of ions. Iron-substituted variants also support essential cellular functions for skin health, such as wound healing and protection against oxidative stress.

Centrifugation tests revealed that the manufactured cosmetic products remained stable under a centrifugal force of 3000 rpm for 5 minutes. The pH values of the freshly prepared products fell within the required range of pH 5-7, but slightly changed over time compared to the control. For products containing 5% of CHA, Fe:CHA, Cu:CHA, and Zn:CHA, the pH values increased negligibly, ranging from 7.08 to 7.12 after 4 months. Additionally, all samples maintained the same colour, smell, and texture. Future research should focus on optimizing the concentration and release mechanisms of the metal ions to balance antimicrobial activity with biocompatibility. Moreover, conducting a dose-response analysis, which is essential in toxicological assessments to determine the safety and efficacy thresholds, could significantly deepen the study's insights.

In conclusion, the addition of zinc enhances antimicrobial efficacy but reduces biocompatibility, while copper maintains both high antimicrobial activity and biocompatibility, making it more suitable for the development of medical or cosmetic materials. Dermal creams containing CHA with copper and iron ions also show significant antimicrobial activity while preserving good cell viability. These results highlight the importance of optimizing the balance between antimicrobial effectiveness and biocompatibility in these materials.

CONCLUSIONS

1. It was demonstrated that cationic substitutions emerged as a powerful tool for improving the chemical, physical, and biological properties of potential biomaterials. Calcium hydroxyapatite (CHA) specimens substituted with transition-metals, especially with silver, iron, copper, and zinc are most promising for applications in future clinical treatment to enhance different therapeutic multifunctional properties. These phosphate nanostructured biomaterials with high biocompatibility and increased antibacterial behaviour are the best candidates for applications in many biomedical fields, such as bone repair and tissue engineering, drug/gene delivery, magnetic targeting and hyperthermia treatment for cancer, bioimaging, and theranostics.
2. It was shown for the first time, that by applying divalent cations as controlling agents for the hydrothermal synthesis conditions (temperature, time) affected the phase purity and morphology of the final CHA products, but the nature and concentration of the foreign ions were the main factors determining the characteristics of the products. Smaller ions (Mg^{2+} and Mn^{2+}) were found to have a stronger inhibiting effect on the hydrolysis process of α-TCP as compared to larger ions (Sr^{2+} and Ba^{2+}). Of all the ions investigated, Mn^{2+} had the highest, and Sr^{2+} had the lowest inhibiting effect. Ba^{2+} had the most prominent effect on the sample morphology.
3. Hydrothermal treatment at 120 °C with 0.1 mol% of various cations resulted in the formation of CHA composed of plate-like crystals. When higher concentrations of metal ions are introduced into the reaction mixture, the formation of both plate-like and hexagonal rod-like particles occurred. In some cases, self-assembly of the rods into flower-like structures was observed. Under the hydrothermal treatment at 200 °C, the formation of the rod-like together with plate-like crystals occurs even when lowest investigated concentration (0.1 mol%) of metal ions is introduced to the reaction mixture. Increasing metal concentrations go hand in hand with an increased fraction of rod-like particles.
4. Crystalline calcium hydroxyapatite coatings with a very high homogeneity and degree of particle size distribution was successfully synthesised from $CaCO_3$ coatings by a dissolution-precipitation method at low temperature of 80 ºC in aqueous media. The low-temperature dissolution-precipitation method was successfully used for the synthesis of partially Cu^{2+} ion-substituted CHA. However, the formation of CHA coatings doped with Zn^{2+} ions by the above method did not proceed as

smoothly as expected. The different synthesis methods tested resulted in the formation of $Zn(OH)(NO_3)(H_2O)$, $Zn_3(OH)_4(NO_3)_2$ on the surface of the coating, leaving unreacted calcium carbonate.

5. Antibacterial property tests showed that no zones of inhibition were detected in pure CHA. In the Cu-HAP and Zn-doped coatings ($Zn_3(OH)_4(NO_3)_2$ coating), after incubation for 24 h at 37 °C, zones of inhibition were detected in the presence of a colony of *B. subtilis* bacteria. However, no zones of inhibition were detected in the presence of *Escherichia coli.*
6. Calcium hydroxyapatite and metal-substituted samples (Fe:CHA, Cu:CHA, and Zn:CHA) were synthesised using wet precipitation of amorphous CaP, followed by solid-state reaction synthesis of α-TCP, and finally hydrothermal synthesis of CHA. The effect of Fe^{3+}, Cu^{2+}, and Zn^{2+} substitution on the phase purity of CHA has been studied. Notably, it highlights the phase purity of CHA and Zn:CHA, while the α- and β-TCP phases have formed in the presence of Fe^{3+} and Cu^{2+} ions.
7. It was found, that metal-substituted CHA samples demonstrate promising antimicrobial potential for medical and materials science applications. These materials exhibit effective antimicrobial properties coupled with favorable biocompatibility profiles.
8. Notably, the addition of zinc enhances antimicrobial efficacy but diminishes biocompatibility, while copper maintains both high antimicrobial activity and biocompatibility, making it an ideal choice for developing medical or cosmetic materials. Dermal creams containing CHA with copper and iron ions also prove to be potent antimicrobial products with good cell viability. These findings highlight the importance of optimizing the balance between antimicrobial activity and biocompatibility in these materials.

REFERENCES

1. DileepKumar VG, Sridhar MS, Aramwit P, Krut'ko VK, Musskaya ON, Glazov IE, et al. A review on the synthesis and properties of hydroxyapatite for biomedical applications. J Biomater Sci Polym Ed. 2022;33(2):229-61.
2. Sadat-Shojai M, Atai M, Nodehi A, Khanlar LN. Hydroxyapatite nanorods as novel fillers for improving the properties of dental adhesives: Synthesis and application. Dental Materials. 2010;26(5):471-82.
3. Tuntun SM, Hossain MS, Uddin MN, Shaikh MAA, Bahadur NM, Ahmed S. Crystallographic characterization and application of copper doped hydroxyapatite as a biomaterial. New Journal of Chemistry. 2023;47(6):2874-85.
4. de Andrade R, Paim TC, Bertaco I, Naasani LS, Buchner S, Kovářík T, et al. Hierarchically porous bioceramics based on geopolymer-hydroxyapatite composite as a novel biomaterial: Structure, mechanical properties and biocompatibility evaluation. Applied Materials Today. 2023;33:101875.
5. Montesissa M, Sassoni E, Boi M, Borciani G, Boanini E, Graziani G. Synthetic or Natural (Bio-Based) Hydroxyapatite? A Systematic Comparison between Biomimetic Nanostructured Coatings Produced by Ionized Jet Deposition. Nanomaterials. 2024;14(16):1332.
6. Ishikawa K, Garskaite E, Kareiva A. Sol–gel synthesis of calcium phosphate-based biomaterials—A review of environmentally benign, simple, and effective synthesis routes. Journal of Sol-Gel Science and Technology. 2020;94:551-72.
7. Ahmed LO, Omer RA. Hydroxyapatite biomaterials: a comprehensive review of their properties, structures, clinical applications, and producing techniques. Reviews in Inorganic Chemistry. 2024.
8. Farazin A, Ghasemi AH. Design, synthesis, and fabrication of chitosan/hydroxyapatite composite scaffold for use as bone replacement tissue by sol–gel method. Journal of Inorganic and Organometallic Polymers and Materials. 2022;32(8):3067-82.
9. George SM, Nayak C, Singh I, Balani K. Multifunctional hydroxyapatite composites for orthopedic applications: a review. ACS biomaterials science & engineering. 2022;8(8):3162-86.
10. Liu Z, Yamada S, Otsuka Y, Galindo TGP, Tagaya M. Surface modification of hydroxyapatite nanoparticles for bone regeneration by controlling their surface hydration and protein adsorption states. Dalton Transactions. 2022;51(25):9572-83.

11. Chatterjee T, Ghosh M, Maji M, Ghosh M, Pradhan SK, Meikap AK. Study of microstructural and electrical properties of silver substituted hydroxyapatite for drug delivery applications. Materials Today Communications. 2022;31:103360.
12. Mondal S, Park S, Choi J, Vu TTH, Doan VHM, Vo TT, et al. Hydroxyapatite: a journey from biomaterials to advanced functional materials. Advances in colloid and interface science. 2023;321:103013.
13. Epple M. Review of potential health risks associated with nanoscopic calcium phosphate. Acta biomaterialia. 2018;77:1-14.
14. Carella F, Degli Esposti L, Adamiano A, Iafisco M. The use of calcium phosphates in cosmetics, state of the art and future perspectives. Materials. 2021;14(21):6398.
15. Chan LKW, Lee KWA, Lee CH. Pilot Study of Microfocused Ultrasound, Incobotulinum Toxin, and Calcium Hydroxyapatite in Triple Therapy for Skin Tightening after Weight Loss. Cosmetics. 2023;10(6):168.
16. Zago Sá Fortes R, Cassol Spanemberg J, Cherubini K, Salum FG. Adverse Events and Satisfaction Outcomes with Calcium Hydroxylapatite and Polycaprolactone Fillers in Facial Aesthetics: A Systematic Review. Cosmetics. 2024;11(5):165.
17. Zhu Y, Hao L, Luo Y, Gao J, Xu F, Li H, et al. A composite dressing combining ultralong hydroxyapatite nanowire bio-paper and a calcium alginate hydrogel accelerates wound healing. Journal of Materials Chemistry B. 2025;13(3):997-1012.
18. Grigoraviciute-Puroniene I, Stankeviciute Z, Ishikawa K, Kareiva A. Formation of calcium hydroxyapatite with high concentration of homogeneously distributed silver. Microporous and Mesoporous Materials. 2020;293:109806.
19. Ishikawa K, Kareiva A. Sol–gel synthesis of calcium phosphate-based coatings–A review. Chemija. 2020;31(1).
20. Tautkus S, Ishikawa K, Ramanauskas R, Kareiva A. Zinc and chromium co-doped calcium hydroxyapatite: Sol-gel synthesis, characterization, behaviour in simulated body fluid and phase transformations. Journal of Solid State Chemistry. 2020;284:121202.
21. Golubevas R, Stankeviciute Z, Zarkov A, Golubevas R, Hansson L, Raudonis R, et al. Acrylate–gelatin–carbonated hydroxyapatite (cHAP) composites for dental bone-tissue applications. Materials Advances. 2020;1(6):1675-84.
22. Sinusaite L, Kareiva A, Zarkov A. Thermally induced crystallization and phase evolution of amorphous calcium phosphate substituted with

divalent cations having different sizes. Crystal Growth & Design. 2021;21(2):1242-8.
23. Griesiute D, Raudonyte-Svirbutaviciene E, Kareiva A, Zarkov A. The influence of annealing conditions on the Ca/P ratio and phase transformations in bulk calcium phosphates. CrystEngComm. 2022;24(6):1166-70.
24. Klimavicius V, Maršalka A, Kizalaite A, Zarkov A, Kareiva A, Aidas K, et al. Step-by-step from amorphous phosphate to nano-structured calcium hydroxyapatite: monitoring by solid-state 1 H and 31 P NMR and spin dynamics. Physical Chemistry Chemical Physics. 2022;24(31):18952-65.
25. Karalkeviciene R.. Development of new methods for the synthesis of bulk and coatings of calcium hydroxyapatite. Vilnius University, Vilnius, Lithuania, 2023, 108 p.
26. Degli Esposti L, Carella F, Adamiano A, Tampieri A, Iafisco M. Calcium phosphate-based nanosystems for advanced targeted nanomedicine. Drug development and industrial pharmacy. 2018;44(8):1223-38.
27. Uskoković V. Ion-doped hydroxyapatite: An impasse or the road to follow? Ceramics International. 2020;46(8):11443-65.
28. Pu'ad NM, Haq RA, Noh HM, Abdullah H, Idris M, Lee T. Synthesis method of hydroxyapatite: A review. Materials Today: Proceedings. 2020;29:233-9.
29. Szcześ A, Hołysz L, Chibowski E. Synthesis of hydroxyapatite for biomedical applications. Advances in colloid and interface science. 2017;249:321-30.
30. Van Rijt S, De Groot K, Leeuwenburgh SC. Calcium phosphate and silicate-based nanoparticles: history and emerging trends. Tissue Engineering Part A. 2022;28(11-12):461-77.
31. Aguilera SB, McCarthy A, Khalifian S, Lorenc ZP, Goldie K, Chernoff WG. The Role of Calcium Hydroxylapatite (Radiesse) as a Regenerative Aesthetic Treatment: A Narrative Review. Aesthet Surg J. 2023;43(10):1063-90.
32. Lotfollahi Z. The anatomy, physiology and function of all skin layers and the impact of ageing on the skin. Wound Practice & Research: Journal of the Australian Wound Management Association. 2024;32(1):6-10.
33. Murphrey MB, Miao JH, Zito PM. Histology, Stratum Corneum. StatPearls. Treasure Island (FL) ineligible companies. Disclosure: Julia Miao declares no relevant financial relationships with ineligible

companies. Disclosure: Patrick Zito declares no relevant financial relationships with ineligible companies.2025.
34. Kabashima K, Honda T, Ginhoux F, Egawa G. The immunological anatomy of the skin. Nat Rev Immunol. 2019;19(1):19-30.
35. Collin M, Bigley V. Many Langerhans make light work of skin immunity. Immunity. 2021;54(10):2188-90.
36. Brown TM, Krishnamurthy K. Histology, Dermis. StatPearls. Treasure Island (FL) ineligible companies. Disclosure: Karthik Krishnamurthy declares no relevant financial relationships with ineligible companies.2025.
37. Hashmi S, Marinkovich MP. Molecular organization of the basement membrane zone. Clin Dermatol. 2011;29(4):398-411.
38. Rawlings AV, Harding CR. Moisturization and skin barrier function. Dermatol Ther. 2004;17 Suppl 1:43-8.
39. Green M, Kashetsky N, Feschuk A, Maibach HI. Transepidermal water loss (TEWL): Environment and pollution-A systematic review. Skin Health Dis. 2022;2(2):e104.
40. Lee HJ, Kim M. Skin Barrier Function and the Microbiome. Int J Mol Sci. 2022;23(21).
41. Dreno B, Araviiskaia E, Berardesca E, Gontijo G, Sanchez Viera M, Xiang LF, et al. Microbiome in healthy skin, update for dermatologists. J Eur Acad Dermatol Venereol. 2016;30(12):2038-47.
42. Elias PM. Stratum corneum acidification: how and why? Exp Dermatol. 2015;24(3):179-80.
43. Novackova A, Sagrafena I, Pullmannova P, Paraskevopoulos G, Dwivedi A, Mazumder A, et al. Acidic pH Is Required for the Multilamellar Assembly of Skin Barrier Lipids In Vitro. J Invest Dermatol. 2021;141(8):1915-21 e4.
44. Picardo M, Ottaviani M, Camera E, Mastrofrancesco A. Sebaceous gland lipids. Dermatoendocrinol. 2009;1(2):68-71.
45. Shamloul G, Khachemoune A. An updated review of the sebaceous gland and its role in health and diseases Part 1: Embryology, evolution, structure, and function of sebaceous glands. Dermatol Ther. 2021;34(1):e14695.
46. Baker LB. Physiology of sweat gland function: The roles of sweating and sweat composition in human health. Temperature (Austin). 2019;6(3):211-59.
47. Murota H, Matsui S, Ono E, Kijima A, Kikuta J, Ishii M, et al. Sweat, the driving force behind normal skin: an emerging perspective on

functional biology and regulatory mechanisms. J Dermatol Sci. 2015;77(1):3-10.
48. Alkilani AZ, McCrudden MT, Donnelly RF. Transdermal Drug Delivery: Innovative Pharmaceutical Developments Based on Disruption of the Barrier Properties of the stratum corneum. Pharmaceutics. 2015;7(4):438-70.
49. Ramadon D, McCrudden MTC, Courtenay AJ, Donnelly RF. Enhancement strategies for transdermal drug delivery systems: current trends and applications. Drug Deliv Transl Res. 2022;12(4):758-91.
50. Zoabi A, Touitou E, Margulis K. Recent advances in nanomaterials for dermal and transdermal applications. Colloids and Interfaces. 2021;5(1):18.
51. Knorr F, Lademann J, Patzelt A, Sterry W, Blume-Peytavi U, Vogt A. Follicular transport route--research progress and future perspectives. Eur J Pharm Biopharm. 2009;71(2):173-80.
52. Bos JD, Meinardi MM. The 500 Dalton rule for the skin penetration of chemical compounds and drugs. Exp Dermatol. 2000;9(3):165-9.
53. Shahzad Y., Louw R., Gerber M., du Plessis J. Breaching the Skin Barrier through Temperature Modulations. J. Control. Release. 2015;202:1–13.
54. Mueller J, Trapp M, Neubert RHH. The effect of hydrophilic penetration/diffusion enhancer on stratum corneum lipid models: Part II*: DMSO. Chem Phys Lipids. 2019;225:104816.
55. Pan S, Goudoulas TB, Jeevanandam J, Tan KX, Chowdhury S, Danquah MK. Therapeutic Applications of Metal and Metal-Oxide Nanoparticles: Dermato-Cosmetic Perspectives. Front Bioeng Biotechnol. 2021;9:724499.
56. Larese Filon F, Mauro M, Adami G, Bovenzi M, Crosera M. Nanoparticles skin absorption: New aspects for a safety profile evaluation. Regul Toxicol Pharmacol. 2015;72(2):310-22.
57. Coelho SG, Patri AK, Wokovich AM, McNeil SE, Howard PC, Miller SA. Repetitive Application of Sunscreen Containing Titanium Dioxide Nanoparticles on Human Skin. JAMA Dermatol. 2016;152(4):470-2.
58. Detoni CB, Coradini K, Back P, Oliveira CM, Andrade DF, Beck RC, et al. Penetration, photo-reactivity and photoprotective properties of nanosized ZnO. Photochem Photobiol Sci. 2014;13(9):1253-60.
59. Yoshioka Y, Kuroda E, Hirai T, Tsutsumi Y, Ishii KJ. Allergic Responses Induced by the Immunomodulatory Effects of Nanomaterials upon Skin Exposure. Front Immunol. 2017;8:169.

60. Jabbar-Lopez ZK, Ung CY, Alexander H, Gurung N, Chalmers J, Danby S, et al. The effect of water hardness on atopic eczema, skin barrier function: A systematic review, meta-analysis. Clin Exp Allergy. 2021;51(3):430-51.
61. Lee SE, Lee SH. Skin Barrier and Calcium. Ann Dermatol. 2018;30(3):265-75.
62. Goldberg DJ, Bass LM, Fitzgerald R, Graivier MH, Lorenc ZP. Expanding Treatment Options for Injectable Agents. Aesthet Surg J. 2018;38(suppl_1):S1-S7.
63. Cunha CS, Castro PJ, Sousa SC, Pullar RC, Tobaldi DM, Piccirillo C, et al. Films of chitosan and natural modified hydroxyapatite as effective UV-protecting, biocompatible and antibacterial wound dressings. Int J Biol Macromol. 2020;159:1177-85.
64. Cruel PTE, dos Santos CPC, Cueto TM, Avila LPV, Buchaim DV, Buchaim RL. Calcium Hydroxyapatite in Its Different Forms in Skin Tissue Repair: A Literature Review. Surgeries. 2024;5(3):640-59.
65. Harwood A, Nassereddin A, Krishnamurthy K. Moisturizers. StatPearls. Treasure Island (FL) ineligible companies. Disclosure: Ali Nassereddin declares no relevant financial relationships with ineligible companies. Disclosure: Karthik Krishnamurthy declares no relevant financial relationships with ineligible companies.2025.
66. Hon KL, Kung JSC, Ng WGG, Leung TF. Emollient treatment of atopic dermatitis: latest evidence and clinical considerations. Drugs Context. 2018;7:212530.
67. Giam YC, Hebert AA, Dizon MV, Van Bever H, Tiongco-Recto M, Kim KH, et al. A review on the role of moisturizers for atopic dermatitis. Asia Pac Allergy. 2016;6(2):120-8.
68. Draelos ZD. New treatments for restoring impaired epidermal barrier permeability: skin barrier repair creams. Clin Dermatol. 2012;30(3):345-8.
69. Blume-Peytavi U, Kanti V. Prevention and treatment of diaper dermatitis. Pediatr Dermatol. 2018;35 Suppl 1:s19-s23.
70. Magnano GC, Carton F, Boccafoschi F, Marussi G, Cocetta E, Crosera M, et al. Evaluating the role of protective creams on the cutaneous penetration of Ni nanoparticles. Environ Pollut. 2023;328:121654.
71. REGULATION (EC) No 1223/2009 OF THE EUROPEAN PARLIAMENT AND OF THE COUNCIL of 30 November 2009 on cosmetic products. OJ L 342 22.12.2009, p. 59.
72. Sörensen A, Landvall P, Lodén M. Moisturizers as cosmetics, medicines, or medical device? The regulatory demands in the European

Union. Treatment of Dry Skin Syndrome: The Art and Science of Moisturizers: Springer; 2012. p. 3-16.
73. Barnes TM, Mijaljica D, Townley JP, Spada F, Harrison IP. Vehicles for Drug Delivery and Cosmetic Moisturizers: Review and Comparison. Pharmaceutics. 2021;13(12).
74. Vanessa VV, Wan Ahmad Kammal WSL, Lai ZW, How KN. A review of moisturizing additives for atopic dermatitis. Cosmetics. 2022;9(4):75.
75. Mawazi SM, Ann J, Othman N, Khan J, Alolayan SO, Al thagfan SS, et al. A review of moisturizers; history, preparation, characterization and applications. Cosmetics. 2022;9(3):61.
76. Kusumawati II, G. Natural Antioxidants in Cosmetics. In Studies in Natural Products Chemistry; Elsevier: Amsterdam, The Netherlands, 2013; Volume 40, pp. 485–505. .
77. Michalak M. Plant-Derived Antioxidants: Significance in Skin Health and the Ageing Process. Int J Mol Sci. 2022;23(2).
78. Czarnowicki T, Malajian D, Khattri S, Correa da Rosa J, Dutt R, Finney R, et al. Petrolatum: Barrier repair and antimicrobial responses underlying this "inert" moisturizer. J Allergy Clin Immunol. 2016;137(4):1091-102 e7.
79. Haftek M, Abdayem R, Guyonnet-Debersac P. Skin Minerals: Key Roles of Inorganic Elements in Skin Physiological Functions. Int J Mol Sci. 2022;23(11).
80. Ma Y, Yoo J. History of sunscreen: An updated view. J Cosmet Dermatol. 2021;20(4):1044-9.
81. Ekstein SF, Hylwa S. Sunscreens: A Review of UV Filters and Their Allergic Potential. Dermatitis. 2023;34(3):176-90.
82. Iannacone MR, Hughes MC, Green AC. Effects of sunscreen on skin cancer and photoaging. Photodermatol Photoimmunol Photomed. 2014;30(2-3):55-61.
83. Marinho A, Nunes C, Reis S. Hyaluronic Acid: A Key Ingredient in the Therapy of Inflammation. Biomolecules. 2021;11(10).
84. Piquero-Casals J, Morgado-Carrasco D, Granger C, Trullas C, Jesus-Silva A, Krutmann J. Urea in Dermatology: A Review of its Emollient, Moisturizing, Keratolytic, Skin Barrier Enhancing and Antimicrobial Properties. Dermatol Ther (Heidelb). 2021;11(6):1905-15.
85. Berson DS, Osborne R, Oblong JE, Hakozaki T, Johnson MB, Bissett DL. Niacinamide. Cosmeceuticals and cosmetic practice. 2013:103-12.
86. Celli A, Tu CL, Lee E, Bikle DD, Mauro TM. Decreased Calcium-Sensing Receptor Expression Controls Calcium Signaling and Cell-To-

Cell Adhesion Defects in Aged Skin. J Invest Dermatol. 2021;141(11):2577-86.
87. Shahi A, Aslani S, Ataollahi M, Mahmoudi M. The role of magnesium in different inflammatory diseases. Inflammopharmacology. 2019;27(4):649-61.
88. Gupta M, Mahajan VK, Mehta KS, Chauhan PS. Zinc therapy in dermatology: a review. Dermatol Res Pract. 2014;2014:709152.
89. Borkow G. Using Copper to Improve the Well-Being of the Skin. Curr Chem Biol. 2014;8(2):89-102.
90. Simoes A, Veiga F, Vitorino C, Figueiras A. A Tutorial for Developing a Topical Cream Formulation Based on the Quality by Design Approach. J Pharm Sci. 2018;107(10):2653-62.
91. Lukić M, Pantelić I, Savić SD. Towards optimal ph of the skin and topical formulations: From the current state of the art to tailored products. Cosmetics. 2021;8(3):69.
92. Schlich M, Musazzi UM, Campani V, Biondi M, Franze S, Lai F, et al. Design and development of topical liposomal formulations in a regulatory perspective. Drug Deliv Transl Res. 2022;12(8):1811-28.
93. Nastiti C, Ponto T, Abd E, Grice JE, Benson HAE, Roberts MS. Topical Nano and Microemulsions for Skin Delivery. Pharmaceutics. 2017;9(4).
94. Ait-Touchente Z, Zine N, Jaffrezic-Renault N, Errachid A, Lebaz N, Fessi H, et al. Exploring the Versatility of Microemulsions in Cutaneous Drug Delivery: Opportunities and Challenges. Nanomaterials (Basel). 2023;13(10).
95. Duarte I, Silveira J, Hafner MFS, Toyota R, Pedroso DMM. Sensitive skin: review of an ascending concept. An Bras Dermatol. 2017;92(4):521-5.
96. Murphy B, Grimshaw S, Hoptroff M, Paterson S, Arnold D, Cawley A, et al. Alteration of barrier properties, stratum corneum ceramides and microbiome composition in response to lotion application on cosmetic dry skin. Sci Rep. 2022;12(1):5223.
97. Tempark T, Shem A, Lueangarun S. Efficacy of ceramides and niacinamide-containing moisturizer versus hydrophilic cream in combination with topical anti-acne treatment in mild to moderate acne vulgaris: A split face, double-blinded, randomized controlled trial. J Cosmet Dermatol. 2024;23(5):1758-65.
98. Purnamawati S, Indrastuti N, Danarti R, Saefudin T. The Role of Moisturizers in Addressing Various Kinds of Dermatitis: A Review. Clin Med Res. 2017;15(3-4):75-87.

99. Mostosi C, Simonart T. Effectiveness of Barrier Creams against Irritant Contact Dermatitis. Dermatology. 2016;232(3):353-62.
100. Mitura S, Sionkowska A, Jaiswal A. Biopolymers for hydrogels in cosmetics: review. J Mater Sci Mater Med. 2020;31(6):50.
101. Alexander H, Brown S, Danby S, Flohr C. Research Techniques Made Simple: Transepidermal Water Loss Measurement as a Research Tool. J Invest Dermatol. 2018;138(11):2295-300 e1.
102. Ali SM, Yosipovitch G. Skin pH: from basic science to basic skin care. Acta Derm Venereol. 2013;93(3):261-7.
103. Wiegand C, Abel M, Ruth P, Elsner P, Hipler UC. In vitro assessment of the antimicrobial activity of wound dressings: influence of the test method selected and impact of the pH. J Mater Sci Mater Med. 2015;26(1):5343.
104. Kuppers V, Kemper M, Abels C. Clinical evaluation of a water-in-oil emulsion with protective and regenerative properties for the anogenital area. Clin Cosmet Investig Dermatol. 2015;8:555-62.
105. Soltanipoor M, Kezic S, Sluiter JK, de Wit F, Bosma AL, van Asperen R, et al. Effectiveness of a skin care programme for the prevention of contact dermatitis in healthcare workers (the Healthy Hands Project): A single-centre, cluster randomized controlled trial. Contact Dermatitis. 2019;80(6):365-73.
106. Commission Regulation (EU) No 655/2013 of 10 July 2013 laying down common criteria for the justification of claims used in relation to cosmetic products. Text with EEA relevance OJ L 190, 11.7.2013, p. 31–34.
107. Dorozhkin SV. Calcium orthophosphates (CaPO(4)): occurrence and properties. Prog Biomater. 2016;5:9-70.
108. Kim Y, Kim D, Lee S, Woo DK, Byun J-H, Kwon K-Y. Synthesis and morphological characterization of calcium phosphates prepared under different naoh concentrations. Bulletin of the Korean Chemical Society. 2014;35(8):2241-2.
109. Mohammad NF, Othman R, Yeoh FY. Controlling the pore characteristics of mesoporous apatite materials: Hydroxyapatite and carbonate apatite. Ceramics International. 2015;41(9):10624-33.
110. van Rijt S, de Groot K, Leeuwenburgh SCG. Calcium Phosphate and Silicate-Based Nanoparticles: History and Emerging Trends. Tissue Eng Part A. 2022;28(11-12):461-77.
111. Clark J. Solubility criteria for the existence of hydroxyapatite. Canadian Journal of Chemistry. 1955;33(11):1696-700.

112. Wang L, Nancollas GH. Calcium orthophosphates: crystallization and dissolution. Chem Rev. 2008;108(11):4628-69.
113. Pompeu LD, Pinton AP, Finger MG, Cadó RG, de Avila Severo V, Pinheiro L, et al. Evaluation of stability of aqueous dispersions using zeta potential data. Disciplinarum Scientia| Naturais e Tecnológicas. 2018;19(3):381-8.
114. Xuchang University. Stable O/W-type Pickering Emulsion by Using Hydroxyapatite Nano Particles and Preparation Method Thereof. CN107595647A. 2018. https://patents.google.com/patent/CN107595647A/en.
115. Jieyao, L.; Wenhan, L.; Yufei, W.; Naiyu, X.; Xueqin, Z.; Le, Z.; Wei, Z.; Yanqing, Z. Compound Composed of Aliphatic Polycarbonate and Inorganic Compound and Application of Compound in Related Fields of Cosmetics. CN111904892A. 2020. https://patents.google.com/patent/CN111904892A/en?oq=CN111904892A.
116. Roveri, N.; Lelli, M.; Masetti, M.; Petraroia, S.; Begotti, S. Compositions Comprising Polyesters of Biological Origin and Biocompatible Inorganic Compounds, and Uses Thereof in the Cosmetics Field. US2019159997A1. 2019. https://patents.google.com/patent/US20190159997A1/en?oq=US20191 59997A1.
117. Kawai K, Larson BJ, Ishise H, Carre AL, Nishimoto S, Longaker M, et al. Calcium-based nanoparticles accelerate skin wound healing. PLoS One. 2011;6(11):e27106.
118. Wu VM, Tang S, Uskokovic V. Calcium Phosphate Nanoparticles as Intrinsic Inorganic Antimicrobials: The Antibacterial Effect. ACS Appl Mater Interfaces. 2018;10(40):34013-28.
119. Abbasi M, Rashnavadi M, Gholami M, Molaei S. Antibacterial property of hydroxyapatite extracted from biological sources and doped with Cu(2+) and Ag(+) by Sol-gels method. Sci Rep. 2025;15(1):12101.
120. Yang F, Xue Y, Wang F, Guo D, He Y, Zhao X, et al. Sustained release of magnesium and zinc ions synergistically accelerates wound healing. Bioact Mater. 2023;26:88-101.
121. Zhang M, Wang AJ, Li JM, Song N, Song Y, He R. Factors influencing the stability and type of hydroxyapatite stabilized Pickering emulsion. Mater Sci Eng C Mater Biol Appl. 2017;70(Pt 1):396-404.
122. Bernauer U, Bodin L, Chaudhry Q, Coenraads P, Dusinska M, Gaffet E, et al. SCCS opinion on Hydroxyapatite (nano)-SCCS 1648/22–Final Opinion: European commission; 2023.
123. Commission Regulation (EU) 2016/621 of 21 April 2016 amending Annex VI to Regulation (EC) No 1223/2009 of the European Parliament

and of the Council on cosmetic products (Text with EEA relevance). C/2016/2222. OJ L 106, 22.4.2016, p. 4–6. ELI: http://data.europa.eu/eli/reg/2016/621/oj.
124. Cassin G. The cosmetic use of hydroxyapatite particles to smooth out wrinkles, bags and rings around the eyes. FR2856593A1. 2003. https://patents.google.com/patent/FR2856593A1/en.
125. Mansouri Z. Topical compositions for the skin comprising ceramic hydroxyapatite as a micro carrier. NZ311461A. 1995. https://patents.google.com/patent/NZ311461A/en.
126. Sliem MA, Karas RA, Harith MA. A promising protected ascorbic acid-hydroxyapatite nanocomposite as a skin anti-ager: A detailed photo-and thermal stability study. J Photochem Photobiol B. 2017;173:661-71.
127. A. Mahanty, D. Shikha, Calcium substituted with magnesium, silver and zinc in hydroxyapatite: a review. Int. J. Mater. Res. 112 (2021) 922-930.
128. O.M. Gomez-Vazquez, B.A. Correa-Pina, L.F. Zubieta-Otero, A.M. Castillo-Paz, S.M. Londono-Restrepo, M.E. Rodriguez-Garcia, Synthesis and characterization of bioinspired nano-hydroxyapatite by wet chemical precipitation. Ceram. Int. 47 (2021) 32775-32785.
129. K. Saito, S. Kagawa, M. Ogasawara, S. Kato, Multiple incorporation of copper and iron ions into the channel of hydroxyapatite. J. Solid State Chem. 317 (2023) 123673.
130. L. Sheikh, S. Sinha, Y.N. Singhababu, V. Verma, S. Tripathy, S. Nayar, Traversing the profile of biomimetically nanoengineered iron substituted hydroxyapatite: synthesis, characterization, property evaluation, and drug release modeling. RSC Adv. 8 (2018) 19389–19401.
131. S. Balakrishnan, V.P. Padmanabhan, R. Kulandaivelu, T.S.S.N. Nellaiappan, S. Sagadevan, S. Paiman, F. Mohammad, H.A. Al-Lohedan, P.K. Obulapuram, W.C. Oh, Influence of iron doping towards the physicochemical and biological characteristics of hydroxyapatite. Ceram. Int. 47 (2021) 5061-5070.
132. M. Kalidoss, R.Y. Basha, M. Doble, T.S.S. Kumar, Theranostic calcium phosphate nanoparticles with potential for multimodal imaging and drug delivery. Front. Bioeng. Biotechnol. 7 (2019) Art. No. 126.
133. M.A.C. Teixeira, C. Piccirillo, D.M. Tobaldi, R.C. Pullar, J.A. Labrincha, M.O. Ferreira, P.M.L. Castro, M.M.E. Pintado, Effect of preparation and processing conditions on UV absorbing properties of hydroxyapatite-Fe_2O_3 sunscreen. Mater. Sci. Eng. C–Mater. Biolog. Appl. 71 (2017) 141-149.

134. M.L. Dittler, P.M. Zelis, A.M. Beltran, R. Destch, C.A. Grillo, M.C. Gonzalez, A.R. Boccaccini, Magnetic 3D scaffolds for tissue engineering applications: bioactive glass (45S5) coated with iron-loaded hydroxyapatite nanoparticles. Biomed. Mater. 16 (2021) 055006.
135. S. Gomes, C. Vichery, S. Descamps, H. Martinez, A. Kaur, A. Jacobs, J.M. Nedelec, G. Renaudin, Cu-doping of calcium phosphate bioceramics: From mechanism to the control of cytotoxicity. Acta Biomater. 65 (2018) 462-474.
136. W.L. Yu, T.W. Sun, Z.Y. Ding, C. Qi, H.K. Zhao, F. Chen, Z.M. Shi, Y.J. Zhu, D.Y. Chen, Y.H. He, Copper-doped mesoporous hydroxyapatite microspheres synthesized by a microwave-hydrothermal method using creatine phosphate as an organic phosphorus source: application in drug delivery and enhanced bone regeneration. J. Mater. Chem. B 5 (2017) 1039-1052.
137. B.M. Hidalgo-Robatto, M. Lopez-Alvarez, A.S. Azevedo, J. Dorado, J. Serra, N.F. Azevedo, P. Gonzalez, Pulsed laser deposition of copper and zinc doped hydroxyapatite coatings for biomedical applications. Surf. Coat. Technol. 333 (2018) 168-177.
138. R.B. Unabia, R.T. Candidato, L. Pawlowski, R. Salvatori, D. Bellucci, V. Cannillo, In vitro studies of solution precursor plasma-sprayed copper-doped hydroxyapatite coatings with increasing copper content. J. Biomed. Mater. Res. B-Appl. Biomater. 108 (2020) 2579-2589.
139. M.S. Fernandes, E.C. Kukulka, J.R. de Souza, A.L.S. Borges, T.M.B. Campos, G.P. Thim, L.M.R. de Vasconcellos, Development and characterization of PCL membranes incorporated with Zn-doped bioactive glass produced by electrospinning for osteogenesis evaluation. J. Polym. Res. 29 (2022) 370.
140. P.V. Gnaneshwar, S.V. Sudakaran, S. Abisegapriyan, J. Sherine, S. Ramakrishna, M.H. Ab Rahim, M.M. Yusoff, R. Jose, J.R. Venugopal, Ramification of zinc oxide doped hydroxyapatite biocomposites for the mineralization of osteoblasts. Mater. Sci. Eng. C-Mater. Biolog. Appl. 96 (2019) 337–346.
141. A. Mahajan, S.S. Sidhu, Surface modification of metallic biomaterials for enhanced functionality: a review. Mater. Technol. 33 (2018) 93–105.
142. Y.C. Su, I. Cockerill, Y.D. Wang, Y.X. Qin, L.Q. Chang, Y.F. Zheng, D.H. Zhu, Zinc-based biomaterials for regeneration and therapy. Trends Biotechnol. 37 (2019) 428–441.

143. N.C. Reger, A.K. Bhargava, I. Ratha, B. Kundu, V.K. Balla, Structural and phase analysis of multi-ion doped hydroxyapatite for biomedical applications. Ceram. Int. 45 (2019) 252–263.
144. Y. Yedekci, E. Gedik, Z. Evis, L. Dogan, G. Ozyigit, M. Gurkaynak, Radiosensitization induced by zinc-doped hydroxyapatite nanoparticles in breast cancer cells. Int. J. Appl. Ceram. Technol. 18 (2021) 563-572.
145. H. Maleki-Ghaleh, M.H. Siadati, Y. Omidi, M. Kavanlouei, J. Barar, A. Akbari-Fakhrabadi, K. Adibkia, Y. Beygi-Khosrowshahi, Synchrotron SAXS/WAXS and TEM studies of zinc doped natural hydroxyapatite nanoparticles and their evaluation on osteogenic differentiation of human mesenchymal stem cells. Mater. Chem. Phys. 276 (2022) 125346.
146. M.A. Badea, M. Balas, M. Popa, T. Borcan, A.C. Bunea, D. Predoi, A. Dinischiotu, Biological Response of Human Gingival Fibroblasts to Zinc-Doped Hydroxyapatite Designed for Dental Applications-An In Vitro Study. Materials 16 (2023) 4145.
147. S. Buyuksungur, P.Y. Huri, J. Schmidt, I. Pana, M. Dinu, C. Vitelaru, A.E. Kiss, D.G. Tamay, V. Hasirci, A. Vladescu, N. Hasirci, In vitro cytotoxicity, corrosion and antibacterial efficiencies of Zn doped hydroxyapatite coated Ti based implant materials. Ceram. Int. 49 (2023) 12570-12584.
148. R.D. Shannon, Revised effective ionic radii and systematic studies of interatomic distances in halides and chalcogenides, Acta Crystallogr. A 32(5) (1976) 751-767.
149. E. Garskaite, L. Alinauskas, M. Drienovsky, J. Krajcovic, R. Cicka, M. Palcut, L. Jonusauskas, M. Malinauskas, Z. Stankeviciute, A. Kareiva, Fabrication of composite of nanocrystalline carbonated hydroxyapatite (cHAP) with polylactic acid (PLA) and its surface topographical structuring with direct laser writing (DLW). RSC Adv. 6 (2016) 72733-72743.
150. Z. Geng, Z. Cui, Z. Li, S. Zhu, Y. Liang, W.W. Lu, X. Yang, Synthesis, characterization and the formation mechanism of magnesium- and strontium-substituted hydroxyapatite, J. Mater. Chem. B 3 (2015) 3738–3746.
151. M. Supova, Substituted hydroxyapatites for biomedical applications: a review, Ceram. Int. 41 (2015) 9203–9231.
152. 152. Yanyan S, Guangxin W, Wuhui L, Yaming W, Hayakawa S, Osaka A. Conversion of sub-μm calcium carbonate (calcite) particles to hollow hydroxyapatite agglomerates in K2HPO4 solutions. Nanotechnol. Rev. 9 (2020) 945-960.

153. Unabia, R.B.; Bonebeau, S.; Candidato Jr, R.T.; Jouin, J.; Noguera, O.; Pawłowski, L. Investigation on the structural and microstructural properties of copper-doped hydroxyapatite coatings deposited using solution precursor plasma spraying. J. Eur. Ceram. Soc. 39 (2019) 4255–4263.
154. Bari A, Bloise N, Fiorilli S, Novajra G, Vallet-Regi M, Bruni G. Copper-containing mesoporous bioactive glass nanoparticles as multifunctional agent for bone regeneration. Acta Biomater. 55 (2017) 493-504.
155. Kalaivani S, Singh RK, Ganesan V, Kannan S. Effect of copper (Cu(2+)) inclusion on the bioactivity and antibacterial behavior of calcium silicate coatings on titanium metal. J. Mater. Chem. B. 2 (2014) 846-858.
156. Arcos D, Vallet-Regi M. Substituted hydroxyapatite coatings of bone implants. J. Mater. Chem. B. 8 (2020) 1781-1800.
157. Jacobs A, Renaudin G, Forestier C, Nedelec JM, Descamps S. Biological properties of copper-doped biomaterials for orthopedic applications: A review of antibacterial, angiogenic and osteogenic aspects. Acta Biomater. 117 (2020) 21-39.
158. Wolf-Brandstetter C, Beutner R, Hess R, Bierbaum S, Wagner K, Scharnweber D. Multifunctional calcium phosphate based coatings on titanium implants with integrated trace elements. Biomed Mater. 15 (2020) 025006.
159. D. Predoi, S.L. Iconaru, M.V. Predoi, G.E. Stan, N. Buton, Synthesis, Characterization, and Antimicrobial Activity of Magnesium-Doped Hydroxyapatite Suspensions. Nanomater. (Basel) 9 (2019) 1295.
160. S.E. Al-Mofty, A.H. Karaly, W.A. Sarhan, H.M.E. Azzazy, Multifunctional Hemostatic PVA/Chitosan Sponges Loaded with Hydroxyapatite and Ciprofloxacin, ACS Omega. 7 (2022) 13210-13220.
161. M. Godoy-Gallardo, U. Eckhard, L.M. Delgado, Y.J.D. de Roo Puente, M. Hoyos-Nogués, F.J. Gil, R.A. Perez. Antibacterial approaches in tissue engineering using metal ions and nanoparticles: From mechanisms to applications, Bioact. Mater. 6 (2021) 4470-4490.
162. C.R. Contessa, G.S. da Rosa, C.C. Moraes, New Active Packaging Based on Biopolymeric Mixture Added with Bacteriocin as Active Compound. Int. J. Molec. Sci. 22 (2021) 10628.
163. S.S. Hashemi, A. Pakdin, A. Mohammadi, A. Keshavarzi, M. Mortazavi, P. Sanati, Study the Effect of Calendula officinalis Extract Loaded on Zinc Oxide Nanoparticle Cream in Burn Wound Healing. ACS Appl. Mater. Interf. 15 (2023) 59269-59279.

SUMMARY (IN LITHUANIAN)

SANTRAUKA

ĮVADAS

Kalcio hidroksiapatitas (Ca_{10} $(PO_4)_6$ $(OH)_2$; CHA) yra plačiai pripažinta biomedžiaga. Įvairų CHA naudojimą biomedicinos srityje lemia jo cheminis panašumas į žmogaus kietuosius audinius: CHA yra pagrindinis dantų ir kaulų mineralinis komponentas, lemiantis jų tvirtumą ir kietumą. Sintetinis CHA pasižymi puikiu osteolaidumu, biologiniu suderinamumu, cheminiu stabilumu ir netoksiškumu. Dėl šių privalumų ir universalių savybių CHA gali būti naudojamas įvairioms medicininėms reikmėms, įskaitant kaulų atstatymą ir regeneraciją, ortopedinius kaulų užpildus, baltymų adsorbciją ir vaistų pernešimą.

Susidomėjimas kalcio fosfatų (CaP) naudojimu kosmetikoje didėja ir ypač matomas pastaraisiais dešimtmečiais. Iš tiesų, minėtos CHA savybės, dėl kurių jie tapo universaliomis medžiagomis medicinoje, gali būti naudingos ir kosmetikos srityje. Visų pirma CHA dėl biologinio saugumo gali pakeisti kosmetikos ingredientus, kurie kelią susirūpinimą sveikatai, saugesnėmis alternatyvomis. CHA savybės leidžia kurti medžiagas, galinčias atlikti įvairias kosmetikos priemonių funkcijas. Mokslinėje literatūroje pateikiami pagrindiniai CHA, kaip kosmetikos sudedamosios dalies, taikymo būdai: burnos priežiūros, odos priežiūros, plaukų priežiūros ir dezodorantų gamybos srityje. Viename atliktame tyrime buvo nustatyta, kad CHA kompozitinis tvarstis yra perspektyvi priemonė ūminėms žaizdoms gydyti ir odos apsaugai.

Sintetinių biomedžiagų, įskaitant CHA, kokybė labai priklauso nuo bendrų susintetintų miltelių savybių ir ypatybių. Tokios savybės yra tankis, grynumas, fazinė sudėtis, kristališkumas, dalelių dydis, dalelių pasiskirstymas pagal dydį, dalelių morfologija ir savitasis paviršiaus plotas. Taigi, visos minėtos biokeramikos savybės yra labai jautrios sintezės sąlygoms ir labai priklauso nuo gautų miltelių kristališkumo, kristalų formos, kristalų dydžio, kristalų dydžio pasiskirstymo ir fazės grynumo.

Šios disertacijos **tikslas** – apžvelgti katijoninio pakeitimo kalcio hidroksiapatite poveikį jo biosavybėms, susintetinti katijonais pakeistas kalcio hidroksiapatito dangas ir birius mėginius bei įvertinti gautų mėginių antibakterines savybes ir galimą jų taikymą kosmetikoje. Šiam tikslui pasiekti buvo suformuluoti pagrindiniai uždaviniai:

1. Apžvelgti katijoninio pakeitimo kalcio hidroksiapatite poveikį jo biologinėms savybėms.

2. Ištirti katijoninio pakeitimo poveikį $Ca_{10}(PO_4)_6(OH)_2$ morfologinėms savybėms.
3. Sukurti antibakterinių kalcio hidroksiapatito dangų sintezės metodą žemoje temperatūroje.
4. Ištirti katijonais pakeistų CHA ir jų turinčių odos kremų antibakterines savybes.

Daktaro disertacijos naujumas ir originalumas

Pirmą kartą įrodyta, kad skirtingas katijoninis pakeitimas (esant mažesniems ir didesniems jonams) daro reikšmingą įtaką kalcio hidroksiapatito morfologinėms savybėms. Iš $CaCO_3$ dangų buvo sėkmingai susintetintos kristalinės kalcio hidroksiapatito dangos tirpinimo-nusodinimo metodu žemoje 80 ^oC temperatūroje vandeninėje terpėje. Šis metodas buvo naudojamas iš dalies Cu^{2+} ir Zn^{2+} jonais pakeistų kalcio hidroksiapatito dangų sintezei. Atlikus mikrobiologinius tyrimus po 24 val. inkubacijos 37 ^oC temperatūroje inhibicijos zonos, nustatytos su šiomis dangomis esant *B. subtilis* bakterijų kolonijai. Nustatyta, kad metalu pakeisti CHA birūs mėginiai pasižymėjo veiksmingomis antimikrobinėmis savybėmis. Cinku pakeisti CHA mėginiai turėjo didesnį antimikrobinį veiksmingumą, bet sumažėjo biologinis suderinamumas, o variu pakeisti mėginiai išlaikė ir didelį antimikrobinį aktyvumą, ir biologinį suderinamumą, kas reikštų idealų pasirinkimą kuriant kosmetikos priemones. Kremai, kurių sudėtyje buvo CHA su vario ir geležies jonais, taip pat pasižymėjo ryškiomis antimikrobinėmis savybėmis ir geru ląstelių gyvybingumu.

Ginamieji disertacijos teigniai:

- Pakeitimas skirtingais katijonais turi reikšmingą poveikį kalcio hidroksiapatito morfologinėms savybėms.
- Tirpinimo-nusodinimo metodas žemoje 80 ^oC temperatūroje vandeninėje terpėje gali būti naudojamas iš dalies Cu^{2+} ir Zn^{2+} jonais pakeistų kalcio hidroksiapatito antibakterinių dangų sintezei.
- Metalais pakeisto kalcio hidroksiapatito bandiniai turi perspektyvų antimikrobinį potencialą medicinoje ir medžiagų moksle.
- Antimikrobinių produktų, pasižyminčių geru ląstelių gyvybingumu, atradimas rodo, kaip svarbu optimizuoti metalais pakeistų kalcio hidroksiapatitų antimikrobinio aktyvumo ir biologinio suderinamumo pusiausvyrą.

1. EKSPERIMENTO METODIKA

1.1. SINTEZĖS METODIKOS

1.1.1. Kalcio hidroksiapatito sintezė

Kalcio nitratas tetrahidratas ($Ca(NO_3)_2 \cdot 4H_2O$, ≥99 %, Roth) ir diamonio vandenilio fosfatas ($(NH_4)_2HPO_4$, ≥98 %, Roth) buvo naudojami kaip pirmtakai ACP sintezei. Geležies nitratas nonahidratas ($Fe(NO_3)_3 \cdot 9H_2O$, ≥98 %, Roth), vario nitratas trihidratas ($Cu(NO_3)_2 \cdot 3H_2O$, ≥99,5 %, Roth) ir cinko nitratas heksahidratas ($Zn(NO_3)_2 \cdot 6H_2O$, ≥99,5 %, Roth) buvo naudojami atitinkamai Fe-, Cu- ir Zn pakeistiems kalcio hidroksiapatito mėginiams sintetinti. Magnio nitratas heksahidratas ($Mg(NO_3)_2 \cdot 6H_2O$, ≥98 %, Roth), mangano nitratas tetrahidratas ($Mn(NO_3)_2 \cdot 4H_2O$, ≥98 %, Roth), stroncio nitratas ($Sr(NO_3)_2$, ≥98 %, Roth) ir bario nitratas ($Ba(NO_3)_2$, ≥99 %, Roth) buvo naudojami atitinkamai Mg-, Mn-, Sr- ir Ba pakeistų kalcio hidroksiapatito mėginių sintezei. ACP sintezei naudotas nusodinimo sintezės metodas, išlaikant Ca ir P santykį 1,5:1. Pirmiausia buvo paruoštas 1 M Ca^{2+} nitrato tirpalas, ištirpinant metalo druską dejonizuotame vandenyje. 0,5 M $(NH_4)_2HPO_4$ tirpalo pH buvo šarmintas iki 10, pridedant koncentruoto amoniako tirpalo (NH_4OH, 25 %), nuolat maišant. Maišant $Ca(NO_3)_2$ ir $(NH_4)_2HPO_4$ 10 min., gautos nuosėdos, kurios buvo nuplautos dejonizuotu vandeniu ir izopropanoliu ir džiovintos 50 °C temperatūroje per naktį. Galiausiai gautas ACP buvo sutrintas agatinėje grūstuvėje ir 5 val. kaitintas 700 °C temperatūroje (oro atmosferoje, kaitinimo greitis 5 °C/min.), siekiant paskatinti trikalcio fosfato (α-TCP) kristalizaciją.

CHA, Fe:CHA, Cu:CHA, Zn:CHA, Mg:CHA, Mn:CHA, Sr:CHA ir Ba:CHA mėginių sintezė buvo atliekama vykstant α-TCP fazinei transformacijai vandeniniame tirpale. Susintetintas α-TCP buvo naudojamas kaip pirmtakas hidroterminei legiruotų ir nelegiruotų CHA bandinių sintezei. α-TCP milteliai (0,3 g) buvo suberti į 90 ml PTFE įdėklą, į kurį įpilta skirtingos koncentracijos (20 ml) įvairių metalų druskų vandeninių tirpalų. Indai buvo uždaryti nerūdijančio plieno reaktoriuose, perkelti į įkaitintą krosnį ir 3 val. kaitinti 200 °C temperatūroje. Mėginiai buvo filtruojami, praplaunami etanoliu ir acetonu ir džiovinami 50 °C temperatūroje per naktį.

1.1.2. Kalcio hidroksiapatito dangų sintezė

CHA dangų sintezė buvo atliekama ant Ti (*Thermo Scientific*; 1,0 mm storio, 99,2 %; CAS 7440-32-6) plokštelių, kurios buvo išpjautos lazeriu (1x1 cm)

atviros prieigos mechanikos centre. Titano plokštelės buvo mechaniškai šlifuojamos, kad būtų pašalinta ore susidariusi oksido plėvelė ir paviršiaus įbrėžimai. Plokštelės buvo šlifuojamos po 1 min. iš kiekvienos pusės. Paskui plokštelės chemiškai apdorotos 30 min. mirkant 70 °C temperatūroje 96 % 5 ml H_2SO_4 ir 7 % 0,35 ml HCl tirpale. Po mirkymo plokštelės buvo plaunamos ultragarso vonioje su distiliuotu vandeniu ir etanoliu 5 minutes. Išvalytos plokštelės buvo džiovinamos per naktį kambario temperatūroje. Paruoštos plokštelės buvo naudojamos $CaCO_3$ ir CHA sintezei.

Tirpalui paruošti buvo pasverta 11,807 g $Ca(NO_3)_2{\cdot}4H_2O$ ir ištirpinta 100 ml etanolio (99,8 %). Tirpalas maišytas magnetinėje maišyklėje 30 °C temperatūroje, kol medžiagos visiškai ištirpo. Tada panardintos plokštelės buvo įdėtos į krosnį termiškai apdoroti. CO_2 praturtinta aplinka krosnyje buvo sukurta šalia panardintų plokščių pastačius aktyvuota anglimi padengtas keramines plokšteles. Krosnyje temperatūra kelta nuo pradinės 20 °C iki 550 °C 3°C/min. greičiu. Pasiekus 550 °C temperatūrą, ji palaikyta 5 val. Reakcijos metu $Ca(NO_3)_2$ termiškai skyla į CaO, paskui CaO reaguoja su CO_2 ir susidaro kalcitas. Prieš išimant plokšteles, krosnis atvėsinta mažinant temperatūrą iki 2 °C 3 °C/min. greičiu.

CHA sintezei tirpalas buvo paruoštas pasveriant 0,14 g Na_2HPO_4 ir 0,6057 g TRIS ($C_4H_{11}NO_3$) buferio. Pasvertos medžiagos ištirpintos 100 ml distiliuoto vandens. Tirpalas buvo maišomas magnetine maišykle kol ištirpo ir palaikomas 30 °C temperatūroje. Tirpalo pH buvo šarminis (maždaug 9–10). Ištirpinus medžiagas, tirpalas buvo supiltas ant $CaCO_3$ sintezuotų plokštelių ir 7 dienas mirkyta 80 °C temperatūroje. Išimti iš tirpalo mėginiai buvo nuplauti distiliuotu vandeniu, išdžiovinti ir panaudoti tolesnei analizei. CHA susidaro po šios reakcijos:

$$10CaCO_3+6Na_2HPO_4+2H_2O = Ca_{(10)}(PO_4)_6(OH)_2+8NaHCO_3+2Na_2CO_3$$

Siekiant įvesti Cu^{2+} jonus, buvo paruoštas 0,5 mol/l koncentracijos $Ca(NO_3)_2$ ir $Cu(NO_3)_2$ mišinys. Pasverta 5,9036 g $Ca(NO_3)_2{\cdot}4H_2O$ ir 5,814 g $Cu(NO_3)_2{\cdot}2{,}5H_2O$ (Sigma-Aldrich). Medžiagos ištirpintos 100 ml etanolio. Paruošus tirpalą, į jį porcelianinėje lėkštelėje buvo panardintos chemiškai ir mechaniškai apdorotos titano plokštelės. Paskui jos buvo kaitinamos krosnyje CO_2 atmosferoje anksčiau minėtu būdu. Po kaitinimo procedūros plokštelės buvo panardintos į 0,14 g Na_2HPO_4+0,6057 g TRIS buferinio tirpalo (ištirpinto distiliuotame vandenyje) ir vieną savaitę mirkytos 80 °C temperatūroje. Panaši procedūra buvo pakartota įterpiant Zn^{2+} jonus (pasverta 7,4365 g $Zn(NO_3)_2{\cdot}6H_2O$; Chempur). Siekiant sėkmingai legiruoti Zn^{2+} jonais, sintezė taip pat buvo vykdoma tiesiogiai panardinant susintetintas CHA padengtas titano plokšteles į $Zn(NO_3)_2{\cdot}6H_2O$ tirpalą. Pasverta 7,4365 g

medžiagos ir ištirpinta 100 ml distiliuoto vandens. Taip pat buvo atlikta dar viena Zn-CHA sintezės modifikacija. Pirmiausia $CaCO_3$ buvo susintetintas pagal aprašytą $CaCO_3$ sintezės ant Ti plokštelių metodiką, tada Ti plokštelės su susintetintu kalcio karbonatu panardintos į 0,14 g Na_2HPO_4+0,6057 g TRIS buferio + 7,4365 g $Zn(NO_3)_2 \cdot 6\ H_2O$ tirpalą, kuris buvo paruoštas ištirpinant šias medžiagas distiliuotame vandenyje.

1.1.3. Kremų ruošimas

Kremams ruošti buvo naudojami šie reagentai: susintetinti CHA, Fe:CHA, Cu:CHA ir Zn:CHA mėginiai, izopropilo miristatas (*Sigma-Aldrich*, ≥90 %), stearino rūgštis (*Sigma-Aldrich*, ≥ 98 %), vazelinas® (*Sigma-Aldrich*, ≥98%), saulėgrąžų aliejus (*Sigma-Aldrich*), eumulginas B25 (*Sigma-Aldrich*, ≥98 %), cetilo alkoholis (*Sigma-Aldrich*, ≥99,5 %), betainas (*Sigma-Aldrich*, ≥98 %), glicerolis (*Sigma-Aldrich*, 99 %), fenoksietanolis (*Sigma-Aldrich*, ≥99 %), etanolis („Vilniaus degtinė“, 92 %) ir dejonizuotas vanduo. Aliejinė fazė buvo tirpinta atskiroje stiklinėje lėtai maišant ir kaitinant aliejinės fazės medžiagas iki 75–80 °C temperatūros. Vandeninės fazės medžiagos taip pat buvo sumaišytos ir kaitinamos iki 75–80 °C temperatūros. Abi fazės, tolygiai sumaišius ingredientus ir pasiekus vienodą 75–80 °C temperatūrą, buvo sumaišytos į vandeninę fazę supilant aliejinę fazę. Po sumaišymo 2 min. buvo homogenizuojama 2000–3000 rpm greičiu, išlaikant tą pačią temperatūrą. Mišinys maišant atvėsintas iki 35 °C temperatūros ir į jį buvo dedamos temperatūrai jautrios sudedamosios dalys. Fazės buvo sujungtos homogenizuojant 2 min. 2000–3000 rpm greičiu.

1.2. Aparatūra ir tyrimo metodai

Medžiagų rentgeno spindulių difrakcinės analizės spektrai buvo užrašyti naudojantis *Rigaku MiniFlex II* difraktometru, skleidžiančiu Ni filtruotą Cu Kα spinduliuotę ir veikiančiu Braggo-Brentano (θ/2θ) geometrija. Renkant duomenis, 2θ kampas buvo keičiamas nuo 10 iki 60°, žingsnio plotis – 0,01°, skenavimo greitis – 5°/min. Ramano spektrai buvo užrašyti kambario temperatūroje naudojant kombinuotą Ramano ir skenuojamąjį artimojo lauko optinį mikroskopą *(SNOM) WiTec Alpha 300 R* (Vokietija) su 532 nm lazerio šaltiniu (galia 40,9 mW). FTIR spektrai buvo užrašyti naudojant *Bruker ALPHA ATR* spektrometrą 4000–400 cm^{-1} diapazone. Mėginių paviršiaus morfologijai tirti naudotas *Hitachi SU-70* skenuojantis elektroninis mikroskopas (FE-SEM). Elementinei analizei bandiniai buvo ištirpinti 5 % azoto rūgštyje (HNO_3, Rotipuran® Supra 69 %, Carl Roth) ir praskiesti iki

atitinkamo tūrio. Kalibraciniai tirpalai buvo paruošti atitinkamai praskiedus pradinius standartinius tirpalus (vieno elemento ICP standartai 1000 mg/l, Carl Roth). Mėginių elementinei sudėčiai nustatyti naudotas *Perkin Elmer Optima 7000 DV ICP-OES* spektrometras.

Susintetintų kosmetikos produktų stabilumas įvertintas dispersinę sistemą veikiant išcentrine jėga. Stabilumo centrifuguojant bandymas atliktas pasveriant vienodą kiekvieno mėginio kiekį į centrifugos mėgintuvėlius, kurie buvo įdėti į centrifugos būgną ir 5 min. veikiami 3000 rpm išcentrinės jėgos. Atlikus bandymą, fazių atsiskyrimas buvo įvertintas vizualiai.

CHA, Fe:CHA, Cu:CHA ir Zn:CHA kremo mėginių citotoksiškumo osteoblastams (U2-OS linija) nustatymas atliktas normatyviniu metodu (ISO 10993: Biologinis medicinos priemonių įvertinimas. 5 dalis. Citotoksiškumo *in vitro* tyrimai. 12 dalis. Mėginių paruošimas ir pamatinės medžiagos (ISO 10993–5:2009 and ISO/IEC 17025:2005). Kondicionuota terpė buvo gauta inkubuojant 200 mg mėginio 1 ml etaloninės terpės, skirtos osteoblastams auginti (Dulbeko modifikuota Eagle terpė su didele gliukozės koncentracija [DMEM], papildyta 10 % embrioninių veršiukų serumu), 24 valandas 37 °C temperatūroje. Tokio pat svorio kremų mėginiai buvo įdėti į terpę ir suformuotos emulsijos naudojant 1 % DMSO. Osteoblastai su kondicionuota terpe buvo kultivuojami 24 valandas. Osteoblastų gyvybingumui įvertinti buvo pasitelktas normatyvinis neutralaus raudonojo (*Neutral Red*) metodas. Kontrolinė grupė buvo osteoblastai, kultivuoti nekondicionuotoje DMEM terpėje. Teigiamai ląstelių žūties kontrolei naudotas 70 % etanolis. Tyrimas pakartotas šešis kartus. Statistinė analizė atlikta naudojant *GraphPad Prism 10.0* programinę įrangą. Pasiskirstymo normalumas patikrintas naudojant Šapiro–Vilko testą. Statistiniam reikšmingumui įvertinti atliktas ANOVA testas su *post hoc* Dunnett'o daugkartiniu palyginimu (0,05).

Eksperimentui tinkamos naudoti kontrolinės medžiagos: gentamicino sulfatas (Sigma-Aldrich), flukonazolas (Pfizer Chemicals) kaip atitinkamai antibakterinės ir priešgrybelinės medžiagos ir 70 % etanolis kaip medžiaga, kuri turi įrodytą citotoksiškumą eukariotinėms ląstelėms. Taikyta Amerikos audinių ir ląstelių kultūrų (ATCC) etaloninė ląstelių linija: osteoblastai U2-OS (*Sigma-Aldrich*). ATCC etaloninės mikrobinės ląstelės: gramteigiamos *Staphylococcus aureus* 6538 (*Merck*) ir gramneigiamos *Pseudomonas aeruginosa* 27853 (*Merck*) bakterijos; grybelis: *Candida albicans* 10231 (*Sigma-Aldrich*).

Susintetintų dangų ant Ti substratų antibakterinių savybių vertinimas buvo atliktas inhibicinės zonos metodu, naudojant gramneigiamas *Escherichia coli* ir gramteigiamas *Bacillus subtilis* bakterijas. Mikrobiologiniai tyrimai atlikti po 24 valandų inkubacijos 37 °C temperatūroje.

REZULTATAI IR APTARIMAS

1.3. DVIVALENČIŲ IR TRIVALENČIŲ KATIJONŲ PAKEITIMO POVEIKIS KALCIO HIDROKSIAPATITO MORFOLOGIJAI

1.3.1. Kalcio hidroksiapatito susidarymo tyrimas, dalyvaujant mažesniems (Mg^{2+}, Mn^{2+}) ir didesniems (Sr^{2+}, Ba^{2+}) jonams

Siekiant ištirti jonų įtaką α-TCP hidrolizės procesui, buvo atliktos keturios hidroterminių sintezių serijos su skirtingais Mg^{2+}, Mn^{2+}, Sr^{2+} ir Ba^{2+} jonų kiekiais. Tirtų jonų joniniai spinduliai (CN = 6) didėja tokia tvarka: Mg^{2+} (0,72 Å) < Mn^{2+} (0,83 Å) < Sr^{2+} (1,18 Å) < Ba^{2+} (1,35 Å). 1 pav. pateikiamos mėginių, paruoštų skirtingomis sąlygomis naudojant dvivalenčius katijonus, XRD difraktogramos. Žemesnėje temperatūroje (120 °C) mažesni katijonai turėjo didžiausią įtaką α-TCP hidrolizės procesui. Net esant vos 0,1 mol % koncentracijai, Mg^{2+} jonų buvimas paskatino nedidelio kiekio β-TCP antrinės fazės susidarymą. Didėjant Mg koncentracijai, šis poveikis darėsi vis akivaizdesnis, o 5 mol % Mg^{2+} visiškai sustabdė hidrolizę ir Mg-5-120 XRD schemoje buvo galima nustatyti tik pradinį α-TCP. Skirtingai nei Mg^{2+} atveju, mažiausia Mn^{2+} koncentracija (0,1 mol %) neskatino β-TCP susidarymo, tačiau β-TCP buvimas išryškėjo Mn-0,5-120 bandinyje. Didesnės Mn^{2+} jonų koncentracijos (1, 5 ir 10 mol % Mn^{2+}) visiškai nuslopino α-TCP hidrolizę.

Sr^{2+} jonai turėjo mažiausią poveikį α-TCP hidrolizei: vienfazis CHA buvo gautas sintezės mišinyje esant net 1 mol % šio katijono; tačiau didesnės Sr koncentracijos sulėtino hidrolizę ir paskatino β-TCP susidarymą. Ba^{2+} jonų poveikis buvo mažesnis: naudojant 0,5 mol% koncentraciją susidarė nedidelis kiekis β-TCP, o 5 mol% Ba^{2+} visiškai užkirto kelią hidrolizės procesui.

Gauti rezultatai rodo, kad β-TCP susidarymą vandeninėje terpėje gali skatinti svetimų jonų buvimas. Padidinus sintezės temperatūrą ir laiką, padidėjo galutinių produktų kristališkumas, kuris matyti iš aštrių difrakcijos smailių. Įdomu tai, kad Ba^{2+}poveikis buvo panašus į Mg^{2+} švelnesnėmis sąlygomis, tačiau aukštesnė temperatūra ir ilgesnis procesas atskleidė reikšmingus šių katijonų poveikio skirtumus.

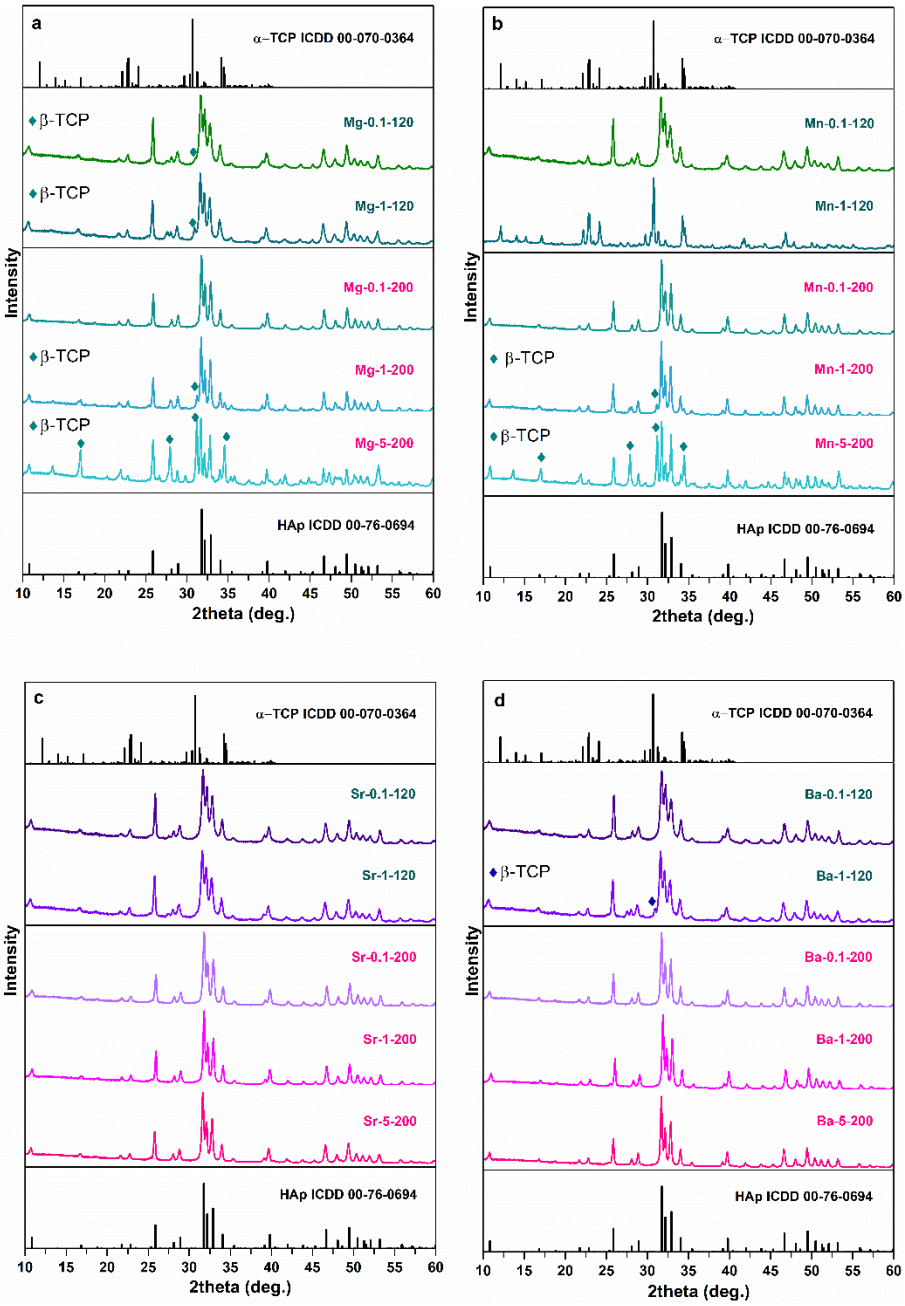

1 pav. Mėginių po hidroterminio apdorojimo 3 val. 120 °C temperatūroje ir 5 val. 200 °C temperatūroje su skirtingais pakaitais XRD difraktogramos

Visuose susintetintų bandinių FTIR spektruose buvo pastebėtos kelios aiškios juostos ties maždaug 940–1180 cm^{-1} ir maždaug 500–660 cm^{-1}. Juostos

1023 cm^{-1} ir 1090 cm^{-1} srityse priskiriamos asimetriniams P-O virpesiams (ν_3), o juosta, kurios smailė yra ties 960 cm^{-1}, atitinka simetrinius P-O virpesius (ν_1), kurie matomi CHA [149]. FTIR spektroskopijos rezultatai gerai sutampa su XRD analizės rezultatais.

Galutinių produktų elementinė analizė buvo atlikta ICP-OES metodu, siekiant nustatyti, ar hidrolizės reakcijos metu metalų jonai iš tirpalo pereina į gautus miltelius, ir įvertinti šių jonų inkorporavimo lygį, palyginti su pradiniu M ir Ca santykiu. ICP-OES analizė parodė, kad į galutinius produktus pateko tik nedidelis metalų jonų kiekis. Akivaizdu, kad mažesnių jonų (Mg^{2+} ir Mn^{2+}) pradinių ir galutinių (gautuose milteliuose) molinių santykių neatitiktys buvo mažesnės, palyginti su Sr^{2+} ir Ba^{2+}. Faktinis Mg^{2+} ir Mn^{2+} jonų procentinis santykis gerai atitiko pradinį katijonų santykį reakcijos mišinyje iki 5 mol %, o tai rodo, kad α-TCP hidrolizės metu šie jonai pereina į sintezės produktus. Didėjant šių jonų koncentracijai reakcijos tirpale, jų kiekis gautuose milteliuose didėjo tik nežymiai. Sr^{2+} atveju buvo gerokai didesnės neatitiktys, o tai rodo, kad po reakcijos tirpale liko didelis kiekis Sr^{2+} jonų. Pavyzdžiui, atlikus reakciją su 5 mol %, produkte buvo gauta tik maždaug pusė šio kiekio. Iš visų tirtų metalų Ba^{2+} jonai pasižymėjo mažiausiu gebėjimu įsijungti į gautą produktą. Skirtumas tarp pradinio katijonų santykio ir faktinio molinio santykio svyravo nuo 34 % iki 84 % ir buvo didesnis mėginiuose, kuriuose buvo didelė pradinė Ba^{2+} koncentracija. Nors Ba^{2+}gali iš dalies pakeisti Ca^{2+} hidroksiapatite, tačiau į CHA struktūrą vandeniniame tirpale galima įterpti tik nedidelius Ba^{2+} kiekius. Taip yra dėl didelio šio jono spindulio. Todėl nenuostabu, kad galutiniame produkte aptinkamas nedidelis Ba^{2+} kiekis.

Paruoštų miltelių dalelių morfologija buvo tiriama skenuojančiu elektroniniu mikroskopu. Didesnio didinimo SEM vaizdai su atrinktų mėginių detalėmis pateikiami 2 ir 3 pav. Mėginių SEM vaizduose galima pastebėti morfologijos skirtumų, priklausančių nuo sintezės sąlygų. Hidrotermiškai apdorojant 120 °C temperatūroje su 0,1 mol % įvairių katijonų, susidarė plokštelės pavidalo kristalai. Į reakcijos mišinį įterpus didesnes metalų jonų koncentracijas, susidarė ir plokštelių, ir šešiakampių lazdelių pavidalo dalelės. Tam tikrais atvejais buvo pastebėtas savaiminis strypelių rinkimasis į gėlės pavidalo struktūras. Hidrotermiškai apdorojant 200 °C temperatūroje, strypelių pavidalo kristalai kartu su plokšteliniais kristalais susidaro net ir tada, kai į reakcijos mišinį įterpiama mažiausia tirta metalo jonų koncentracija (0,1 mol %). Didėjant metalų koncentracijai, kartu didėja ir strypelių pavidalo dalelių dalis.

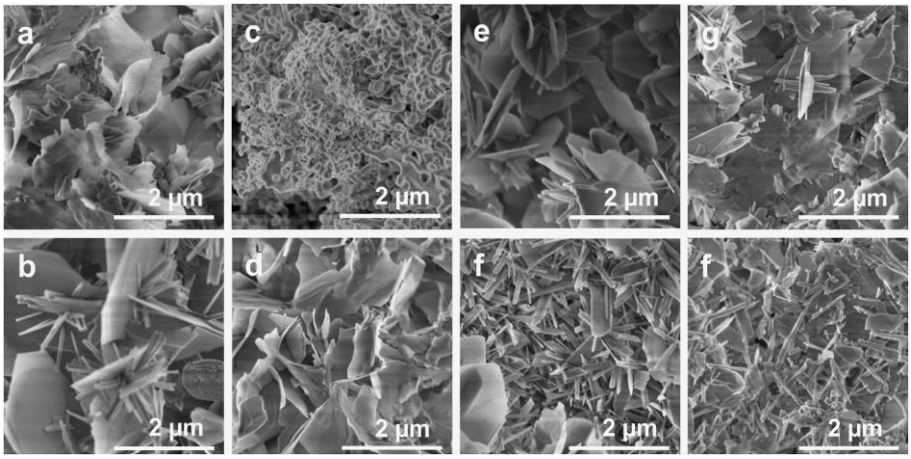

2 pav. Mėginių po hidroterminio apdorojimo 120 °C temperatūroje 3 val. SEM vaizdai: a) Mg-0,1-120; b) Mg-1-120; c) Mn-0,1-120; d) Mn-1-120; e) Sr-1-120; f) Sr-5- 120; g) Ba-0,1-120; h) Ba-1-120

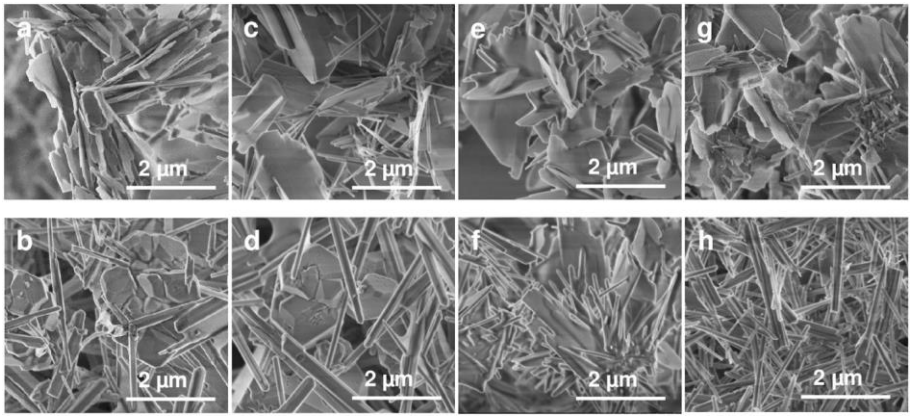

3 pav. Mėginių po hidroterminio apdorojimo 200 °C temperatūroje 5 val. SEM vaizdai: (a) Mg-0,1-200); (b) Mg-5-200; (c) Mn-0,1-200; (d) Mn-5-200; (e) Sr-0,1-200; (f) Sr-5-200; (g) Ba-0,1-200; (h) Ba-5-200

Mėginį, paruoštą su 5 mol% Ba^{2+}, sudarė tik šešiakampės lazdelių pavidalo dalelės. Atsižvelgiant į ryškiausią Ba^{2+} jonų įtaką lazdeliniams CHA kristalams susidaryti, 200 °C temperatūroje buvo atlikta papildoma eksperimentų serija su skirtingomis Ba^{2+} koncentracijomis (1, 2, 3 ir 4 mol %). Mėginiuose, paruoštuose su 1 ir 2 mol % Ba^{2+}, vis dar buvo tam tikrų plokštelių pavidalo struktūrų. Tokių struktūrų nepastebėta mėginių, paruoštų su 3 ir 4 mol % Ba^{2+}, SEM vaizduose, šie mėginiai buvo panašūs į paruoštus su 5 mol % Ba^{2+} ir buvo sudaryti iš lazdelių pavidalo dalelių. Vidutinis strypelių skersmuo ir ilgis buvo

atitinkamai apie 0,2 ir 4 μm. Ba^{2+} jonų koncentracija neturėjo didelės įtakos gautų CHA strypelių matmenims.

Šie rezultatai aiškiai rodo, kad galutinių produktų morfologija priklauso nuo hidroterminės sintezės sąlygų, tačiau svetimų jonų koncentracija ir pobūdis šiame procese vaidina svarbų vaidmenį.

Apibendrinant galima teigti, kad hidroterminės sintezės metu naudojant dvivalenčius katijonus kaip kontroliuojančius agentus, buvo pasiekta legiruoto hidroksiapatito su kalcio trūkumu morfologijos kontrolė. Hidroterminės sintezės sąlygos (temperatūra, laikas) turėjo įtakos galutinių produktų fazės grynumui ir morfologijai, tačiau svetimų jonų pobūdis ir koncentracija buvo pagrindiniai veiksniai, lemiantys produktų savybes. Nustatyta, kad mažesni jonai (Mn^{2+} ir Mg^{2+}), palyginti su didesniais jonais (Ba^{2+} ir Sr^{2+}) , turėjo stipresnį slopinamąjį poveikį α-TCP hidrolizės procesui. Aukštesnė temperatūra ir ilgesnis reakcijos laikas lemia vienfazės CHA susidarymą, esant didesnėms metalų jonų koncentracijoms. Tai ypač pastebima Ba^{2+}ir Sr^{2+} atveju. Be to, padidinus hidroterminės sintezės temperatūrą ir laiką, padidėjo galutinių produktų kristališkumas. Pakeitus sintezės sąlygas, buvo gauti mėginiai, sudaryti tik iš plokštelės pavidalo (atidengtos *c plokštumos*) arba lazdelių pavidalo (atidengtos *a(b)-plokštumos*) CHA kristalų.

1.3.2. Kalcio hidroksiapatito susidarymo, dalyvaujant Fe^{3+}, Cu^{2+} ir Zn^{2+} jonams, tyrimas

CHA ir metalais legiruoti mėginiai Fe:CHA, Cu:CHA ir Zn:CHA taip pat buvo susintetinti naudojant anksčiau aprašytą metodą. Metalais pakeistų mėginių (Fe:CHA, Cu:CHA ir Zn:CHA) XRD difraktogramos pateikiamos 4 paveiksle. Esant Fe^{3+} ir Cu^{2+}jonams, akivaizdu, kad susidaro antrinės TCP fazės (β-TCP ir α-TCP). Skirtingai nei Fe^{3+} ir Cu^{2+} jonai, Zn^{2+} jonai neskatino β-TCP ar α-TCP susidarymo.

Visų susintetintų bandinių FTIR spektrai buvo labai panašūs, nepriklausomai nuo metalo pakeitimo, kaip rodo du tipiniai CHA mėginių FTIR spektrai (5 pav.). Šie FTIR rezultatai vėlgi gerai sutampa su XRD duomenimis. ICP-OES analizė parodė, kad į galutinius produktus pateko tik nedideli kiekiai Fe^{3+} ir Cu^{2+}jonų. Zn^{2+} jonai CHA struktūroje beveik visiškai pakeitė Ca^{2+} jonus. Susintetintų mėginių CHA, Fe:CHA, Cu:CHA ir Zn:CHA SEM vaizdai pateikiami 6 paveiksle. Vaizduose matomi nedideli morfologiniai skirtumai, priklausantys nuo pakaitalo tipo. Hidrotermiškai apdorojant nepakeistą α-TCP 200 °C temperatūroje, susidarė skirtingai orientuoti ir šiek tiek aglomeruoti plokšteliniai CHA kristalai. Atskiros dalelės buvo maždaug 50 nm dydžio. Į reakcijos mišinį įterpus metalų jonų, susidarė

papildomų formų ir didesnio aglomeracijos laipsnio plokštelinės dalelės. Fe^{3+} turintį mėginį sudarė panašaus dydžio (~ 50 nm) plokštelės ir adatos formos dalelės. Mėginys su 10 mol% Cu^{2+} pasižymėjo didelėmis plokštelės pavidalo struktūromis su mažesnėmis dalelėmis, tolygiai pasiskirsčiusiomis plokštelės paviršiuje. Zn^{2+} pakeisto CHA atveju miltelius sudarė ir plokštelinės, ir pluoštinės dalelės, kurių dydis svyravo nuo 50 iki 100 nm.

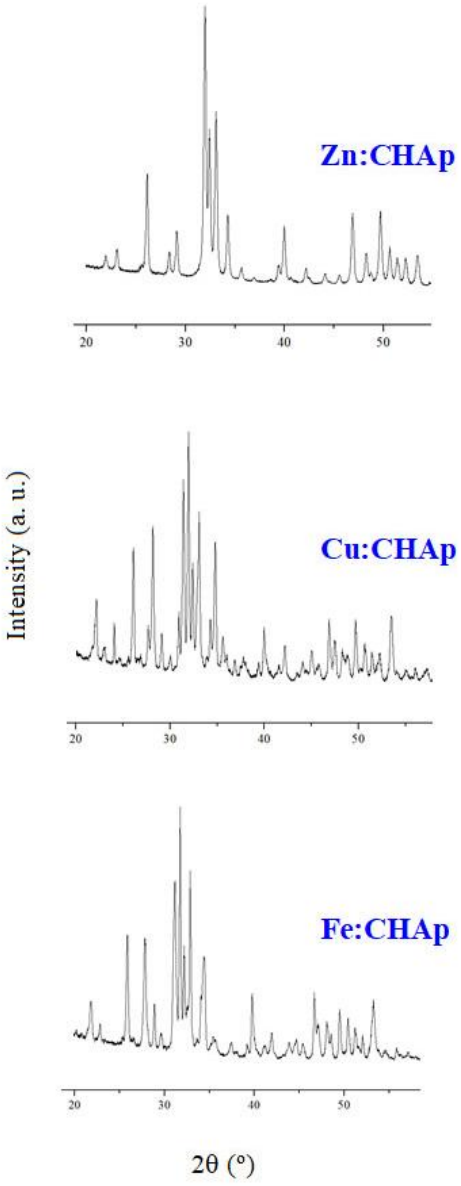

4 pav. Fe:CHA, Cu:CHA ir Zn:CHA mėginių XRD difraktogramos

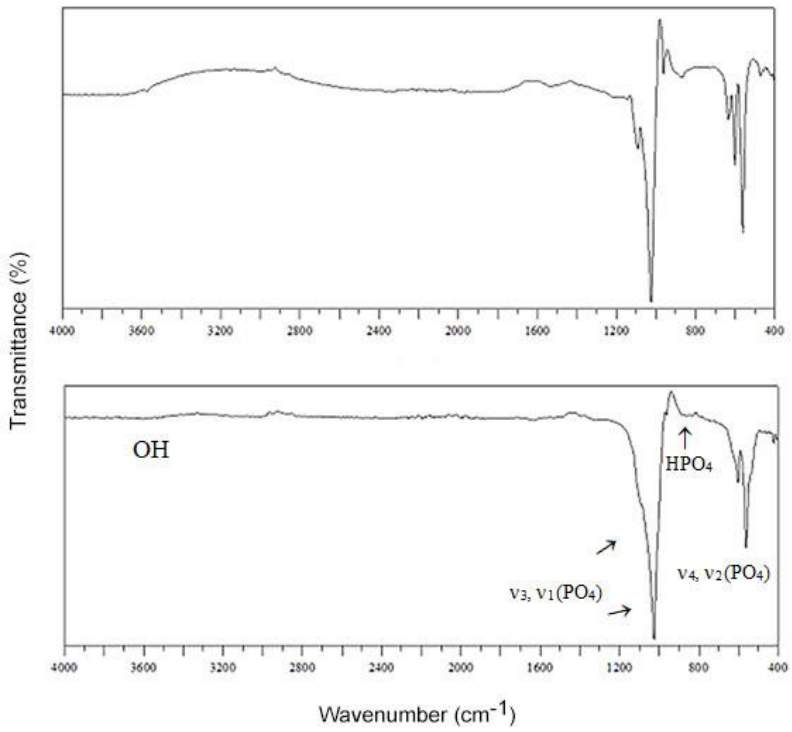

5 pav. Cu:CHA (apačioje) ir Zn:CHA (viršuje) mėginių FTIR spektrai

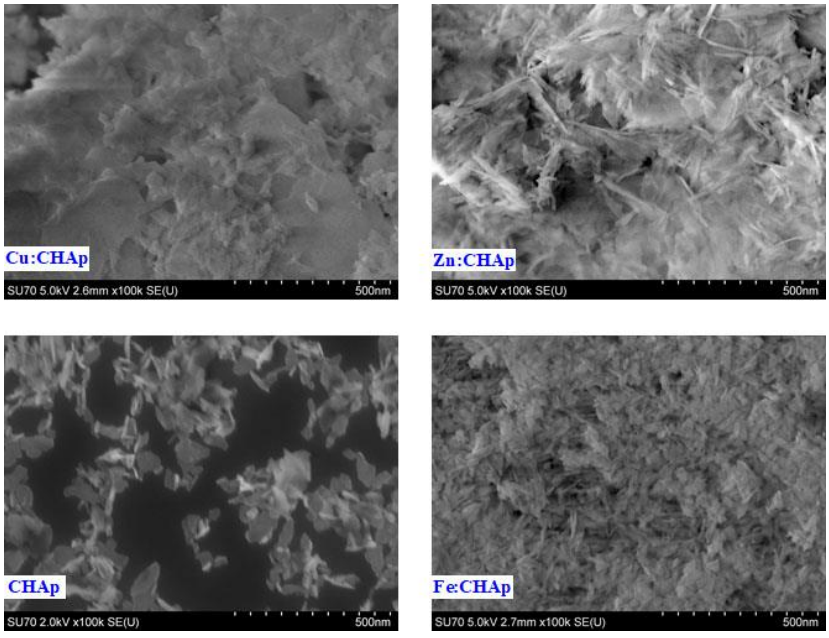

6 pav. CHA, Fe:CHA, Cu:CHA ir Zn:CHA mėginių SEM nuotraukos

Nustatyta, kad Fe^{3+}, Cu^{2+} ir Zn^{2+} katijonai veikia CHA fazinį grynumą ir morfologiją. Susintetinti nanodydžio CHA, Fe:CHA, Cu:CHA ir Zn:CHA mėginiai buvo naudojami kaip priedai odos kremams gaminti.

1.4. KALCIO HIDROKSIAPATITO DANGŲ SINTEZĖ ŽEMOJE TEMPERATŪROJE

1.4.1. Kalcio hidroksiapatito dangų sintezė ir apibūdinimas

CHA akytųjų sluoksnių sintezė buvo atliekama ant Ti plokštelių. Paruoštos plokštelės iš pradžių buvo naudojamos $CaCO_3$ dangoms sintetinti. Vėliau naudojant tirpinimo ir nusodinimo metodą žemoje temperatūroje (80 ^oC) iš šių $CaCO_3$ dangų buvo susintetintas kristalinis kalcio hidroksiapatitas. Dangų fazinė sudėtis buvo nustatyta naudojant XRD. Iš XRD difraktogramų matyti, kad ant Ti padėklo susidarė $CaCO_3$ sluoksnis. Ties $2\theta = 29{,}4°$ matoma intensyviausia kalcitui ($CaCO_3$) būdinga smailė. Kaip jau buvo minėta, CHA vėliau buvo susintetintas iš šių $CaCO_3$ dangų tirpinimo ir nusodinimo metodu. XRD rezultatai aiškiai parodė, kad susidaro CHA su būdingais atspindžiais 31–32,5° 2θ kampų intervale (žr. 7 pav.).

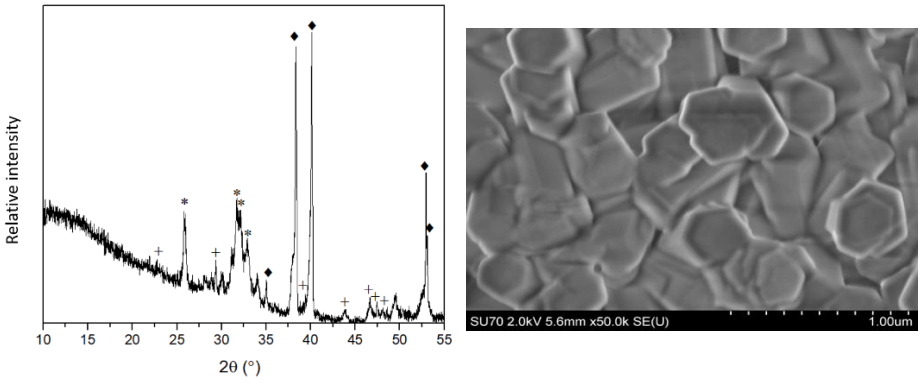

7 pav. Kalcio hidroksiapatito dangos ant Ti padėklo XRD difraktograma (kairėje) ir SEM nuotrauka (dešinėje). Difrakciniai atspindžiai: * – HAP [PDF: 96-431-7044];♦ – Ti [PDF: 96-901-6191]; + $CaCO_3$[PDF: 96-154-7348]

Taip pat identifikuotos $CaCO_3$ smailės, o tai įrodo, kad dalis $CaCO_3$ vis dar lieka nesureagavusi. Be to, matomos intensyvios Ti padėklo difrakcijos smailės. Taigi, galima daryti išvadą, kad ant Ti susidarė kalcio hidroksiapatito sluoksnis. Gauti Ramano ir FTIR spektroskopijos rezultatai patvirtino

rentgeno spinduliuotės difrakcijos duomenis apie sėkmingą $Ca_{10}(PO_4)_6(OH)_2$ dangų formavimąsi ant Ti padėklo. Žemoje temperatūroje susidarė 20 nm dydžio šešiakampės CHA dalelės. Ypatinga susintetintų CHA morfologinė savybė (7 pav.) yra ta, kad pasiektas labai didelis dalelių homogeniškumas ir jų dydžio pasiskirstymas.

1.4.2. Cu^{2+}ir Zn^{2+} pakeistų kalcio hidroksiapatito dangų sintezė ir jų savybės

Cu^{2+} pakeistų CHA bandinių, susintetintų žematemperatūriniu zolių-gelių ir tirpinimo-nusodinimo metodu, fazinis grynumas taip pat buvo ištirtas naudojant XRD analizę. Nustatyta, kad, kaitinant $Ca(NO_3)_2$ ir $Cu(NO_3)_2$ tirpalų mišinį CO_2 atmosferoje, be $CaCO_3$, susidarė vario hidroksido karbonatas $Cu_2(OH)_2CO_3$ (malachitas). 8 pav. pavaizduota CHA dangos, kurioje Ca^{2+} jonai pakeisti Cu^{2+} jonais, XRD difraktograma.

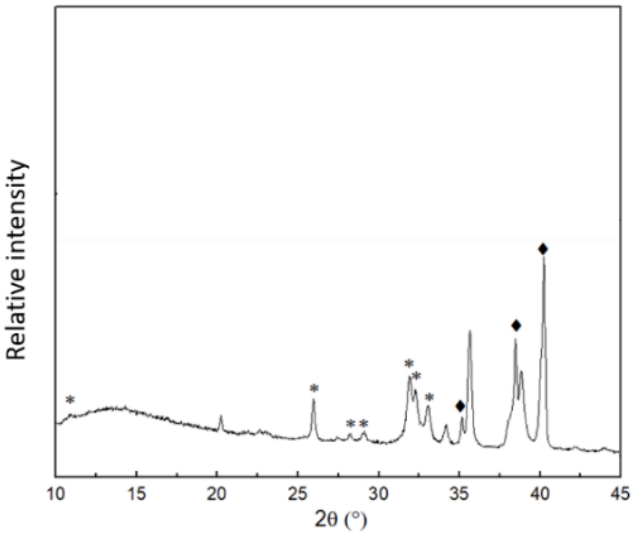

8 pav. Cu-CHA dangos, gautos ant Ti, XRD difraktograma. Difrakciniai atspindžiai: * – CHA; ♦ – Ti

XRD rezultatai rodo, kad iš dalies Cu^{2+} jonais pakeisto CHA sintezei galima sėkmingai naudoti žemos temperatūros nusodinimo-tirpinimo metodą. Tačiau CHA dangos, pakeistos Zn^{2+} jonais, pirmiau minėtu paruošimo būdu nesusidarė. Ant Ti plokštelės vietoj Zn-CHA susidarė beveik vienfazis cinko hidroksido nitrato monohidratas $Zn(OH)(NO_3)(H_2O)$. SEM vaizdai aiškiai parodė, kad į CHA pridėjus vario taip pat pasikeitė dalelių morfologija. Vietoj

šešiakampių 20 nm CHA dalelių susiformavo maždaug 1 μm ilgio snaigės formos pluoštiniai kristalitai (žr. 9 pav.).

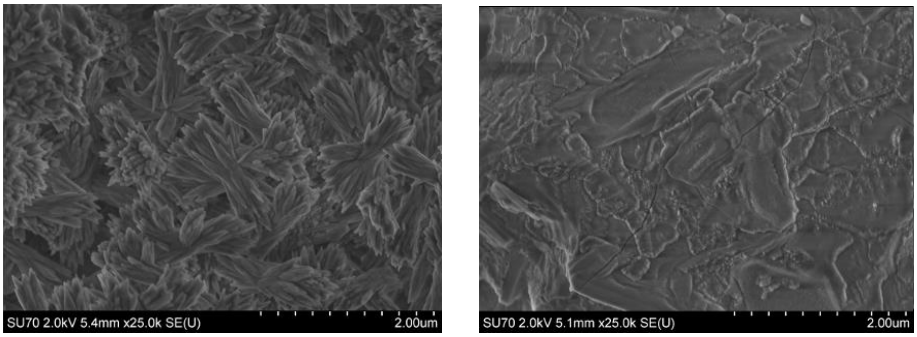

9 pav. Cu-CHA (kairėje) ir $Zn_3(OH)_4(NO_3)_2$ dangų (dešinėje), pagamintų ant Ti plokštelės, SEM nuotraukos

Naudojant Zn^{2+} turinčius mėginius susiformavo homogeninės dangos su tam tikrais įtrūkiais. Dangos sudarytos iš plokštuminių didesnių nei 1 μm kristalų, sudarančių ištisinę dangą. Ti paviršiuje taip pat matyti keletas mažesnių dalelių sankaupų.

Susintetintų Cu ir Zn turinčių dangų elementinė analizė buvo atlikta EDX analizės metodu. Nustatyta, kad Cu-CHA dangos atveju Ca/P santykis ~ 1,62 beveik sutampa su kalcio ir fosforo santykiu stechiometriniame CHA (1,67). Kalcio ir vario molinis santykis buvo Ca:Cu = 1:0,033, t. y. apie 3,3 mol % kalcio buvo pakeista variu. Tada sintezės produkto formulę būtų galima užrašyti $Ca_{9,7}Cu_{0,3}(PO_4)_6(OH)_2$ arba $Ca_{9,85}Cu_{0,15}(PO_4)_6(OH)_2$, jei reakcijos metu susidarytų stechiometrinis vario hidroksido kiekis. Iš mėginio su cinku EDX matavimų nustatytas Ca/P santykis buvo visiškai nepagrįstas, nes neatitiko jokio galimo kalcio ir fosforo santykio žinomuose fosfatuose. Tikėtina, kad dangoje liko didelis kiekis amorfinio kalcio karbonato ir (arba) labai nedidelis kiekis kalcio hidroksiapatito. EDX spektras rodė, kad susintetintoje dangoje yra didelis kiekis cinko.

1.4.3. Antibakterinių savybių tyrimas

Įvertinus susintetintų dangų antibakterines savybes ant Ti padėklų, nenustatyta CHA slopinimo zonų, esant gramneigiamoms *Escherichia coli* ir gramteigiamoms *Bacillus subtilis* bakterijoms. Vėlesni mikrobiologiniai tyrimai, atlikti po 24 val. inkubacijos 37 °C temperatūroje, parodė Cu-CHA turinčių mėginių slopinimo zonas, *B. subtilis* kolonijoms (žr. 10 pav.).

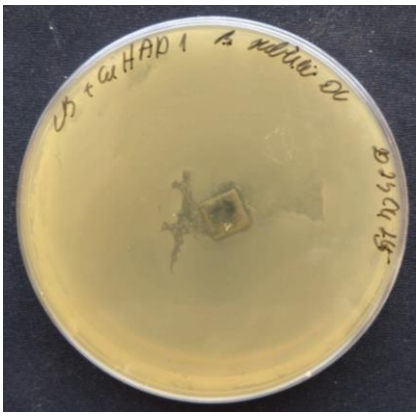

10 pav. Žemoje temperatūroje susintetintos Cu-CHA dangos ant Ti antibakterinio veiksmingumo tyrimų su *B. subtilis* rezultatai

11 pav. pavaizduotos Zn^{2+} jonais legiruotų mėginių slopinimo zonos, veikiant *B. subtilis* kolonijas. Tačiau veikiant *E. coli* inhibicijos zonų nepastebėta.

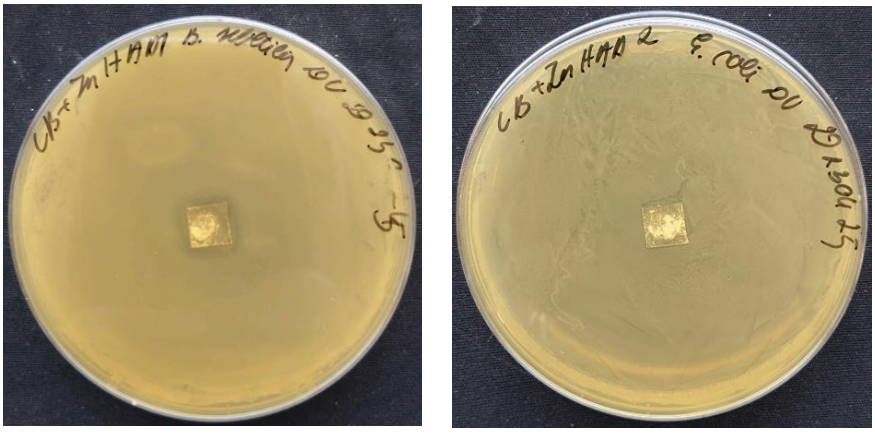

11 pav. Žemoje temperatūroje susintetintų dangų su Zn^{2+} jonais ant Ti antibakterinio veiksmingumo tyrimų rezultatai su (kairėje) *B. subtilis* ir (dešinėje*) E. coli* bakterijomis

Dangos su Cu-CHA ant Ti slopinimo zona buvo 10,5 mm±0,5 mm vidutiniškai iš 9 matavimų, plokštelės su $Zn_3(OH)_4(NO_3)_2$ danga – 15 mm± 1,8 mm.

1.5. SUSINTETINTŲ KALCIO HIDROKSIAPATITO MĖGINIŲ NAUDOJIMAS KOSMETIKOJE

Šioje disertacijos dalyje apibendrinamas Fe^{3+}, Cu^{2+}ir Zn^{2+}pakeitimo CHA poveikis CHA antimikrobinėms savybėms. Pagamintų kremo mėginių nuotraukos pateikiamos 12 paveiksle.

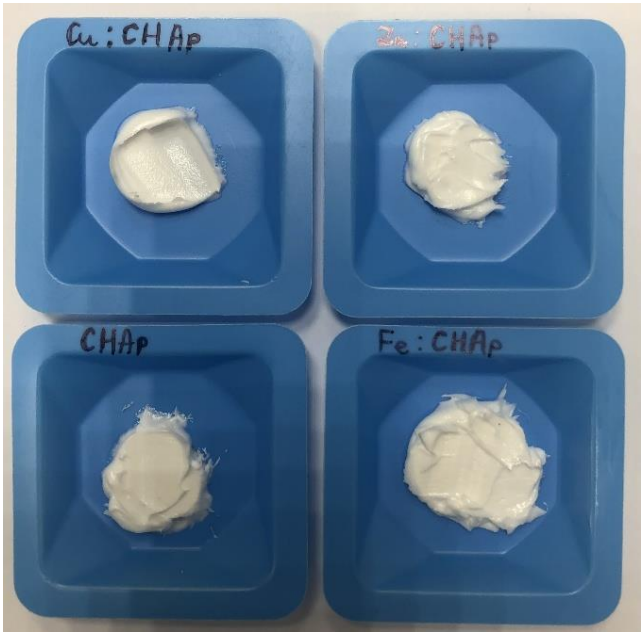

12 pav. Pagamintų kremo mėginių, naudojant CHA (apačioje, kairėje), Fe:CHA (apačioje, dešinėje), Cu:CHA (viršuje, kairėje) ir Zn:CHA (viršuje, dešinėje) mėginius, nuotraukos

Iš šių vaizdų matyti, kad visų kremų, pagamintų naudojant skirtingus CHA, išvaizda yra beveik identiška. Kremo mėginių morfologija taip pat atrodė beveik vienoda visuose preparatuose nepriklausomai nuo naudoto kalcio hidroksiapatito tipo.

1.5.1. Biologinio suderinamumo vertinimas

Biologinio suderinamumo vertinimas atliktas naudojant osteoblastus. Osteoblastų gyvybingumo tyrimų rezultatai (13 pav.) rodo, kad nemodifikuotas CHA nesukėlė ląstelių žūties, o tai patvirtina jo biosuderinamumą lyginant su neapdorota kontroline medžiaga (C+). Tiek Fe^{3+}, tiek Cu^{2+} legiruotas CHA taip pat nepasižymėjo didele ląstelių žūtimi,

taigi jų biosuderinamumas buvo išlaikytas. Priešingai, Zn pakeistas CHA sukėlė daugiau kaip 30 % osteoblastų žūtį, o tai rodo galimą citotoksiškumą.

Analizuojant kremų mėginius (14 pav.), nustatytas stipresnis poveikis osteoblastų gyvybingumui.

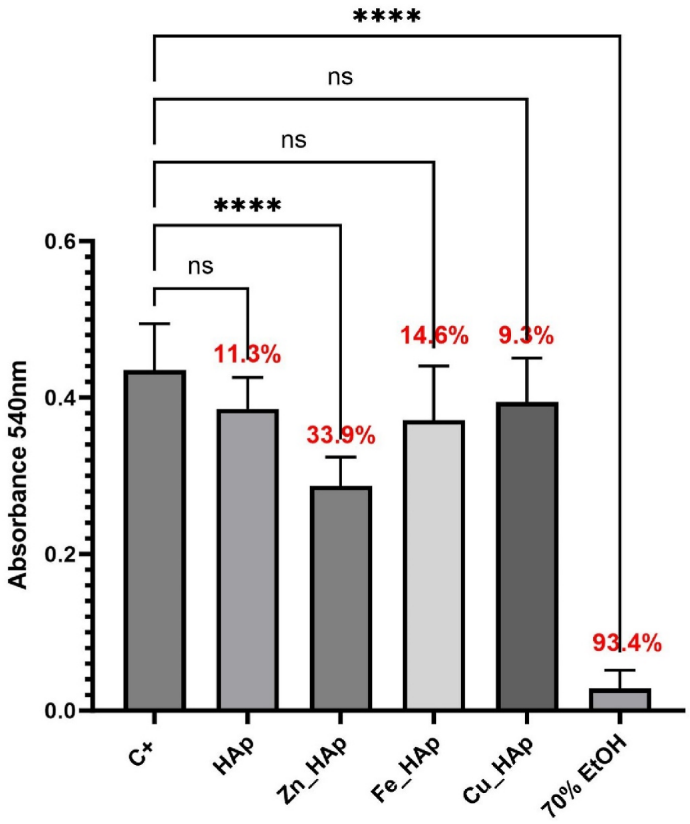

13 pav. Osteoblastų, paveiktų tiriamomis medžiagomis, išgyvenamumas / citotoksiškumas. C+ – augimo kontrolė, t. y. osteoblastai, kultivuoti nekondicionuotoje DMEM terpėje. Stulpeliai rodo ląstelių augimo lygį, o procentinės vertės – konkrečių mėginių citotoksiškumą. Žvaigždutės rodo statistinį reikšmingumą, o ns – statistinio reikšmingumo nėra.

Kremas su CHA be metalo priedų gerokai sumažino ląstelių gyvybingumą, tačiau toksikologiniuose standartuose paprastai laikoma, kad sumažėjimas apie 20 % arba mažiau yra nereikšmingas. Šie rezultatai rodo, kad kremai, kurių sudėtyje yra Cu ir Fe, yra tokie pat biologiškai suderinami kaip ir mėginys be metalų. Priešingai, kremas, kurio sudėtyje yra Zn, kaip ir Zn:CHA, pasižymėjo galimu citotoksiškumu, todėl kyla abejonių dėl jo tinkamumo klinikiniam ar kosmetiniam naudojimui.

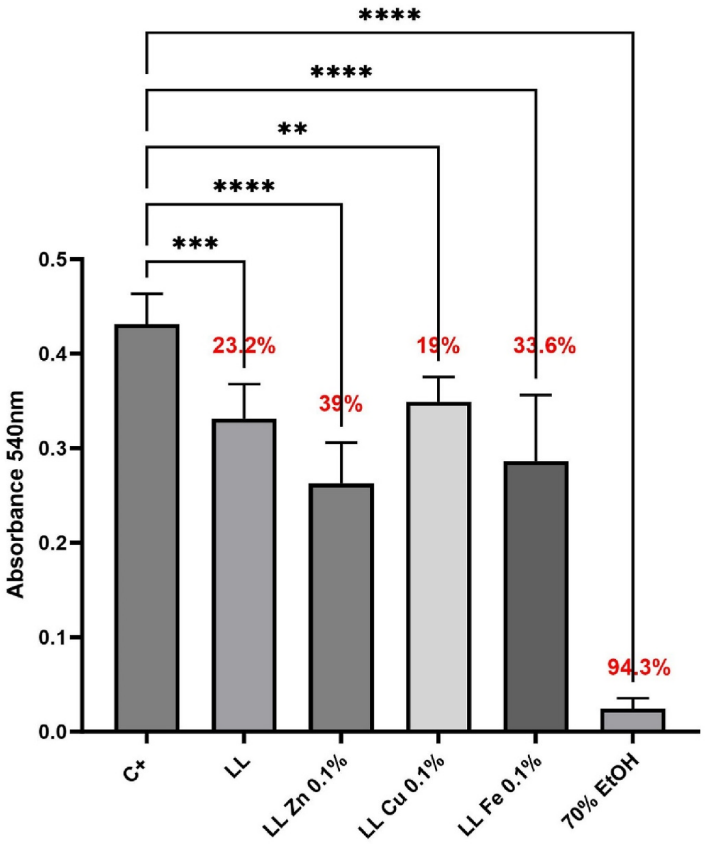

14 pav. Osteoblastų, paveiktų tiriamais kremų mėginiais, išgyvenamumas / citotoksiškumas. C+ – augimo kontrolė, t. y. osteoblastai, kultivuoti nekondicionuotoje DMEM terpėje. Stulpeliai rodo ląstelių augimo lygį, o procentinės vertės – konkrečių mėginių citotoksiškumą. Žvaigždutės rodo statistinį reikšmingumą, o ns – statistinio reikšmingumo nėra.

1.5.2. Antibakterinis aktyvumas

Medžiagų antimikrobinis veiksmingumas buvo įvertintas pagal poveikį dviem bakterijų padermėms – *Staphylococcus aureus* (gramteigiamas) ir *Pseudomonas aeruginosa* (gramneigiamas) – bei mielių *Candida albicans* padermei. Tikėtina, kad plokščias polistireninis daugiabriaunės plokštelės paviršius buvo mažiau palankus mikrobams augti, palyginti su porėtu hidroksiapatito paviršiumi, ir tuo galima paaiškinti ant pastarojo matomą stipresnį bakterijų augimą. Todėl, siekiant įvertinti mikroorganizmų augimo sumažėjimą, buvo atlikti du palyginimai: kaip kontrolinis paviršius buvo naudoti polistireno paviršius (C+) arba hidroksiapatitas. CHA, legiruoti Zn^{2+} ir Cu^{2+} veiksmingai sumažino gramteigiamų bakterijų ir mielių bioplėvelės

formavimąsi, tačiau buvo mažiau veiksmingi pagal poveikį gramneigiamoms bakterijoms. Įdomu, kad, kremai, kuriuose CHA legiruoti metalais, buvo veiksmingi pagal poveikį abiejų tipų bakterijoms, o Zn turintys mėginiai pasižymėjo ir priešgrybelinėmis savybėmis (15–17 pav.).

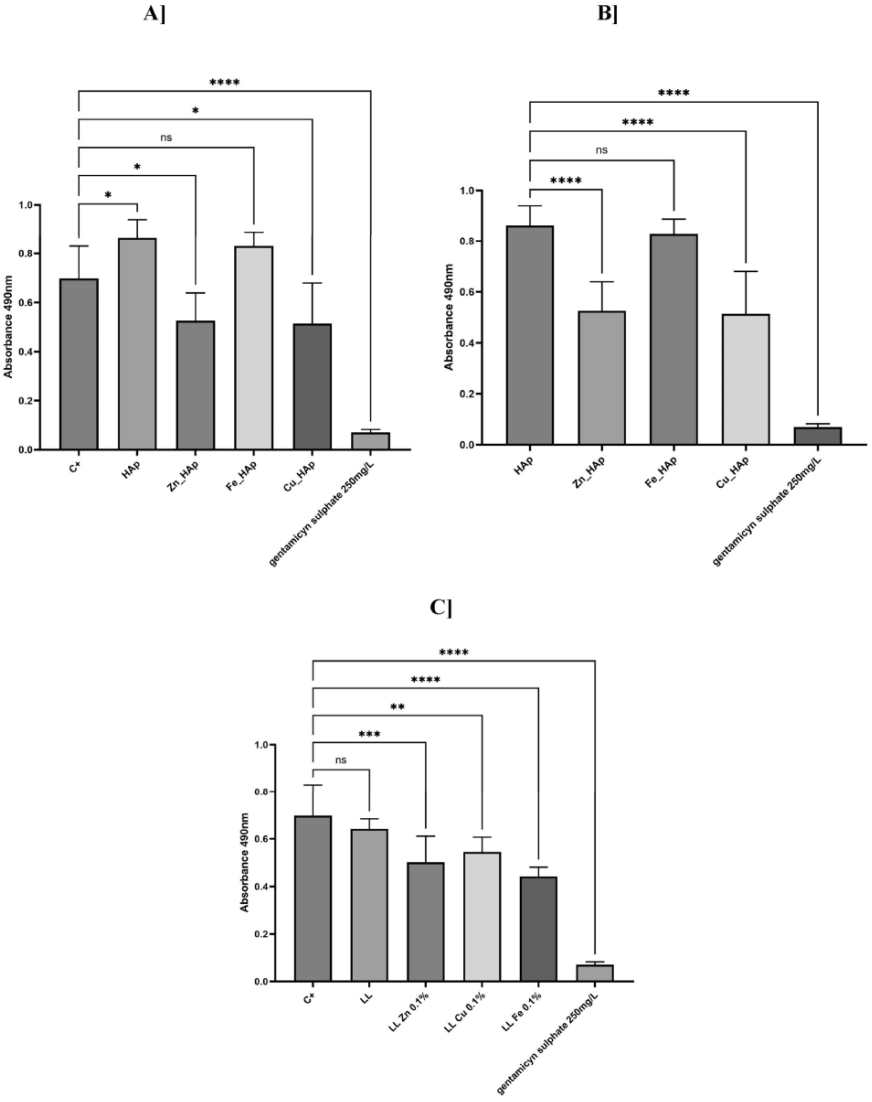

15 pav. *S. aureus* augimo sumažėjimas veikiant tiriamaisiais mėginiais: A) ir B) milteliai; C) kremai. Pasirinkus kaip tiriamąjį mėginį miltelius, buvo pateiktos dvi diagramos su skirtingais teigiamų kontrolių rinkiniais (C+ arba CHA). Žvaigždutės rodo statistinį reikšmingumą, o ns – statistinio reikšmingumo nėra

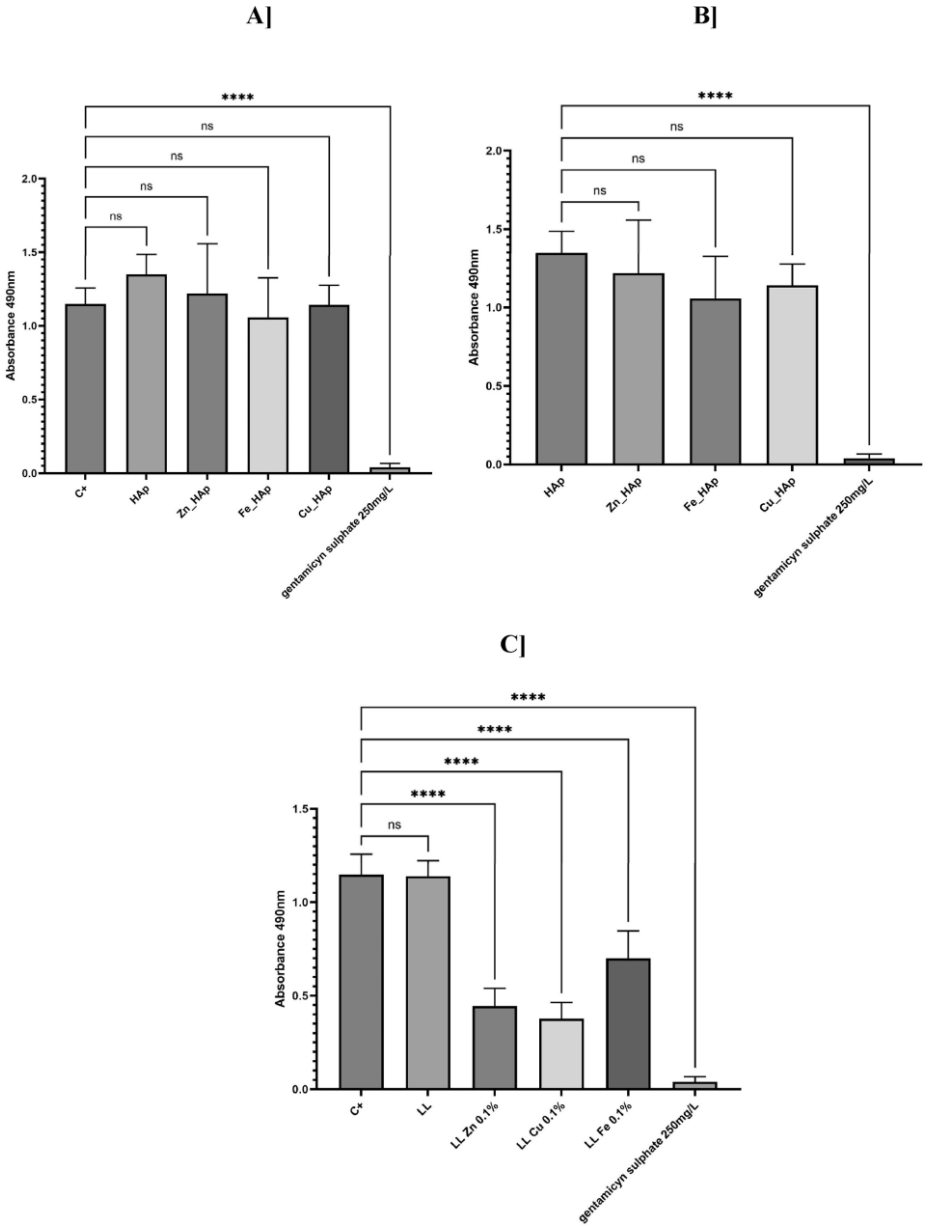

16 pav. *P. aeruginosa* augimo sumažėjimas veikiant tiriamaisiais mėginiais: A) ir B) milteliai; C) kremai. Pasirinkus kaip tiriamąjį mėginį miltelius, pateikti du grafikai su skirtingais kontroliniais rinkiniais (C+ arba CHA). Žvaigždutės rodo statistinį reikšmingumą, o ns – statistinio reikšmingumo nėra

Tikėtina, kad tokį skirtingą poveikį lemia unikalios mikroorganizmų ląstelių sienelių struktūros ir paviršiaus krūviai, kurie turi įtakos jų sąveikai su metalu legiruotomis medžiagomis. Antimikrobinių savybių santrauka pateikiama 1 lentelėje.

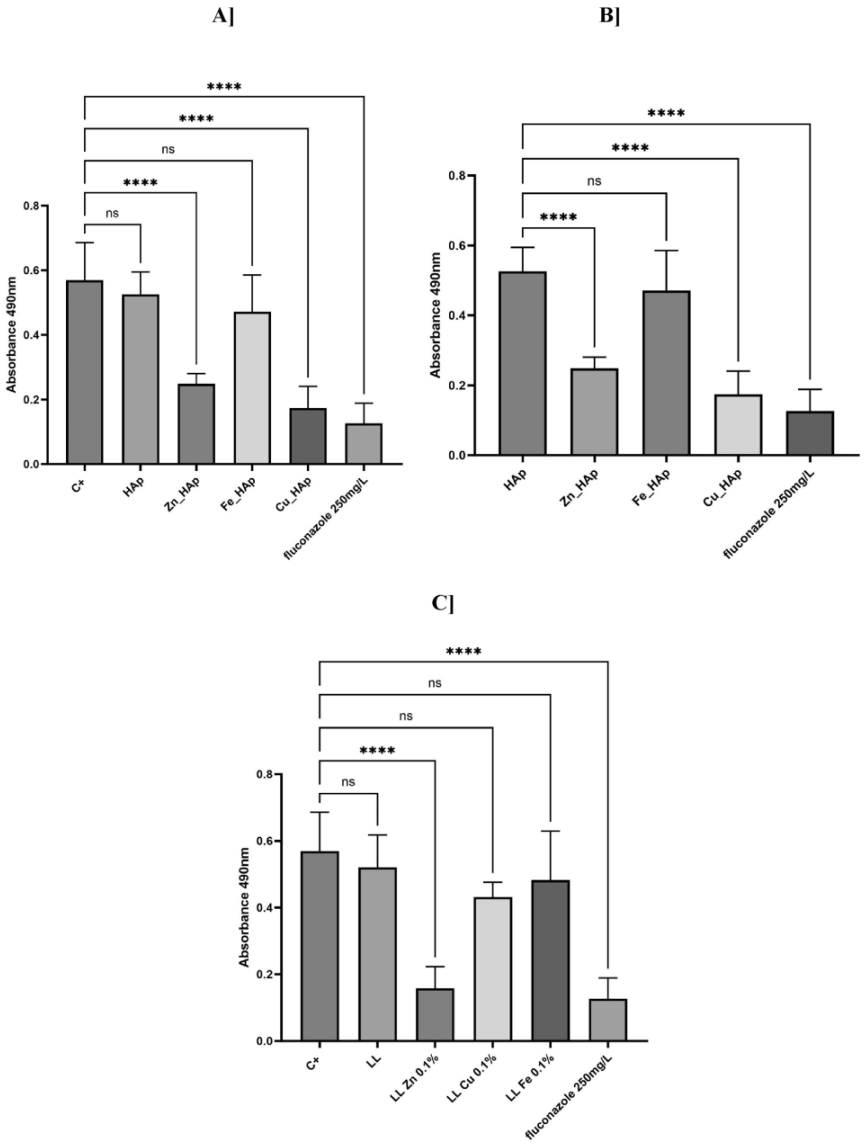

17 pav. *C. albicans* augimo sumažėjimas veikiant tiriamaisiais mėginiais: A) ir B) milteliai; C) kremai. Pasirinkus kaip tiriamąjį mėginį miltelius, pateikti du grafikai su skirtingais kontroliniais rinkiniais (C+ arba CHA).

Žvaigždutės rodo statistinį reikšmingumą, o ns – statistinio reikšmingumo nėra

1 lentelė. Apibendrintos tirtų miltelių ir kremų antimikrobinės savybės. „–“ – aktyvumo nėra; „+“ – silpnas aktyvumas prieš patogeną; „++“ – stipresnis aktyvumas prieš patogeną

Medžiaga	**Patogenas**		
	S. aureus	***P. aeruginosa***	***C. albicans***
CHA	−	−	−
Zn:CHA	+	−	++
Fe:CHA	−	−	−
Cu:CHA	+	−	++
LL	−	−	−
LL Zn	+	++	++
LL Cu	+	++	+
LL Fe	+	+	−

Metalais legiruotų hidroksiapatitų įterpimas į odos kremus davė daug žadančių rezultatų, ypač dėl biologinio suderinamumo ir antimikrobinių savybių. Hidroksiapatito antimikrobinis poveikis pirmiausia siejamas su didele kalcio jonų koncentracija, kuri sukelia kalcio stresą bakterijų ląstelėse ir lemia ląstelių žūtį. Tai reikšmingas atradimas, parodantis, kad mikrobų augimą galima kontroliuoti ne tik antibiotikais, o tai gali būti ypač vertinga dėl vis didėjančio atsparumo antibiotikams. Šį antimikrobinį poveikį sustiprina hidroksiapatito legiravimas metalų jonais. Biologinio suderinamumo tyrimai rodo, kad cinku ir variu pakeisti hidroksiapatitai yra citosuderinami, greičiausiai dėl mikroporėtos paviršiaus struktūros ir naudingo jonų išsiskyrimo bendro poveikio. Geležies pakaitalų variantai taip pat palaiko odos sveikatai svarbias ląstelių funkcijas, pavyzdžiui, žaizdų gijimą ir apsaugą nuo oksidacinio streso.

Atlikus centrifugavimo bandymus (5 minutes veikiant 3000 aps./min. išcentrinei jėgai) paaiškėjo, kad tiriamieji kosmetikos gaminiai išliko stabilūs. Šviežiai pagamintų produktų pH vertės pateko į reikiamą pH 5–7 intervalą, tačiau laikui bėgant šiek tiek pakito, palyginti su kontroliniais produktais. Produktų, kurių sudėtyje buvo 5 % CHA, Fe:CHA, Cu:CHA ir Zn:CHA, pH vertės po 4 mėnesių padidėjo nežymiai ir svyravo nuo 7,08 iki 7,12. Be to, visi mėginiai išlaikė tą pačią spalvą, kvapą ir tekstūrą. Ateityje atliekant tyrimus reikėtų sutelkti dėmesį į metalų jonų koncentracijos ir išsiskyrimo

mechanizmų optimizavimą, siekiant suderinti antimikrobinį aktyvumą ir biologinį suderinamumą. Be to, atlikus dozės ir atsako analizę, kuri yra labai svarbi darant toksikologinius vertinimus, siekiant nustatyti saugos ir veiksmingumo ribas, būtų galima gerokai pagilinti tyrimo įžvalgas.

Apibendrinant galima teigti, kad cinko priedas padidina antimikrobinį veiksmingumą, tačiau sumažina biologinį suderinamumą, o varis išlaiko ir didelį antimikrobinį aktyvumą, ir biologinį suderinamumą, todėl yra tinkamesnis kuriant medicinines ar kosmetines medžiagas. Kremai, kurių sudėtyje yra CHA su vario ir geležies jonais, taip pat pasižymi dideliu antimikrobiniu aktyvumu, kartu išsaugant gerą ląstelių gyvybingumą. Šie rezultatai rodo, kad svarbu optimizuoti šių medžiagų antimikrobinio veiksmingumo ir biologinio suderinamumo pusiausvyrą.

IŠVADOS

1. Katijoniniai pakaitalai pagerina biokeraminių medžiagų chemines, fizikines ir biologines savybes. Kalcio hidroksiapatito (CHA) pavyzdžiai, pakeisti pereinamaisiais metalais, ypač sidabru, geležimi, variu ir cinku, yra perspektyviausi, nes ateityje juos bus galima taikyti klinikinėje praktikoje, siekiant pagerinti įvairias terapines daugiafunkcines savybes. Šios fosfatinės nanostruktūrizuotos biomedžiagos, pasižyminčios dideliu biologiniu suderinamumu ir antibakteriniu poveikiu, yra labiausiai tinkamos taikyti daugelyje biomedicinos sričių, tokių kaip kaulų atstatymas ir audinių inžinerija, vaistų ir genų transportas, magnetinė taikinių terapija ir hiperterminis vėžio gydymas, biologinis vaizdinimas ir teranostika.
2. Pirmą kartą parodyta, kad, taikant skirtingo dydžio dvivalenčius katijonus hidroterminėmis sintezės sąlygomis (temperatūra, laikas), buvo matomas poveikis galutinių CHA produktų fazių grynumui ir morfologijai, o įterptų jonų pobūdis ir koncentracija buvo pagrindiniai veiksniai, lemiantys produktų savybes. Nustatyta, kad mažesni jonai (Mg^{2+} ir Mn^{2+}), palyginti su didesniais jonais (Sr^{2+} ir $Ba^{2+)}$, turėjo stipresnį slopinamąjį poveikį α-TCP hidrolizei. Iš visų tirtų jonų Mn^{2+} turėjo didžiausią, o Sr^{2+} – mažiausią slopinamąjį poveikį. Ba^{2+}turėjo didžiausią poveikį mėginio morfologijai.
3. Hidrotermiškai apdorojant 120 °C temperatūroje su 0,1 mol % įvairių katijonų, susidarė plokštelinių kristalitų pavidalo CHA. Į reakcijos mišinį įterpus didesnes metalų jonų koncentracijas, susidarė ir plokštelinių, ir šešiakampių lazdelių pavidalo dalelių. Tam tikrais atvejais buvo matomas savaiminis strypelių rinkimasis į gėlės pavidalo struktūras. Hidrotermiškai apdorojant 200 °C temperatūroje, strypelių pavidalo kristalai kartu su

plokšteliniais kristalais susidarė net ir tada, kai į reakcijos mišinį įterptamažiausia tirta metalo jonų koncentracija (0,1 mol %). Didėjant metalų koncentracijai, kartu didėjo ir strypelių pavidalo dalelių dalis.

4. Kristalinės kalcio hidroksiapatito dangos, pasižyminčios labai dideliu homogeniškumu ir dalelių dydžio pasiskirstymo laipsniu, buvo sėkmingai susintetintos iš $CaCO_3$ dangų naudojant tirpinimo ir nusodinimo metodą žemoje 80 ºC temperatūroje vandeninėje terpėje. Žemos temperatūros nusodinimo-tirpinimo metodas sėkmingai panaudotas iš dalies Cu^{2+} jonais pakeisto CHA sintezei. Tačiau CHA dangų, legiruotų Zn^{2+} jonais, formavimas minėtu metodu vyko ne taip sklandžiai, kaip tikėtasi. Išbandžius skirtingus sintezės metodus, dangos paviršiuje susidarė $Zn(OH)(NO_3)(H_2O)$, $Zn_3(OH)_4(NO_3)_2$, tačiau liko nesureagavusio kalcio karbonato.
5. Antibakterinis tyrimas su grynąja CHA danga neparodė jokių slopinimo zonų. Tyrime su Cu-CHA ir Zn legiruotomis dangomis ($Zn_3(OH)_4(NO_3)_2$ danga) po 24 val. inkubacijos 37 °C temperatūroje buvo aptiktos slopinimo zonos su *B. subtilis* bakterijų kolonijomis. Tačiau *E. coli* bakterijų kolonijai inhibicijos zonų neaptikta.
6. Kalcio hidroksiapatito ir metalų pakaitų pavyzdžiai (Fe:CHA, Cu:CHA ir Zn:CHA) buvo susintetinti nusodinimo metodu iš amorfinio CaP, paskui – kietafazių reakcijų su α-TCP būdu ir galiausiai atliekant CHA hidroterminę sintezę. Ištirtas Fe^{3+}, Cu^{2+} ir Zn^{2+} pakeitimo poveikis CHA fazės grynumui. Ypač išryškėjo CHA ir Zn:CHA fazių grynumas, o α- ir β-TCP fazės susidarė esant Fe^{3+} ir Cu^{2+} jonams.
7. Nustatyta, kad metalais pakeisti CHA mėginiai pasižymi perspektyviu antimikrobiniu potencialu, kuris gali būti naudojamas medicinoje ir medžiagų moksle. Šios medžiagos pasižymi ne tik veiksmingomis antimikrobinėmis savybėmis, bet ir palankiu biosuderinamumo profiliu.
8. Pridėjus cinko padidėja antimikrobinis veiksmingumas, tačiau sumažėja biologinis suderinamumas, o varis išlaiko ir didelį antimikrobinį aktyvumą, ir biologinį suderinamumą, todėl yra idealus pasirinkimas kuriant medicinines ar kosmetines medžiagas. Kremai, kurių sudėtyje yra CHA su vario ir geležies jonais, taip pat pasirodė esantys stiprūs antimikrobiniai produktai, pasižymintys geru ląstelių gyvybingumu. Šie rezultatai rodo, kad svarbu optimizuoti šių medžiagų antimikrobinio aktyvumo ir biologinio suderinamumo pusiausvyrą.

CURRICULUM VITAE

Laura Lukavičiūtė-Navickienė

Education

2012–2018 m.	Faculty of Medicine, Vilnius University	Medical Doctor (Master's degree, *cum laude*)
2018–2020 m.	Faculty of Medicine, Vilnius University; Institute of Clinical Medicine; Clinic of Infectious Diseases and Dermatovenereology	Junior Resident, Dermatovenereology Residency Programme
2020–2022 m.	Faculty of Medicine, Vilnius University; Institute of Clinical Medicine; Clinic of Infectious Diseases and Dermatovenereology	Senior Resident, Dermatovenereology Residency Programme
2021–2025 m.	Faculty of Chemistry, Vilnius University; Department of Inorganic Chemistry	PhD Candidate

Since 2022, I have been practising as a dermatologist-venereologist. My clinical experience encompasses dermato-oncology, dermatological surgery, inflammatory skin diseases, and aesthetic dermatology, and I continually refine these competencies within a leading tertiary-level healthcare institution.

In terms of professional service, I am a long-standing member of the Lithuanian Association of Dermatologists and Venereologists, the European Academy of Dermatology and Venereology, and the International Dermoscopy Society. I participate in volunteer initiatives to raise skin cancer awareness and deliver education, and I have contributed to the development of national guidelines for melanoma diagnosis and treatment.

Academically, I am a Junior Research Fellow and Lecturer at Vilnius University, teaching dermatovenereology to students of medicine, dentistry, and public health in Lithuanian and English; I lead a student research network dedicated to advancing dermatological science; my interests include the synthesis of calcium hydroxyapatite, structure–property–function relationships, and applications in cosmetics and aesthetic dermatology; and I routinely participate in research spanning interdisciplinary studies at the interface of mental health and dermatology, as well as clinical trials on laser

tattoo-removal technologies and on biologic therapies for psoriasis and hidradenitis suppurativa.

For professional development and scientific collaboration, I regularly attend dermatology conferences and congresses in Lithuania, Europe, and the United States, and participate in hands-on clinical training in Greece, Belgium, Portugal, and the Czech Republic.

ACKNOWLEDGEMENTS

The achievement of this PhD thesis has been both a challenge and a rewarding journey, which would not have been possible without the help and support of many people around me.

Foremost, I would like to express my deepest gratitude to my scientific supervisor, Prof. habil. Dr. Aivaras Kareiva, for his invaluable guidance, constant encouragement, and inspiring motivation throughout the course of my doctoral studies. His expertise, constructive advice, and continuous support were of great significance for the successful completion of this work. I am also sincerely thankful to my supervisor Assoc. Prof. Dr. Edita Garškaitė.

I would like to extend my sincere appreciation to my PhD thesis consultant, Assoc. Prof. Dr. Rūta Gancevičienė, for her professional guidance, valuable insights, and kind understanding. As a dermatologist and researcher, her expertise was not only scientifically enriching but also personally inspiring, and her advice was of great importance throughout my research.

Furthermore, I am very grateful to all members of the sol-gel research group for their assistance, cooperation, and support during my studies. I would like to express special thanks to Assoc. Prof. Dr. Živilė Stankevičiūtė and to Dr. Eva Raudonytė-Svirbutavičienė for their continuous help, valuable suggestions, and encouragement, which were essential during the preparation of this thesis.

Finally, my heartfelt gratitude goes to my family for their love, patience, and unwavering support. I owe special thanks to my husband, who stood by me at every step of this journey. Their understanding and encouragement have been indispensable in the completion of this work.

LIST OF PUBLICATIONS SUMMARIZED IN PHD THESIS WITH CONFERENCE PARTICIPATION

LIST OF PUBLICATIONS

E. Raudonyte-Svirbutaviciene, **L. Lukaviciute**, Z. Moravec, J. Pinkas, T. Goto, T. Sekino, A. Zarkov, A. Kareiva. Tailoring hydroxyapatite morphology via the effect of divalent cations on the hydrolysis of α-TCP: Oriented crystal growth towards the application in water treatment. *Ceramics International,* **49** (2023) 32816-32825.

L. Lukaviciute, J. Karciauskaite, I. Grigoraviciute, D. Vasiliauskiene, D. Sokol, A. Kareiva. Calcium Hydroxyapatite Coatings: Low Temperature Synthesis and Investigation of Antibacterial Properties. *Coatings*, **13** (2023) 1991.

E. Raudonyte-Svirbutaviciene, G. Klydziute, **L. Lukaviciute**, A. Antuzevics, A. Balciunaite, E. Norkus, A. Beganskiene, A. Zarkov, A. Kareiva. Hydrothermal synthesis of Mn^{2+} and Cu^{2+} - doped calcium hydroxyapatite: morphological features and importance of EPR insights. *Ceramics International,* **50** (2024) 4005-4013.

L. Lukaviciute, R. Ganceviciene, K. Tsuru, K. Ishikawa, J.-C. Yang, I. Grigoraviciute, A. Kareiva. Cationic Substitution Effects in Phosphate-Based Bioceramics - A Way Towards Superior Bioproperties. *Ceramics International,* **50** (2024) 34479-34509.

L. Lukaviciute, A. Lukowiak, Z. Stankeviciute, A. Junka, M. Mortimer, A. Zarkov, J.-C. Yang, R. Ganceviciene, A. Kareiva. Cytocompatible and antibacterial Fe-, Cu- and Zn-substituted calcium hydroxyapatite materials for skin applications. *Ceramics International,* **51** (2025) 11286-11296.

CONFERENCE PARTICIPATION

L. Lukavičiūtė, G. Klydžiūtė, E. Raudonytė-Svirbutavičienė, A. Žarkov, A. Kareiva. Hydrothermal Synthesis and Characterisation of Fe^{2+} doped calcium-deficient hydroxyapatite. 24th International Conference-School "Advanced Materials and Technologies 2024". Palanga, Lithuania, August 22-26, (2022).

L. Lukaviciute, G. Klydziute, E. Raudonyte-Svirbutaviciene, A. Zarkov, A. Beganskiene, A. Kareiva. The Influence of Fe2+ on the Transformation of α-TCP. Int. Conference „Functional Inorganic Materials 2022", Vilnius, Lithuania, October 6-8, (2022) 47.

L. Lukaviciute, A. Lukowiak, Z. Stankeviciute, A. Junka, M. Mortimer, A. Zarkov, A. Kareiva. Metal-substituted calcium hydroxyapatite: synthesis and application in the production of cosmetic products. 2nd International Conference on Advanced Materials for Bio-Related Applications ”AMBRA 2024”, Wroclaw, Poland, May 19-23, (2024) 42.

COPIES OF PUBLICATIONS

Ceramics International 49 (2023) 32816–32825

Contents lists available at ScienceDirect

Ceramics International

journal homepage: www.elsevier.com/locate/ceramint

Tailoring hydroxyapatite morphology via the effect of divalent cations on the hydrolysis of α-TCP: Oriented crystal growth towards the application in water treatment

Eva Raudonyte-Svirbutaviciene [a,*], Laura Lukaviciute [a], Zdenek Moravec [b], Jiří Pinkas [b], Tomoyo Goto [c,d], Tohru Sekino [c], Aleksej Zarkov [a,**], Aivaras Kareiva [a]

[a] Institute of Chemistry, Faculty of Chemistry and Geosciences, Vilnius University, Naugarduko 24, LT-03225, Vilnius, Lithuania
[b] Department of Chemistry, Faculty of Science, Masaryk University, Kotlarska 2, CZ-61137, Brno, Czech Republic
[c] SANKEN (The Institute of Scientific and Industrial Research), Osaka University, 8–1 Mihogaoka, Ibaraki, Osaka, 567-0047, Japan
[d] Institute for Advanced Co-Creation Studies, Osaka University, 1-1 Yamadaoka, Suita, Osaka, 565-0871, Japan

ARTICLE INFO

Keywords:
Hydrothermal synthesis
Hydroxyapatite
Divalent cations
Crystal growth
Adsorption

ABSTRACT

The hydrothermal synthesis method to produce calcium hydroxyapatite (HA) of controlled morphology without the use of organic additives is developed in this study. The influence of smaller (Mg^{2+}, Mn^{2+}) and larger (Sr^{2+}, Ba^{2+}) ions on the hydrolysis of α-TCP and crystal growth of HA particles was investigated. It was revealed that both the hydrothermal synthesis conditions (temperature, time) and the nature and concentration of the foreign ion affected the phase purity and morphology of the final products. Of all the ions investigated, Mn^{2+} had the highest, and Sr^{2+} had the lowest inhibiting effect on the hydrolysis process of α-TCP. Under certain synthesis conditions, we were able to obtain samples consisting of plate-like or rod-like particles only. The dye adsorption test revealed that the adsorption of plate-like particles for cationic dyes was more efficient, possibly, due to the higher surface area (S_{BET}). Upon normalizing the test results to S_{BET}, it became apparent that the electrostatic attraction between HA particles and dye molecules also impacted the adsorption efficiency. Rod-like particles had a higher ratio of exposed (*a,m*)-planes and hence lower zeta potential, resulting in increased adsorption of the cationic dye.

coatings

MDPI

Article

Calcium Hydroxyapatite Coatings: Low-Temperature Synthesis and Investigation of Antibacterial Properties

Laura Lukaviciute [1], Justina Karciauskaite [1], Inga Grigoraviciute [1], Dovile Vasiliauskiene [2], Denis Sokol [1] and Aivaras Kareiva [1,*]

[1] Institute of Chemistry, Vilnius University, Naugarduko 24, LT-03225 Vilnius, Lithuania; lukaviciute.laura@gmail.com (L.L.); justina.karciauskaite@chgf.stud.vu.lt (J.K.); inga.grigoraviciute@gmail.com (I.G.); denis.sokol@chgf.vu.lt (D.S.)

[2] Department of Chemistry and Bioengineering, Vilnius Gediminas Technical University, Saulėtekio al. 11, LT-10223 Vilnius, Lithuania; dovile.vasiliauskiene@vilniustech.lt

* Correspondence: aivaras.kareiva@chgf.vu.lt

Abstract: In the present work, the low-temperature synthesis of substituted calcium hydroxyapatite ($Ca_{10}(PO_4)_6(OH)_2$, HAP) with copper and zinc ions on titanium substrates was performed. Initially, $CaCO_3$ coatings were synthesised on titanium substrate using the sol-gel method at 550 °C in a CO_2 atmosphere. Crystalline calcium hydroxyapatite was then synthesised from these $CaCO_3$ coatings through the dissolution-precipitation method at low temperature (80 °C). X-ray diffraction (XRD) analysis, FTIR and Raman spectroscopies, and scanning electron microscopy (SEM) were employed to evaluate the phase composition, surface functional groups, crystallinity, and morphology of the coatings. The results showed the formation of hexagonal HAP particles with a size of 20 nm at low temperature, exhibiting high homogeneity in particle size distribution. In the calcium hydroxyapatite, some of the Ca^{2+} ions were replaced by Cu^{2+} ions. Heating the mixture of $Ca(NO_3)_2$ and $Cu(NO_3)_2$ solutions at 550 °C in a CO_2 atmosphere led to the formation of copper hydroxide carbonate (malachite, $Cu_2(OH)_2CO_3$) along with $CaCO_3$. The reaction between the sol-gel precursor obtained and Na_2HPO_4 resulted in the formation of copper-substituted hydroxyapatite (Cu-HAP). Different synthesis methods were tested with Zn^{2+} ions, and on the surface of the coating, $Zn(OH)(NO_3)(H_2O)$, $Zn_3(OH)_4(NO_3)_2$, and unreacted $CaCO_3$ were formed. Antibacterial properties of the coatings were tested using the inhibition zone method. No inhibition zones were observed for HAP. However, in the Cu and Zn containing coatings, inhibition zones were observed in the presence of a colony of *B. subtilis* bacteria. However, no inhibition zones were detected in the presence of *E. coli* bacteria.

Keywords: $Ca_{10}(PO_4)_6(OH)_2$; Cu and Zn containing hydroxyapatite; coatings; sol-gel method; dissolution-precipitation method

check for updates

Citation: Lukaviciute, L.; Karciauskaite, J.; Grigoraviciute, I.; Vasiliauskiene, D.; Sokol, D.; Kareiva, A. Calcium Hydroxyapatite Coatings: Low-Temperature Synthesis and Investigation of Antibacterial Properties. *Coatings* **2023**, *13*, 1991. https://doi.org/10.3390/coatings13121991

Academic Editors: Egemen Avcu, Mert Guney and Yasemin Yıldıran Avcu

Received: 23 October 2023
Revised: 20 November 2023
Accepted: 20 November 2023
Published: 23 November 2023

1. Introduction

Calcium hydroxyapatite ($Ca_{10}(PO_4)_6(OH)_2$, HAP) constitutes the primary inorganic component of bone tissue and exhibits exemplary biocompatibility [1]. Morphologically, hydroxyapatite particles in bone can manifest in diverse geometries—spherical, plate-like, or needle-like—and typically exhibit dimensions on the order of 40–60 nm in length, 20 nm in width, and 1.5–5 nm in thickness [2,3]. Hydroxyapatite accounts for up to 60% of bone tissue by weight and as much as 97% in tooth enamel [1]. Due to its high surface-area-to-volume ratio, reactivity, and biomimetic properties, nano-HAP serves as an optimal material for orthopaedic implant coatings and bone-substitute fillers [4].

Hydroxyapatite-based implant materials often feature a porous, interlinked architecture that mimics the intracellular matrix, thus facilitating cellular proliferation and tissue regeneration [5,6]. This structural design also enhances osseointegration by establishing a rigid mechanical interface with the surrounding biological tissues, thereby minimising fibrous tissue formation [7,8].

This ionic flexibility is in alignment with the naturally occurring human bone mineral, which comprises non-stoichiometric nanocrystalline apatites. These apatites possess structural imperfections owing to the substitution of calcium, phosphate, and hydroxide ions by a range of ions such as Na, Mg, Zn, Sr, K, F, Cl, Si, and CO_3^{2-} [9–11]. Such adaptability underlines the modifiable bioactive properties of HAP through lattice incorporation of diverse substituents [12,13].

Despite the promise of hydroxyapatite coatings, challenges persist in optimising their synthesis and functional properties. Various substrates such as titanium, quartz, and silicon have been employed for the deposition of HAP coatings via the aqueous sol-gel method, which is contingent upon precise control of temperature, pH, and precursor concentrations [14]. This technique, however, typically necessitates elevated temperatures to facilitate the crystallisation of hydroxyapatite, potentially resulting in heterogeneous coatings with domains of varying grain sizes [14]. Furthermore, synthesis of hydroxyapatite coatings on titanium substrates at elevated temperatures may induce the formation of a TiO_2 phase, thereby compromising adhesion to the substrate [15]. Consequently, there is an ongoing pursuit to develop innovative methodologies for synthesising hydroxyapatite coatings that faithfully replicate the characteristics of natural bone tissue.

The objective of this study is to investigate the potential of substituting Ca^{2+} ions with Zn^{2+} and Cu^{2+} ions in HAP coatings using a low-temperature sol-gel dissolution-precipitation deposition approach. The suggested method is promising for the preparation of Cu-HAP coatings; however, the formation of Zn-HAP did not proceed. It was found that in the Cu and Zn containing coatings, inhibition zones were observed in the presence of a colony of *B. subtilis* bacteria. However, no inhibition zones were detected in the presence of *E. coli* bacteria.

2. Materials and Methods

2.1. Synthesis and Materials

2.1.1. Synthesis of Calcium Carbonate

The synthesis of the HAP porous layers was carried out on Ti (Thermo Scientific, Waltham, MA, USA; 1.0 mm thick, 99.2%; CAS 7440-32-6) wafers, which were laser cut (1 × 1 cm) in the open access mechanics centre. The titanium wafers were mechanically abraded to remove the oxide film formed in the air and surface scratches. The titanium plates were mechanically abraded with sandpaper of different grit sizes (1000–2500 grit). The plates were scrubbed for 1 min on each side. The plates were then chemically treated by soaking for 30 min at 70 °C in a solution of 96% 5 mL H_2SO_4 (Chempur, Karlsruhe, Germany, 99.7%) and 7% 0.35 mL HCl (Chempur, 37%). After soaking, the plates were washed in an ultrasonic bath with distilled water and ethanol for 5 min. The cleaned plates were dried overnight at room temperature. The prepared plates were used for the synthesis of $CaCO_3$ and HAP.

For the preparation of the solution, 11.807 g of $Ca(NO_3)_2{\cdot}4H_2O$ (Alfa Aesar, Ward Hill, MA, USA, 99.6%) was weighed and dissolved in 100 mL of ethanol (Vilniaus degtine, Vilniaus, Lithuania, 99.8%). Concentration was 0.5 mol/l. The solution was subjected to magnetic stirring at a temperature of 30 °C until complete dissolution was confirmed. The submerged plates were then placed in a furnace, manufactured by Nabertherm, New Castle, Germany, for heat treatment. A CO_2-rich environment within the furnace was established by positioning ceramic plates coated with activated carbon adjacent to the submerged plates. The furnace was programmed to elevate its internal temperature from an initial 20 °C to 550 °C at a rate of 3 °C/min. Upon reaching 550 °C, this temperature was maintained for a duration of 5 h. During the reaction, $Ca(NO_3)_2$ was thermally decomposed into CaO, followed by a reaction of the CaO with the CO_2 to form calcite. Before removal from the furnace, the furnace was cooled by lowering the temperature to 20 °C at a rate of 3 °C/min.

2.1.2. Synthesis of Calcium Hydroxyapatite

For the synthesis of HAP, a solution was prepared by weighing 0.14 g of Na_2HPO_4 (Carl Roth, Karlsruhe, Germany, 99%) and 0.6057 g of TRIS ($C_4H_{11}NO_3$) (Carl Roth, 99%) buffer. The weighed materials were dissolved in 100 mL of distilled water. The solution was stirred on a magnetic stirrer until dissolved and maintained at 30 °C. The pH of the solution was alkaline (approximately 9–10). After the dissolution of the materials, the solution was poured onto $CaCO_3$-synthesised plates and soaked for 7 days at 80 °C. After removal from the solution, the samples were washed with distilled water, dried, and used for further analysis. The formation of HAP follows this reaction:

$$10\ CaCO_3 + 6Na_2HPO_4 + 2\ H_2O = Ca_{10}(PO_4)_6(OH)_2 + 8\ NaHCO_3 + 2\ Na_2CO_3 \quad (1)$$

2.1.3. Synthesis of Substituted Calcium Hydroxyapatite

In order to introduce Cu^{2+} ions, a mixture of $Ca(NO_3)_2$ and $Cu(NO_3)_2$ was prepared at a concentration of 0.5 mol/l. 5.9036 g of $Ca(NO_3)_2{\cdot}4H_2O$ and 5.814 g of $Cu(NO_3)_2{\cdot}2.5H_2O$ (Sigma-Aldrich, St. Louis, MO, USA, 99.8%) were weighed. The substances were dissolved in 100 mL of ethanol. After the solution had been prepared, the chemically and mechanically treated titanium plates were dropped into the solution in a porcelain dish to submerge. This was then heated in an oven under a CO_2 atmosphere in a previously mentioned manner. After the heating procedure, the plates were dipped into a solution of 0.14 g Na_2HPO_4 + 0.6057 g TRIS buffer (dissolved in distilled water) and soaked for one week at 80 °C. A similar procedure was repeated for the introduction of Zn^{2+} ions (weighed 7.4365 g $Zn(NO_3)_2{\cdot}6\ H_2O$; Chempur, 99.7%). To successfully alloy Zn^{2+} ions, the synthesis was also carried out by direct dropping of already synthesised HAP onto titanium plates into $Zn(NO_3)_2{\cdot}6H_2O$ solution. In total, 7.4365 g of the material was weighed and dissolved in 100 mL of distilled water. A further modification of the Zn-HAP synthesis was also performed. First, $CaCO_3$ was synthesised according to the methodology described for the synthesis of $CaCO_3$ on Ti substrates, then Ti plates containing the synthesised calcium carbonate were dipped into a solution of 0.14 g Na_2HPO_4 + 0.6057 g TRIS buffer + 7.4365 g $Zn(NO_3)_2{\cdot}6$ H2O, which was prepared by dissolving these materials in distilled water.

2.2. Characterisation

X-ray diffraction measurements were carried out to determine the phase composition of the synthesised products. This method of analysis is used to study the crystalline structure. The measurements were carried out on a Rigaku miniFlex II diffractometer (Applied Rigaku Technologies, Inc., Cedar Park, TX, USA) (Cu-Kα radiation, λ = 0.1542 nm at 30 kV 15 mA). The diffracted X-rays were recorded between 10° and 70° (2θ). A Hitachi TM3000 and a Hitachi SU70 (Tokyo, Japan) scanning electron microscope were used to study the morphology and microstructure of the samples. These microscopes were used for EDX analysis of the samples. Raman spectra were recorded at room temperature using a combined Raman and scanning near-field optical microscope (SNOM) WiTec Alpha 300 R (WiTec, Ulm, Germany) with a 532 nm excitation laser source (power 40.9 mW). Fourier transform infrared (FTIR) spectroscopy measurements were carried out on an FTIR spectrometer (PerkinElmer, Inc., Waltham, MA, USA). Evaluation of the antibacterial properties of synthesised coatings on Ti substrates revealed no zones of hydroxyapatite (HAP) inhibition in the presence of Gram-negative Escherichia coli and Gram-positive Bacillus subtilis bacteria. The cultures of *E. coli* and *B. subtilis* bacteria were incubated overnight in liquid LB medium, 10 g/L NaCl, 5 g/L yeast extract, at 37 ° C temperature. After this the culture of bacteria were centrifuged and diluted in sterile 0.9% NaCl to 10^6 units/mL. 100 µL of pre-pared bacteria culture were inoculated in LB agar medium. Plates with HAP, Cu-HAP, and $Zn_3(OH)_4(NO_3)_2$ were placed on these *E. coli* and *B. subtilis* inoculants; prepared samples were incubated at 37 °C temperature for 24 h. After these hours emerges zone of inhibition of HAP, Cu-HAP, and $Zn_3(OH)_4(NO_3)_2$ coatings.

Two or three measurements were conducted in all of the sample preparation and any data processing steps.

3. Results

3.1. Synthesis and Characterization of HAP

The phase composition of the coatings was determined by XRD. The XRD patterns showed that a layer of $CaCO_3$ [PDF:96-154-7348] was formed on the Ti substrate. At $2\theta = 29.4°$, the most intense peak characteristic of calcite ($CaCO_3$) was visible. The data were in a good agreement with literature [16]. Crystalline calcium hydroxyapatite was then synthesised from these $CaCO_3$ coatings through the dissolution-precipitation method at low temperature (80 °C). The XRD results clearly showed the formation of HAP [PDF: 96-431-7044] with characteristic reflections in the 31–32.5° 2θ angle range (Figure 1). The peaks of $CaCO_3$ [PDF: 96-154-7348] are also identified, proving that some $CaCO_3$ still remains unreacted. In addition, intense diffraction peaks of the Ti substrate are visible. Thus, it can be concluded that a layer of calcium hydroxyapatite has formed on the titanium substrate, which is supported by the literature data [17]. The Raman absorption bands (1084 cm-1, symmetric stretching), (716 cm-1, in-plane bending), (276 and 146 cm- 1, lattice modes) of $CaCO_3$ coating are consistent with calcite [18]. Figure 1 also shows Raman spectrum of HAP coating. The PO_4^{3-} peaks at 590, 950, and 1085 cm^{-1} of the phosphate group oscillations belonging to HAP. The peak around 285 cm^{-1} is attributed to Ca-PO_4 and Ca-OH bonds. The FTIR spectrum of the calcium hydroxyapatite layer on a Ti substrate is depicted in Figure 1 as well. The FTIR spectra shown here identify absorption peaks for PO_4^{3-} (560–600 cm^{-1}, ~600 cm^{-1} and 1000–1100 cm^{-1}), OH^- (3600–3500 cm^{-1} and 630 cm^{-1}), CO_3^{2-} (1460–1530 cm^{-1}), as well as for HPO_4^{2-} (610–615 cm^{-1}) [19]. Thus, it can be concluded that the Raman and FTIR spectroscopy results obtained confirmed the X-ray diffraction data for the successful formation of $Ca_{10}(PO_4)_6(OH)_2$ coatings on the Ti substrate.

The morphological features of the $CaCO_3$ and $Ca_{10}(PO_4)_6(OH)_2$ coatings were investigated by SEM. The calcium carbonate layers were composed of sub-micrometre (up to 1 μm) rhombohedral particles which form a continuous calcite layer. Hexagonal HAP particles of 20 nm in size were formed at low temperature. A particular morphological feature of the synthesised HAP (Figure 1) is that a very high degree of homogeneity and distribution of particle size is achieved.

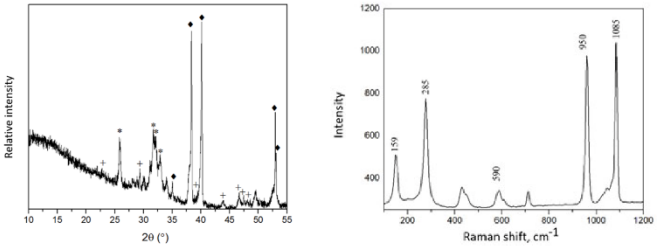

Figure 1. *Cont.*

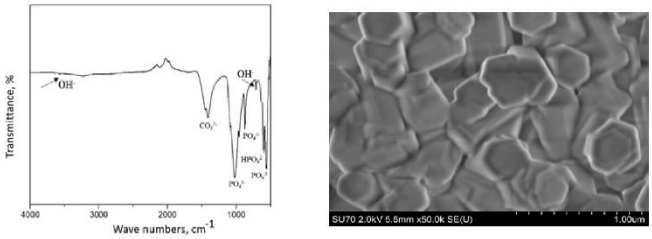

Figure 1. XRD pattern (**top**, **left**), Raman spectrum (**top**, **right**), FTIR spectrum (**bottom**, **left**), and SEM micrograph (**bottom**, **right**) of a calcium hydroxyapatite coating on a Ti substrate. Diffraction reflections: *—HAP [PDF: 96-431-7044]; ♦—Ti [PDF: 96-901-6191]; +—$CaCO_3$ [PDF: 96-154-7348].

3.2. Synthesis and Characterization of Cu-HAP

The phase crystallinity and purity of Cu^{2+}-substituted HAP specimens synthesised by low-temperature sol-gel and dissolution-precipitation method were also investigated by means of XRD analysis. It was determined that during the heating of mixture of $Ca(NO_3)_2$ and $Cu(NO_3)_2$ solutions in a CO_2 atmosphere, in addition to $CaCO_3$, a copper hydroxide carbonate $Cu_2(OH)_2CO_3$ (malachite) had also formed. It is not surprising, since it is known that pure $CuCO_3$ does not form in an aqueous media under normal conditions:

$$2\,Cu(NO_3)_2 + CO_2 + 4\,NaOH \rightarrow Cu_2(OH)_2CO_3 + 4\,NaNO_3 + H_2O \quad (2)$$

Figure 2 represents the XRD patterns of the HAP coatings where Ca^{2+} ions are substituted by Cu^{2+} ions.

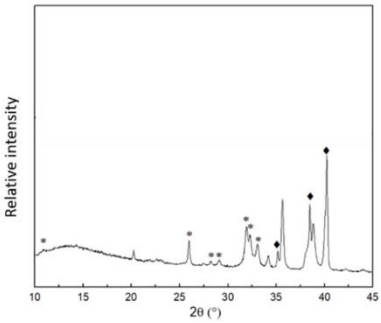

Figure 2. XRD pattern of the Cu-HAP coating obtained on the Ti substrate. Diffraction reflections: *—HAP [PDF: 96-431-7044]; ♦—Ti [PDF:96-901-6191.

The XRD results indicate that the low-temperature precipitation-dissolution method can be successfully used for the synthesis of partially Cu^{2+} ion-substituted HAP. Treatment

of $CaCO_3$ containing a small amount of impure $Cu_2(OH)_2CO_3$ with sodium hydrogen phosphate produces copper-substituted hydroxyapatite (Cu-HAP):

$$10-x\ CaCO_3 + x\ Cu_2(OH)_2CO_3 + 6\ Na_2HPO_4 + 2\ H_2O = Ca_{10-x}Cu_x(PO_4)_6(OH)_2 + x\ Cu(OH)_2 + 8\ NaHCO_3 + 2\ Na_2CO_3 \quad (3)$$

Figure 3 shows the FTIR spectrum of the Cu-HAP coating. The absorption bands at 970 and 1031 cm^{-1} correspond to symmetric and asymmetric vibrations in the PO_4^{3-} ion. Bending vibrations in the PO_4^{3-} ion correspond to absorption bands at 599-567 cm^{-1}. The absorption bands of carbonate are at 870 and 1400 cm^{-1} [20].

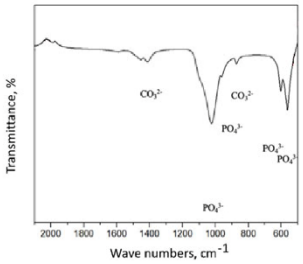

Figure 3. FTIR spectrum of the Cu-HAP coating obtained on the Ti substrate.

Figure 4 represents the Raman spectrum of a HAP coating substituted with Cu^{2+} ions. In this Raman spectrum, the band at 428 cm^{-1} of the phosphate group vibrations are visible, while the bands at 590, 607 cm^{-1} also belong to the PO_4^{3-} asymmetric vibrations of the HAP. The band at 957 cm^{-1} corresponds to a fully symmetric stretching of PO_4^{3-}. The sharpness of this band confirms a good crystallinity of the Cu-HAP coating [21].

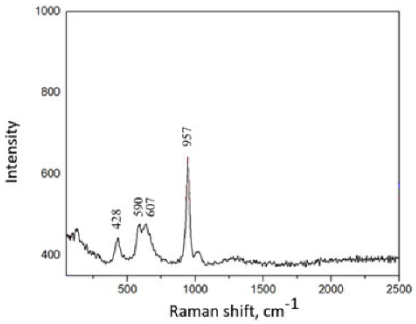

Figure 4. Raman spectrum of the Cu-HAP coating obtained on the Ti substrate.

3.3. Synthesis and Characterization of Zn-HAP

However, the formation of HAP coatings substituted with Zn^{2+} ions by the above preparation method did not proceed. The results presented in the XRD pattern of the coating synthesised by the low-temperature precipitation-dissolution method (by forming

mixed carbonates from a mixture of $Zn(NO_3)_2 \cdot 6H_2O$ and $Ca(NO_3)_2 \cdot 4H_2O$ and dropping the product into Na_2HPO_4 + TRIS buffer solution) confirmed only formation of calcite which was not transformed to the Zn-HAP. Once again, we can conclude that HAP substituted by zinc ions has not formed by this synthesis method. The XRD patterns contained only diffraction reflections of calcium carbonate.

Therefore, different variations of the proposed synthesis method were tested to obtain a Zn-HAP coating on Ti substrate. An attempt was made to synthesise the Zn-HAP coating by direct immersing of the already synthesised HAP coating on Ti into $Zn(NO_3)_2$ solution. The reaction was carried out under the same conditions at 80 °C for one week. The XRD pattern of the resulting product is shown in Figure 5.

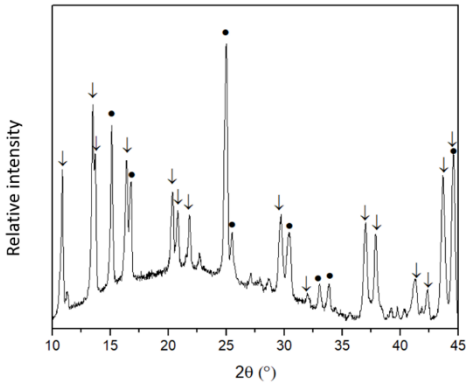

Figure 5. XRD pattern of HAP doped with Zn^{2+} coatings synthesised by immersing the HAP coating on Ti in zinc nitrate solution. Diffraction reflections: •—TiO_2 [PDF: 96-152-8779]; ↓—$Zn(OH)(NO_3)(H_2O)$ [PDF:96-152-9913].

Unexpectedly, the Zn-HAP did not form, and also the HAP coating dissolved, although the solubility of HAP is very low. An even more unexpected result was the formation of almost single phase zinc hydroxide nitrate monohydrate $Zn(OH)(NO_3)(H_2O)$ on the Ti substrate. Thus, during this synthetic approach almost monophasic $Zn(OH)(NO_3)(H_2O)$ instead of Zn-HAP has formed on Ti substrate.

A third synthetic approach was also selected to obtain the Zn-HAP coating. The $CaCO_3$ coating synthesised on Ti substrate was dipped into a solution of Na_2HPO_4 + TRIS buffer + $Zn(NO_3)_2 \cdot 6H_2O$ and stored therein for one week at 80 °C. Again, instead of Zn-HAP, the formation of $Zn(OH)(NO_3)(H_2O)$ along with small amount of $Zn_3(OH)_4(NO_3)_2$ and unreacted calcium carbonate was observed on the Ti surface.

3.4. SEM and EDX Analysis

The SEM images clearly showed that the addition of copper to the HAP also changes the morphology of the particles. Instead of the hexagonal 20 nm particles of HAP, fibrous crystallites with a snowflake shape of about 1 μm have formed (see Figure 6). The volumetric snowflake crystallites are composed of interlocking needles between 0.5 nm and 1 nm in size. Both the partially altered Cu-HAP samples are characterised by a high degree of homogeneity in particle size distribution. The morphology of the Zn^{2+}-containing samples synthesised by forming mixed carbonates from a mixture of $Zn(NO_3)_2 \cdot 6H_2O$ and $Ca(NO_3)_2 \cdot 4H_2O$ and immersing the product into a Na_2HPO_4 + TRIS buffer solution

differs considerably from that of the HAP and Cu-HAP. The representative SEM image of this sample is also shown in Figure 6. It can be seen that homogeneous coatings with some cracks have formed. The coatings are composed of planar crystals larger than 1 µm forming a continuous coating. Few accumulations of smaller particles are also visible on the Ti surface.

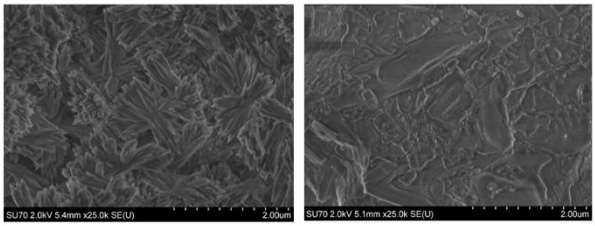

Figure 6. SEM micrographs of Cu-HAP (**left**) of $Zn_3(OH)_4(NO_3)_2$ coatings (**right**) fabricated on Ti substrate.

Elemental analysis of the synthesised Cu and Zn containing coatings was carried out using EDX analysis. The EDX spectra of both samples are presented in Figure 7.

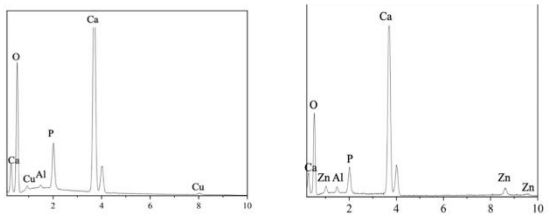

Figure 7. EDX spectra of Cu-HAP (**left**) of $Zn_3(OH)_4(NO_3)_2$ coatings (**right**) fabricated on Ti substrate.

In the case of Cu-HAP coating, the Ca/P ratio of ~1,62 was found to be almost identical to the calcium/phosphorus ratio in stoichiometric HAP (1,67). The molar ratio of calcium to copper was Ca:Cu = 1:0.033, i.e., about 3.3 mol% of the calcium was likely replaced by copper. The formula for the synthesis product could then be written $Ca_{9,7}Cu_{0,3}(PO_4)_6(OH)_2$ or $Ca_{9,85}Cu_{0,15}(PO_4)_6(OH)_2$, if the reaction (see Equation (3)) produced a further stoichiometric amount of copper hydroxide. From the EDX measurements of the sample with zinc, the Ca/P ratio determined was completely unreasonable as it did not correspond to any possible calcium/phosphorus ratio in known phosphates. Although calcium and phosphorus were detected in the synthesised coating, XRD analysis failed to detect calcium phosphate crystalline phases. It is likely that a significant amount of amorphous calcium carbonate and/or a very small amount of calcium hydroxyapatite remained in the coating. The EDX spectrum shows that the coating synthesised contains a significant amount of zinc.

3.5. Antibacterial Properties

Evaluation of the antibacterial properties of synthesised coatings on Ti substrates revealed no zones of hydroxyapatite (HAP) inhibition in the presence of Gram-negative *Escherichia coli* and Gram-positive *Bacillus subtilis* bacteria (Figure 8).

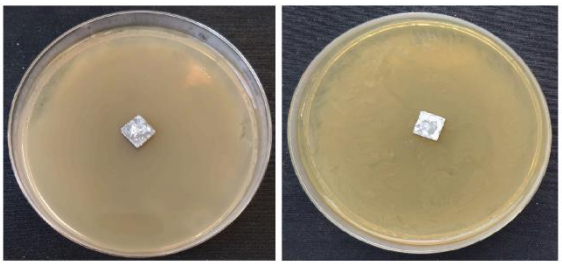

Figure 8. Results of antibacterial performance tests of low-temperature synthesised HAP coatings on Ti with (**left**) *B. subtilis* and (**right**) *E. coli* bacteria.

Subsequent microbiological tests conducted after 24 h of incubation at 37 °C demonstrated zones of inhibition in samples containing Cu-HAP when exposed to a colony of *B. subtilis* (see Figure 9).

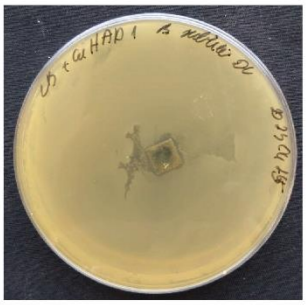

Figure 9. Results of antibacterial performance tests of low-temperature synthesised Cu-HAP coating on Ti with *B. subtilis*.

According to existing literature [22], Gram-positive bacteria possess a negatively charged cell surface and a substantial peptidoglycan membrane, ranging from 20 to 80 nm in thickness. In contrast, Cu^{2+} ions are positively charged and adhere to these negatively charged surfaces, thereby inducing apoptosis in Gram-positive bacteria. Similar observations on the effects of Cu-doped titanium alloy coatings on Gram-positive bacteria have been reported in a study by Kalaivani, S. et al. [23]. Figure 10 illustrates the zones of inhibition associated with samples doped with Zn^{2+} ions when exposed to a *B. subtilis* colony. However, no zones of inhibition were observed in the presence of *E. coli*.

Inhibition zone of coating with Cu-HAP coating on Ti were 10.5mm $\pm$ 0.5 mm average from nine measurement; the plate with the $Zn_3(OH)_4(NO_3)_2$ coatings were 15 mm $\pm$ 1.8 mm. Several factors may explain the lack of inhibition zones in some cases with Cu^{2+} and Zn^{2+} ion coatings. One plausible explanation is that materials from coatings do not substantially diffuse into the medium; the fraction that does diffuse exhibits inhibitory effects solely against B. subtilis. Another possibility is the absence of direct contact between the metal

ions and the bacteria. Alternatively, the concentrations of metal ions may be insufficient for inhibition.

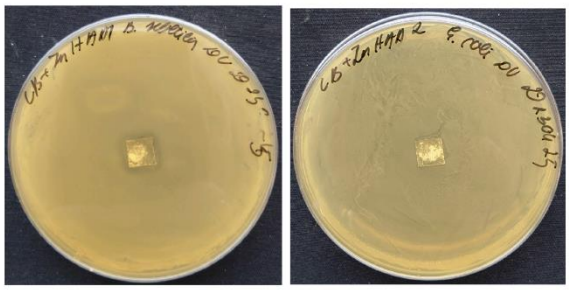

Figure 10. Results of antibacterial performance tests of low-temperature synthesised coatings with Zn^{2+} ions on Ti with (**left**) *B. subtilis* and (**right**) *E. coli* bacteria.

4. Discussion

Bone is a biologically rigid and strong material that lasts for more than 50 years without damage in human bodies [24]. However, an array of factors, including mechanical trauma, age-related weakening, and pathological conditions, necessitate the implantation of synthetic prostheses. [25]. There are different types of bone implants that can be used to help restore or replace bone tissue. The most common are:

1. Metal implants. These implants are usually made of titanium or stainless steel and are used for fracture fixation, joint replacement, and spinal surgery [26].
2. Ceramic implants. These implants are usually made of zirconium and are used for joint replacement surgery [27].
3. Polymer implants. These implants are routinely made of polyethylene and are used for joint replacement surgery, particularly in hips and knees [28].
4. Bone grafts. Bone tissue is taken from another part of the patient's body or from a donor and is used to promote healing of damaged or missing bone [29].

Titanium and calcium phosphate ceramics have emerged as the gold standard in orthopaedic applications. Titanium alloys exhibit commendable mechanical strength and resistance to physiological corrosion, courtesy of an intrinsic oxide layer. Calcium phosphates, particularly hydroxyapatite (HAP), offer unparalleled biocompatibility, accelerating biological responses and promoting strong bone-implant interfaces. Despite their advantages, calcium phosphates are mechanically inferior, leading to research efforts focused on material modification for enhanced bioavailability [25]. HAP has strong osteopermeability properties, making it particularly attractive for biomedical applications [30]. When HAP-based ceramics are implanted, a fibrous layer is formed on the surface of the ceramics, which helps the implant to bond to the living bone. This stabilises the implant and anchors it to the surrounding tissue. Synthetic HAPs are also used to cover metal implants or bone grafts. In addition, a PhD thesis [13] suggests that HAP particles can inhibit the growth of various types of cancer cells. HAP-based materials find utilisation in medical and dental fields as bone graft substitutes, dental implant coatings, and even as facial fillers [31–33].

Various synthesis methodologies have been explored, including wet, dry, and high-temperature techniques, sometimes leveraging bio-waste as precursors, which offers an economical and sustainable approach [34]. Bio-wastes include vertebrate bones, eggshells, and marine shells, the use of which is not only cost-effective but also contributes to sustainability and adds value. The properties of the final product produced depend on the type of

precursor used and the synthesis protocols used. Wet methods are further subdivided into precipitation, sol-gel, hydrothermal, microwave, and sonochemical methods. The precipitation method remains the prevalent approach for synthesising hydroxyapatite (HAP). This technique involves the incremental addition of precursors under constant mixing, while maintaining an alkaline pH. Subsequent to reaction completion, the precipitate is isolated via centrifugation, oven-dried, and mechanically processed. Key variables influencing the material's characteristics include the Ca/P ratio, rate of precursor addition, reaction temperature, and pH, as well as any added dispersants [35]. Advantages of this methodology encompass simplicity, low-temperature synthesis, cost-effectiveness, and high product purity. Limitations include particle non-uniformity and agglomeration, which can be mitigated through meticulous control of reaction parameters [36]. The sol-gel synthesis method is a method for the synthesis of HAP under mild conditions. When the crystallisation of the calcium and phosphate precursors takes place in a mild environment, the resulting HAP has high purity. The rate of gel formation and HAP growth depends on the type of solvent, the precursors used, the pH, and the temperature used in the process. Inaccuracies in these parameters lead to the formation of calcium-containing impurities during the process [37]. Another disadvantage of the sol-gel method is that it is time consuming.

Another widely used method for the preparation of HAP is the hydrothermal method, which involves chemical reactions between calcium and phosphate precursors at temperatures and pressures above ambient conditions. This method produces HAP with high crystallinity and stoichiometry. The morphology, crystallinity, and porosity of the HAP can be controlled by proper control of the pressure and temperature of the reaction vessel [37]. In the microwave (MW) irradiation method, a rapid heating source is used and monodisperse HAP nanoparticles can be synthesised in a short time. In addition, MW methods are energy efficient, the results are reproducible, and the final product has high crystallinity. The method can also be integrated with traditional methods (such as MW-deposition, MW-sol-gel, MW-hydrothermal, etc.) [38]. Research has shown that MW heating can enhance the antibacterial properties of HAP [39]. The sonochemical method is very fast and energy efficient, using ultrasound to synthesise HAP. It has been shown that prolonging the duration of the ultrasound produces small rod-shaped HAP nanoparticles of almost uniform size [40]. Naturally occurring biological resources like animal bones, eggshells, and plant extracts serve as viable precursors for hydroxyapatite (HAP) synthesis. These resources offer cost-effectiveness and waste treatment benefits, alongside yielding biomimetic, biocompatible, and bioactive HAP that is non-stoichiometric due to trace elements, making it analogous to human bone composition [36,41]. Mammalian bones, such as those from cows and pigs, are particularly favoured for their physicochemical resemblance to human bone. The extraction process involves a pre-processing step of cleaning and boiling, followed by high-temperature burning to remove organic compounds [42]. The resultant HAP's properties are influenced by the heating parameters [43–45]. Eggshells, predominantly composed of calcium carbonate, undergo cleaning and heating to form CaO, which is then converted to $Ca(OH)_2$. This is mixed with a phosphorus precursor to synthesise HAP [46]. Plant-derived biomolecules like pectin can modulate HAP morphology. For example, pectin from banana bark has been demonstrated to produce low-crystalline HAP with uniformly distributed nanoparticles [47–49].

In our study, the incorporation of Zn^{2+} ions into hydroxyapatite (HAP) was investigated. Zinc (Zn) is a critical trace element in humans, constituting approximately 3 g in the adult body. It serves both catalytic and structural roles in various biological processes, including metabolism, cell division, and gene transcription. Zinc deficiency is detrimental, particularly affecting the immune system [12]. Zinc is found as a trace element in bone. The introduction of Zn cations into the HAP structure is a popular area of research. The substitution of Zn^{2+} ions for Ca^{2+} results in a decrease in the lattice parameters a and c. This is due to the difference in the ionic radii of these cations (Zn^{2+} (0.074 nm) and Ca^{2+} (0.099 nm)). Scientific publications have reported that zinc stimulates bone formation by activating osteoblast proliferation and differentiation [50,51]. Zn-HAP also has antibacterial

properties against Gram-negative and Gram-positive bacteria. HAP doped with less than 1% zinc ions exhibits effective biological activity [12].

In previous studies, Zn-HAP coatings have been obtained by different methods, e.g., plasma spraying, sputtering, sol-gel method, magnetron sputtering. The Zn-HAP samples obtained by the different methods show a different distribution of zinc in the coating. For example, sputtering produces homogeneous Zn-HAP coatings, whereas magnetron sputtering produces Zn-HAP coatings with a higher concentration of zinc ions on the coating surface [12]. The dependence of the Zn-HAP biological response on the zinc content has been investigated in various experiments. Webster et al. have shown that even small amounts of Zn (from 1.3%) increase the osteoblast response [52]. In vitro adhesion and proliferation studies have shown that human osteoblast cells respond better to Zn-HAP layers compared to pure HAP coatings. Zn substitution was shown to affect the adhesion of HAP coatings on Ti substrates.

Another cation included in our research was Cu^{2+}. The introduction of Cu ions into the HAP structure also provides antibacterial properties to the HAP, which reduces the risk of inflammation after implantation. Additionally, our research examines the incorporation of Cu^{2+} ions into hydroxyapatite (HAP). Copper ions enhance protein absorption and osteogenic differentiation, and facilitate bone-like apatite formation at implant sites [53]. While Cu-based nanoparticles have catalytic applications due to copper's variable oxidation states (0, I, II, III) [54], the impact of Cu^{2+} substitution on HAP structure remains understudied. Cu has antibacterial properties, promotes angiogenesis, and has low cytotoxicity. Despite promising applications in orthopaedics, the literature shows that commercial success is still a long way off. This is not only due to the burden of the regulatory processes involved in bringing metal-doped materials to the health market, but also due to the difficulty in proving the effect of the element experimentally. Today's challenges are to combine in the same study all the characteristics related to the element: material studies (chemical composition, phase composition, formation, biomechanical aspects, brittleness, mechanical strength, and oxidation resistance) and biological aspects (cytotoxicity, bactericidal, osteogenic and angiogenic properties) [55]. Cu is a trace element essential for numerous physiological functions, including respiration, energy production, and tissue formation [56]. It is crucial for bone collagen maturation and osteoblast function [57,58]. In a 70 kg adult, approximately 100 mg of Cu is distributed primarily in the skeleton, muscles, liver, and brain [59]. While the maximum adult dose is 10 mg/day, deficiency can result in conditions like anaemia, leucopenia, and bone fragility [55]. Prado et al. demonstrated experimentally that after 48 h, MRSA, *Klebsiella pneumoniae*, and *Acinetobacter baumannii* did not adhere to Cu-containing samples, unlike stainless steel [60]. Another study investigated the incidence of infections over one year in an intensive care unit. Some patients were placed in wards with Cu-alloy surfaces and others in conventional wards. The proportion of patients who developed an infection with MRSA or VRE (vancomycin-resistant enterococcus) was compared between the two types of wards. In wards with Cu, 7.1% of patients developed nosocomial infection, compared with 12.3% in standard wards, indicating that Cu-alloy surfaces significantly reduced nosocomial infections [61]. Three main mechanisms are described in the literature: (a) membrane and cell wall damage due to direct interaction with microbial surfaces; (b) release of component divalent metal ions; (c) generation of reactive oxygen species (ROS), which are known to be toxic to bacteria.

In 2008, the EPA acknowledged copper's antimicrobial properties, leading to its incorporation in various biomedical materials, including calcium phosphate bioceramics [62,63]. Key studies have substantiated the antimicrobial efficacy of Cu-doped hydroxyapatite (HAP). For instance, Stanic et al. reported a 95% reduction in *Escherichia coli*, *S. aureus*, and *Candida albicans* [64], while Li et al. found less than a 1% survival rate of *E. coli* after 24 h [64]. In 2019, Bhattacharjee et al. confirmed the material's effectiveness against *E. coli* and *S. aureus* [65]. In 2015, Huang et al. synthesised Cu-doped HAP coatings on titanium. The coatings were found to have an antimicrobial effect of >75% against *E. coli* [66]. In a study by Kalaivani et al., copper-doped $CaSiO_3$ coatings were synthesised and evaluated

for their antibacterial properties against *E. coli* and *S. aureus*. The results showed that the pure powder did not exhibit antibacterial properties, but the antibacterial activity gradually increased with increasing Cu content in the doped coatings [23]. Ghosh et al. coated Cu-doped hydroxyapatite on titanium with varying Cu content and tested these samples against *E. coli* and *S. aureus*. Their results showed that the number of viable bacteria decreased as the Cu content of the coatings increased, while the antibacterial activity of the Cu-free hydroxyapatite was very low. After 8 h of cultivation, the antibacterial activity of *E. coli* on Cu-HAP was 78% and that of *S. aureus* was 83%. Wolf-Brandstetter et al. performed similar studies with titanium implants coated with Cu-HAP layers. After 2 h of cultivation with *E. coli*, the coatings with the highest Cu content showed a significantly lower number of viable bacteria and this effect was prolonged to 12 h. The results also showed a reduction in adherent bacteria on implant surfaces after 12 h [67]. Although Cu-based biomaterials are generally effective against bacteria, the efficacy is influenced by various parameters, such as bacterial type (Gram-positive or Gram-negative), testing methodologies, experimental conditions, and Cu content variation. The ion release rate in biological media also plays a role. Gram-positive bacteria, with their negatively charged and thick peptidoglycan membranes (20–80 nm), are more susceptible to Cu-induced apoptosis, whereas Gram-negative bacteria possess a thinner peptidoglycan layer (6–15 nm) and an outer membrane that can act as a diffusion barrier [22,68]. A paramount strength of this study resides in its innovative approach to the low-temperature synthesis of hydroxyapatite (HAP) coatings; thereby the adhesion to titanium substrate is better and formation of TiO_2 is avoided. The incorporation of copper and zinc ions as dopants not only adds complexity to the material but also offers a platform for the exploration of multifunctional properties. Significantly, the study takes the crucial step of evaluating the antibacterial efficacy of these doped coatings, filling a gap in current research on HAP-based biomaterials. Analytical methods used in the study provide a robust foundation for the reported findings. Nevertheless, the study is not devoid of limitations. A comprehensive analysis of the coatings' mechanical properties, aside from their antibacterial attributes, could provide a more holistic understanding of their potential applications [69–71]. Moreover, the study would benefit from a broader comparative framework that situates the findings in relation to existing methods and materials for HAP coatings.

5. Conclusions

A crystalline calcium hydroxyapatite (HAP) with a very high homogeneity and degree of particle size distribution was successfully synthesised from $CaCO_3$ coatings by a dissolution-precipitation method at low temperature of 80 °C in aqueous media. The low-temperature precipitation-dissolution method was successfully used for the synthesis of partially Cu^{2+} ion-substituted HAP. However, the formation of HAP coatings doped with Zn^{2+} ions by the above method did not proceed as smoothly as expected. The different synthesis methods tested resulted in the formation of $Zn(OH)(NO_3)(H_2O)$, $Zn_3(OH)_4(NO_3)_2$ on the surface of the coating, leaving unreacted calcium carbonate. Antibacterial property tests showed that no zones of inhibition were detected in pure HAP. In the Cu-HAP and Zn-HAP coating, after incubation for 24 h at 37 °C, zones of inhibition were detected in the presence of a colony of *B. subtilis* bacteria. However, no zones of inhibition were detected in the presence of *Escherichia coli*.

Author Contributions: Conceptualisation, I.G. and D.S.; methodology, A.K.; formal analysis, L.L., D.V. and J.K. resources, A.K.; writing—original draft preparation, A.K and L.L.; writing—review and editing, A.K.; visualisation, I.G.; supervision, A.K. All authors have read and agreed to the published version of the manuscript.

Funding: This research received no external funding.

Institutional Review Board Statement: Not applicable.

Informed Consent Statement: Not applicable.

Data Availability Statement: Data are contained within the article.

Conflicts of Interest: The authors declare no conflict of interest.

References

1. In, Y.; Amornkitbamrung, U.; Hong, M.H.; Shin, H. On the Crystallization of Hydroxyapatite under Hydrothermal Conditions: Role of Sebacic Acid as an Additive. *ACS Omega* **2020**, *5*, 27204–27210. [CrossRef]
2. Szewczyk, A.; Skwira, A.; Ginter, M.; Tajer, D.; Prokopowicz, M. Microwave-Assisted Fabrication of Mesoporous Silica-Calcium Phosphate Composites for Dental Application. *Polymers* **2020**, *13*, 53. [CrossRef] [PubMed]
3. Teotia, A.K.; Raina, D.B.; Singh, C.; Sinha, N.; Isaksson, H.; Tagil, M.; Lidgren, L.; Kumar, A. Nano-Hydroxyapatite Bone Substitute Functionalized with Bone Active Molecules for Enhanced Cranial Bone Regeneration. *ACS Appl. Mater. Interfaces* **2017**, *9*, 6816–6828. [CrossRef] [PubMed]
4. Tas, A.C. Synthesis of biomimetic Ca-hydroxyapatite powders at 37 degrees C in synthetic body fluids. *Biomaterials* **2000**, *21*, 1429–1438. [CrossRef] [PubMed]
5. Kumar, M.; Kumar, R.; Kumar, S. Coatings on orthopedic implants to overcome present problems and challenges: A focused review. *Mater. Today Proc.* **2021**, *45*, 5269–5276. [CrossRef]
6. Cheng, Y.; Zhao, G.; Liu, H. Histological evaluation of collagen-hydroxyapatite composite as osseous implants in the repair of mandibular defect. *Chin. J. Reparative Reconstr. Surg.* **1998**, *12*, 74–76.
7. Park, J.; Kim, B.J.; Hwang, J.Y.; Yoon, Y.W.; Cho, H.S.; Kim, D.H.; Lee, J.K.; Yoon, S.Y. In-Vitro Mechanical Performance Study of Biodegradable Polylactic Acid/Hydroxyapatite Nanocomposites for Fixation Medical Devices. *J. Nanosci. Nanotechnol.* **2018**, *18*, 837–841. [CrossRef] [PubMed]
8. Shi, P.; Liu, M.; Fan, F.; Yu, C.; Lu, W.; Du, M. Characterization of natural hydroxyapatite originated from fish bone and its biocompatibility with osteoblasts. *Mater. Sci. Eng. C Mater. Biol. Appl.* **2018**, *90*, 706–712. [CrossRef]
9. Eliaz, N.; Metoki, N. Calcium Phosphate Bioceramics: A Review of Their History, Structure, Properties, Coating Technologies and Biomedical Applications. *Materials* **2017**, *10*, 334. [CrossRef]
10. Yasukawa, A.; Gotoh, K.; Tanaka, H.; Kandori, K. Preparation and structure of calcium hydroxyapatite substituted with light rare earth ions. *Colloids Surf. A: Physicochem. Eng. Asp.* **2012**, *393*, 53–59. [CrossRef]
11. Lin, K.; Chang, J. Structure and properties of hydroxyapatite for biomedical applications. In *Hydroxyapatite (HAp) for Biomedical Applications*; Elsevier: Amsterdam, The Netherlands, 2015; pp. 3–19.
12. Arcos, D.; Vallet-Regi, M. Substituted hydroxyapatite coatings of bone implants. *J. Mater. Chem. B* **2020**, *8*, 1781–1800. [CrossRef] [PubMed]
13. Trinkunaite-Felsen, J. Investigation of Calcium Hydroxyapatite Synthesized Using Natural Precursors. Ph.D. Thesis, Vilnius University, Vilnius, Lithuania, 2014.
14. Ishikawa, K.; Kareiva, A. Sol–gel synthesis of calcium phosphate-based coatings—A review. *Chemija* **2020**, *31*, 25–41. [CrossRef]
15. Jonauske, V.; Stanionyte, S.; Chen, S.-W.; Zarkov, A.; Juskenas, R.; Selskis, A.; Matijosius, T.; Yang, T.C.; Ishikawa, K.; Ramanauskas, R. Characterization of sol-gel derived calcium hydroxyapatite coatings fabricated on patterned rough stainless steel surface. *Coatings* **2019**, *9*, 334. [CrossRef]
16. Shi, R.; Hayashi, K.; Bang, L.T.; Ishikawa, K. Effects of surface roughening and calcite coating of titanium on cell growth and differentiation. *J. Biomater. Appl.* **2020**, *34*, 917–927. [CrossRef] [PubMed]
17. Yanyan, S.; Guangxin, W.; Wuhui, L.; Yaming, W.; Hayakawa, S.; Osaka, A. Conversion of sub-μm calcium carbonate (calcite) particles to hollow hydroxyapatite agglomerates in K2HPO4 solutions. *Nanotechnol. Rev.* **2020**, *9*, 945–960. [CrossRef]
18. Harris, J.; Mey, I.; Hajir, M.; Mondeshki, M.; Wolf, S.E. Pseudomorphic transformation of amorphous calcium carbonate films follows spherulitic growth mechanisms and can give rise to crystal lattice tilting. *CrystEngComm* **2015**, *17*, 6831–6837. [CrossRef]
19. Gheisari, H.; Karamian, E.; Abdellahi, M. A novel hydroxyapatite—Hardystonite nanocomposite ceramic. *Ceram. Int.* **2015**, *41*, 5967–5975. [CrossRef]
20. Shanmugam, S.; Gopal, B. Copper substituted hydroxyapatite and fluorapatite: Synthesis, characterization and antimicrobial properties. *Ceram. Int.* **2014**, *40*, 15655–15662. [CrossRef]
21. Unabia, R.B.; Bonebeau, S.; Candidato Jr, R.T.; Jouin, J.; Noguera, O.; Pawłowski, L. Investigation on the structural and microstructural properties of copper-doped hydroxyapatite coatings deposited using solution precursor plasma spraying. *J. Eur. Ceram. Soc.* **2019**, *39*, 4255–4263. [CrossRef]
22. Bari, A.; Bloise, N.; Fiorilli, S.; Novajra, G.; Vallet-Regi, M.; Bruni, G.; Torres-Pardo, A.; Gonzalez-Calbet, J.M.; Visai, L.; Vitale-Brovarone, C. Copper-containing mesoporous bioactive glass nanoparticles as multifunctional agent for bone regeneration. *Acta Biomater.* **2017**, *55*, 493–504. [CrossRef]
23. Kalaivani, S.; Singh, R.K.; Ganesan, V.; Kannan, S. Effect of copper (Cu(2+)) inclusion on the bioactivity and antibacterial behavior of calcium silicate coatings on titanium metal. *J. Mater. Chem. B* **2014**, *2*, 846–858. [CrossRef]
24. Chandra, G.; Pandey, A. Biodegradable bone implants in orthopedic applications: A review. *Biocybern. Biomed. Eng.* **2020**, *40*, 596–610. [CrossRef]
25. León, B.; Jansen, J.A. *Thin Calcium Phosphate Coatings for Medical Implants*; Springer: Berlin/Heidelberg, Germany, 2009; Volume 309.

26. Prasad, K.; Bazaka, O.; Chua, M.; Rochford, M.; Fedrick, L.; Spoor, J.; Symes, R.; Tieppo, M.; Collins, C.; Cao, A.; et al. Metallic Biomaterials: Current Challenges and Opportunities. *Materials* **2017**, *10*, 884. [CrossRef]
27. Rieu, J.; Goeuriot, P. Ceramic composites for biomedical applications. *Clin. Mater.* **1993**, *12*, 211–217. [CrossRef]
28. Tang, X.; Thankappan, S.K.; Lee, P.; Fard, S.E.; Harmon, M.D.; Tran, K.; Yu, X. Polymeric biomaterials in tissue engineering and regenerative medicine. In *Natural and Synthetic Biomedical Polymers*; Elsevier: Amsterdam, The Netherlands, 2014; pp. 351–371.
29. De Long, W.G., Jr.; Einhorn, T.A.; Koval, K.; McKee, M.; Smith, W.; Sanders, R.; Watson, T. Bone grafts and bone graft substitutes in orthopaedic trauma surgery. *A critical analysis. J. Bone Jt. Surg. Am.* **2007**, *89*, 649–658. [CrossRef]
30. Fox, K.; Tran, P.A.; Tran, N. Recent advances in research applications of nanophase hydroxyapatite. *Chemphyschem* **2012**, *13*, 2495–2506. [CrossRef] [PubMed]
31. Siddiqui, H.A.; Pickering, K.L.; Mucalo, M.R. A Review on the Use of Hydroxyapatite-Carbonaceous Structure Composites in Bone Replacement Materials for Strengthening Purposes. *Materials* **2018**, *11*, 1813. [CrossRef] [PubMed]
32. Nasar, A. Hydroxyapatite and its coatings in dental implants. In *Applications of Nanocomposite Materials in Dentistry*; Elsevier: Amsterdam, The Netherlands, 2019; pp. 145–160.
33. Jeong, S.H.; Fan, Y.F.; Baek, J.U.; Song, J.; Choi, T.H.; Kim, S.W.; Kim, H.E. Long-lasting and bioactive hyaluronic acid-hydroxyapatite composite hydrogels for injectable dermal fillers: Physical properties and in vivo durability. *J. Biomater. Appl.* **2016**, *31*, 464–474. [CrossRef] [PubMed]
34. Sadat-Shojai, M.; Khorasani, M.T.; Dinpanah-Khoshdargi, E.; Jamshidi, A. Synthesis methods for nanosized hydroxyapatite with diverse structures. *Acta Biomater.* **2013**, *9*, 7591–7621. [CrossRef] [PubMed]
35. Ma, G. Three common preparation methods of hydroxyapatite. *Proc. IOP Conf. Ser. Mater. Sci. Eng.* **2019**, *688*, 033057. [CrossRef]
36. Pu'ad, N.M.; Haq, R.A.; Noh, H.M.; Abdullah, H.; Idris, M.; Lee, T. Synthesis method of hydroxyapatite: A review. *Mater. Today Proc.* **2020**, *29*, 233–239. [CrossRef]
37. Fihri, A.; Len, C.; Varma, R.S.; Solhy, A. Hydroxyapatite: A review of syntheses, structure and applications in heterogeneous catalysis. *Coord. Chem. Rev.* **2017**, *347*, 48–76. [CrossRef]
38. Kalita, S.J.; Verma, S. Nanocrystalline hydroxyapatite bioceramic using microwave radiation: Synthesis and characterization. *Mater. Sci. Eng. C Mater. Biol. Appl.* **2010**, *30*, 295–303. [CrossRef] [PubMed]
39. Lamkhao, S.; Phaya, M.; Jansakun, C.; Chandet, N.; Thongkorn, K.; Rujijanagul, G.; Bangrak, P.; Randorn, C. Synthesis of Hydroxyapatite with Antibacterial Properties Using a Microwave-Assisted Combustion Method. *Sci. Rep.* **2019**, *9*, 4015. [CrossRef] [PubMed]
40. Utara, S.; Klinkaewnarong, J. Effect of sonication time on the characteristics of nanophase hydroxyapatite crystals synthesised by the sol–gel technique. *Micro Nano Lett.* **2015**, *10*, 1–4. [CrossRef]
41. Akram, M.; Ahmed, R.; Shakir, I.; Ibrahim, W.A.W.; Hussain, R. Extracting hydroxyapatite and its precursors from natural resources. *J. Mater. Sci.* **2014**, *49*, 1461–1475. [CrossRef]
42. Sun, R.-X.; Lv, Y.; Niu, Y.-R.; Zhao, X.-H.; Cao, D.-S.; Tang, J.; Sun, X.-C.; Chen, K.-Z. Physicochemical and biological properties of bovine-derived porous hydroxyapatite/collagen composite and its hydroxyapatite powders. *Ceram. Int.* **2017**, *43*, 16792–16798. [CrossRef]
43. Googerdchian, F.; Moheb, A.; Emadi, R.; Asgari, M. Optimization of Pb(II) ions adsorption on nanohydroxyapatite adsorbents by applying Taguchi method. *J. Hazard. Mater.* **2018**, *349*, 186–194. [CrossRef] [PubMed]
44. Khoo, W.; Nor, F.; Ardhyananta, H.; Kurniawan, D. Preparation of natural hydroxyapatite from bovine femur bones using calcination at various temperatures. *Procedia Manuf.* **2015**, *2*, 196–201. [CrossRef]
45. Öksüz, K.E.; Kilinç, S.; Özer, A. Effect of calcination on microstructure development and properties of hydroxyapatite powders extracted from human and bovine bones. *Trans. Indian Ceram. Soc.* **2019**, *78*, 41–45. [CrossRef]
46. Varadavenkatesan, T.; Vinayagam, R.; Pai, S.; Kathirvel, B.; Pugazhendhi, A.; Selvaraj, R. Synthesis, biological and environmental applications of hydroxyapatite and its composites with organic and inorganic coatings. *Prog. Org. Coat.* **2021**, *151*, 106056. [CrossRef]
47. Gopi, D.; Kanimozhi, K.; Bhuvaneshwari, N.; Indira, J.; Kavitha, L. Novel banana peel pectin mediated green route for the synthesis of hydroxyapatite nanoparticles and their spectral characterization. *Spectrochim. Acta A Mol. Biomol. Spectrosc.* **2014**, *118*, 589–597. [CrossRef] [PubMed]
48. Gopi, D.; Kanimozhi, K.; Kavitha, L. Opuntia ficus indica peel derived pectin mediated hydroxyapatite nanoparticles: Synthesis, spectral characterization, biological and antimicrobial activities. *Spectrochim. Acta A Mol. Biomol. Spectrosc.* **2015**, *141*, 135–143. [CrossRef]
49. Begum, Y.; Deka, S. Green synthesis of pectin mediated hydroxyapatite nanoparticles from culinary banana bract and its characterization. *Acta Aliment.* **2017**, *46*, 428–438. [CrossRef]
50. Yamaguchi, M.; Oishi, H.; Suketa, Y. Stimulatory effect of zinc on bone formation in tissue culture. *Biochem. Pharmacol.* **1987**, *36*, 4007–4012. [CrossRef]
51. Yamaguchi, M. Role of zinc in bone formation and bone resorption. *J. Trace Elem. Exp. Med. Off. Publ. Int. Soc. Trace Elem. Res. Hum.* **1998**, *11*, 119–135. [CrossRef]
52. Webster, T.J.; Massa-Schlueter, E.A.; Smith, J.L.; Slamovich, E.B. Osteoblast response to hydroxyapatite doped with divalent and trivalent cations. *Biomaterials* **2004**, *25*, 2111–2121. [CrossRef] [PubMed]

53. Bulina, N.V.; Eremina, N.V.; Vinokurova, O.B.; Ishchenko, A.V.; Chaikina, M.V. Diffusion of Copper Ions in the Lattice of Substituted Hydroxyapatite during Heat Treatment. *Materials* **2022**, *15*, 5759. [CrossRef]
54. Othmani, M.; Bachoua, H.; Ghandour, Y.; Aissa, A.; Debbabi, M. Synthesis, characterization and catalytic properties of copper-substituted hydroxyapatite nanocrystals. *Mater. Res. Bull.* **2018**, *97*, 560–566. [CrossRef]
55. Jacobs, A.; Renaudin, G.; Forestier, C.; Nedelec, J.M.; Descamps, S. Biological properties of copper-doped biomaterials for orthopedic applications: A review of antibacterial, angiogenic and osteogenic aspects. *Acta Biomater.* **2020**, *117*, 21–39. [CrossRef]
56. Chellan, P.; Sadler, P.J. The elements of life and medicines. *Philos. Trans. A Math. Phys. Eng. Sci.* **2015**, *373*, 20140182. [CrossRef] [PubMed]
57. Opsahl, W.; Zeronian, H.; Ellison, M.; Lewis, D.; Rucker, R.B.; Riggins, R.S. Role of copper in collagen cross-linking and its influence on selected mechanical properties of chick bone and tendon. *J. Nutr.* **1982**, *112*, 708–716. [CrossRef] [PubMed]
58. Lowe, N.M.; Lowe, N.M.; Fraser, W.D.; Jackson, M.J. Is there a potential therapeutic value of copper and zinc for osteoporosis? *Proc. Nutr. Soc.* **2002**, *61*, 181–185. [CrossRef]
59. Ingle, A.P.; Paralikar, P.; Shende, S.; Gupta, I.; Biswas, J.K.; da Silva Martins, L.H.; Rai, M. Copper in medicine: Perspectives and toxicity. In *Biomedical Applications of Metals*; Springer: Berlin/Heidelberg, Germany, 2018; pp. 95–112.
60. Prado, J.V.; Esparza, M.M.; Vidal, A.R.; Duran, T.C. Adherence to copper and stainless steel metal coupons of common nosocomial bacterial strains. *Rev. Med. Chil.* **2013**, *141*, 291–297. [CrossRef]
61. Salgado, C.D.; Sepkowitz, K.A.; John, J.F.; Cantey, J.R.; Attaway, H.H.; Freeman, K.D.; Sharpe, P.A.; Michels, H.T.; Schmidt, M.G. Copper surfaces reduce the rate of healthcare-acquired infections in the intensive care unit. *Infect. Control Hosp. Epidemiol.* **2013**, *34*, 479–486. [CrossRef] [PubMed]
62. Prather, V. Copper, brass and bronze kill pathogens-including "superbug" MRSA-responsible for hospital- and community-acquired infections. *CDA Press Release* **2008**, *25*, 1.
63. Dorozhkin, S.V. Calcium orthophosphates. *J. Mater. Sci.* **2007**, *42*, 1061–1095. [CrossRef]
64. Stanić, V.; Dimitrijević, S.; Antić-Stanković, J.; Mitrić, M.; Jokić, B.; Plećaš, I.B.; Raičević, S. Synthesis, characterization and antimicrobial activity of copper and zinc-doped hydroxyapatite nanopowders. *Appl. Surf. Sci.* **2010**, *256*, 6083–6089. [CrossRef]
65. Bhattacharjee, A.; Fang, Y.; Hooper, T.J.N.; Kelly, N.L.; Gupta, D.; Balani, K.; Manna, I.; Baikie, T.; Bishop, P.T.; White, T.J.; et al. Crystal Chemistry and Antibacterial Properties of Cupriferous Hydroxyapatite. *Materials* **2019**, *12*, 1814. [CrossRef] [PubMed]
66. Huang, Y.; Zhang, X.; Zhao, R.; Mao, H.; Yan, Y.; Pang, X. Antibacterial efficacy, corrosion resistance, and cytotoxicity studies of copper-substituted carbonated hydroxyapatite coating on titanium substrate. *J. Mater. Sci.* **2015**, *50*, 1688–1700. [CrossRef]
67. Wolf-Brandstetter, C.; Beutner, R.; Hess, R.; Bierbaum, S.; Wagner, K.; Scharnweber, D.; Gbureck, U.; Moseke, C. Multifunctional calcium phosphate based coatings on titanium implants with integrated trace elements. *Biomed. Mater.* **2020**, *15*, 025006. [CrossRef] [PubMed]
68. Nan, L.; Liu, Y.; Lu, M.; Yang, K. Study on antibacterial mechanism of copper-bearing austenitic antibacterial stainless steel by atomic force microscopy. *J. Mater. Sci. Mater. Med.* **2008**, *19*, 3057–3062. [CrossRef] [PubMed]
69. Thakur, A.; Sharma, S.; Ganjoo, R.; Assad, H.; Kumar, A. Anti-Corrosive Potential of the Sustainable Corrosion Inhibitors Based on Biomass Waste: A Review on Preceding and Perspective Research. *J. Phys. Conf. Series* **2022**, *2267*, 012079. [CrossRef]
70. Hikku, G.S.; Arthi, C.; Jeen Robert, R.B.; Jeyasubramanian, K.; Murugesan, R. Calcium phosphate conversion technique: A versatile route to develop corrosion resistant hydroxyapatite coating over Mg/Mg alloys based implants. *J. Magnes. Alloys* **2022**, *10*, 1821–1845. [CrossRef]
71. Singh, J.; Singh Chatha, S.; Singh, H. Microstructural and in-vitro characteristics of functional calcium silicate topcoat on hydroxyapatite coating for bio-implant applications. *Prog. Biomater.* **2022**, *11*, 95–108. [CrossRef]

Ceramics International 50 (2024) 4005–4013

Contents lists available at ScienceDirect

Ceramics International

journal homepage: www.elsevier.com/locate/ceramint

Hydrothermal synthesis of Mn^{2+}- and Cu^{2+}-doped calcium hydroxyapatite: morphological features and importance of EPR insights

Eva Raudonyte-Svirbutaviciene [a,*], Gabriele Klydziute [a], Laura Lukaviciute [a], Andris Antuzevics [a,b], Aldona Balciunaite [c], Eugenijus Norkus [c], Aldona Beganskiene [a], Aleksej Zarkov [a,**], Aivaras Kareiva [a]

[a] Institute of Chemistry, Vilnius University, Naugarduko 24, LT-03225, Vilnius, Lithuania
[b] Institute of Solid State Physics, University of Latvia, Kengaraga 8, LV-1063, Riga, Latvia
[c] Department of Catalysis, Center for Physical Sciences and Technology, Saulėtekio ave. 3, Vilnius, LT-10257, Lithuania

ARTICLE INFO

Keywords:
Hydroxyapatite
Hydrothermal synthesis
Crystal growth
Morphology control
Mn doping
Cu doping

ABSTRACT

This study aims to explore the effects of various hydroxyapatite (HA) doping techniques in depth. For this purpose, two ions with comparable sizes, namely Mn^{2+} and Cu^{2+}, were selected based on their suitability as dopants for HA in biomedical applications. Moreover, their paramagnetic properties enable sample characterization through electron paramagnetic resonance (EPR) spectroscopy. Two different approaches were employed: (I) ion-substituted α-TCP was used as starting material; (II) foreign ions presented in the solution during the transformation of undoped α-TCP to HA. The foreign ions influenced the hydrolysis process of α-TCP, altering the phase purity and morphology of the products. Doped α-TCP showed a weaker effect, while adding ions to the synthesis solution had substantial impact. Mn-doped α-TCP transformed into plate-like HA particles while Mn^{2+} ions present in the solution led to the formation of both plate- and rod-shaped particles. In contrast, Cu^{2+} ions induced the formation of rod-like particles independently of the doping process. Plate-like particles demonstrated higher Brunauer–Emmet–Teller surface area (S_{BET}) than rod-like HA. Each sample exhibited a combination of mesopores and macropores, with mesopores in the range of 15–17 Å being dominant. EPR investigations revealed that Mn^{2+} and Cu^{2+} are excellent paramagnetic probes to monitor synthesis reactions of HA and determine the localisation of foreign ions in the material.

Ceramics International 50 (2024) 34479–34509

Contents lists available at ScienceDirect

Ceramics International

journal homepage: www.elsevier.com/locate/ceramint

Review article

Cationic substitution effects in phosphate-based bioceramics - A way towards superior bioproperties

Laura Lukaviciute [a], Ruta Ganceviciene [b], Kanji Tsuru [c], Kunio Ishikawa [d], Jen-Chang Yang [e], Inga Grigoraviciute [a,*], Aivaras Kareiva [a]

[a] Institute of Chemistry, Vilnius University, Naugarduko 24, 03225, Vilnius, Lithuania
[b] Faculty of Medicine, Clinic of Infectious Diseases and Dermatovenereology, Vilnius University, M. K. Ciurlionio 21/27, 03101, Vilnius, Lithuania
[c] Section of Bioengineering, Department of Dental Engineering, Fukuoka, Dental College, Fukuoka, Japan
[d] Department of Biomaterials, Faculty of Dental Science, Kyushu University, Maidashi, Higashi-Ku, Fukuoka, Japan
[e] Graduate Institute of Nanomedicine and Medical Engineering, International Ph.D. Program in Biomedical Engineering, College of Biomedical Engineering, Research Center of Biomedical Device, Research Center of Digital Oral Science and Technology, Taipei Medical University, Taiwan

ARTICLE INFO

Handling Editor: Dr P. Vincenzini

Keywords:
Calcium phosphates
Cationic substitution
Co-substitution
Bioproperties

ABSTRACT

This review summarises the available results on the effects of cation substitution on the antibacterial and other bioproperties of different phosphates. Attention is given to bulk cation-substituted phosphates (alkali, alkaline earth, transition and lanthanide metals) and to thin films, glasses, and various composite materials. The cationic effects on the biological properties of phosphate bioceramics are also documented. These phosphate-based biomaterials, especially nanostructured ones, show high biocompatibility and enhanced antibacterial behaviour. Numerous articles have concluded that the cationically substituted phosphates are the best candidates for applications in many biomedical fields such as bone repair, tissue engineering, drug and gene delivery, magnetic targeting and hyperthermia treatment for cancer, bioimaging, and theranostics.

Ceramics International 51 (2025) 11286–11296

Contents lists available at ScienceDirect

Ceramics International

journal homepage: www.elsevier.com/locate/ceramint

Cytocompatible and antibacterial Fe-, Cu- and Zn-substituted calcium hydroxyapatite materials for skin applications

L. Lukaviciute [a,*], A. Lukowiak [b], Z. Stankeviciute [a], A. Junka [c], M. Mortimer [d], A. Zarkov [a], J.-C. Yang [e], R. Ganceviciene [f], A. Kareiva [a]

[a] Faculty of Chemistry and Geosciences, Vilnius University, Naugarduko st. 24, 03225, Vilnius, Lithuania
[b] Institute of Low Temperature and Structure Research, Polish Academy of Sciences, Okolna 2, 50422, Wroclaw, Poland
[c] Department of Pharmaceutical Microbiology and Parasitology, Wroclaw Medical University, Borowska 211A, 50556, Wroclaw, Poland
[d] Laboratory of Environmental Toxicology, National Institute of Chemical Physics and Biophysics, Akadeemia tee 23, 12618, Tallinn, Estonia
[e] Graduate Institute of Nanomedicine and Medical Engineering, International Ph.D. Program in Biomedical Engineering, College of Biomedical Engineering, Research Center of Biomedical Device, Research Center of Digital Oral Science and Technology, Taipei Medical University, Taiwan
[f] Faculty of Medicine, Vilnius University, M.K. Ciurlionio st. 21, 03101, Vilnius, Lithuania

ARTICLE INFO

Handling Editor: Dr P. Vincenzini

Keywords:
Hydroxyapatite
Hydrothermal synthesis
Substitution effects
Skin creams
Bioproperties

ABSTRACT

Calcium hydroxyapatite ($C_{10}(PO_4)_6(OH)_2$; CHAp) and metal-substituted samples (Fe:CHAp, Cu:CHAp, and Zn:CHAp) were synthesized using a recently developed method. This method involved the wet precipitation of amorphous calcium phosphate (ACP), followed by solid-state reaction synthesis of α-tricalcium phosphate (α-TCP), and finally hydrothermal synthesis of CHAp. The effect of Fe^{3+}, Cu^{2+}, and Zn^{2+} substitution on the phase purity and antimicrobial properties of CHAp are summarized in this study. Notably, it highlights the phase purity of CHAp and Zn:CHAp (in the presence of Fe^{3+} and Cu^{2+} ions, the α- and β-TCP phases have formed) as well as the antimicrobial activity of Zn:CHAp and Cu:CHAp against *Staphylococcus aureus* and *Candida albicans*. The synthesized nanosized CHAp, Fe:CHAp, Cu:CHAp, and Zn:CHAp samples were used as additives in the preparation of skin creams. *In vitro* biological studies of the resulting skin creams demonstrated their antimicrobial activity against *Pseudomonas aeruginosa*, and showed a reduction in osteoblasts cells viability of in the range of 20–40 %. The addition of zinc enhances antimicrobial efficacy but reduces biocompatibility, while copper maintains both high antimicrobial activity and biocompatibility, making it more suitable for the development of medical or cosmetic materials. Dermal creams containing CHAp with copper and iron ions also show significant antimicrobial activity while preserving good cell viability. These results highlight the importance of optimizing the balance between antimicrobial effectiveness and biocompatibility in these materials.

Vilnius University Press
9 Saulėtekio Ave., Building III, LT-10222 Vilnius
Email: info@leidykla.vu.lt, www.leidykla.vu.lt
bookshop.vu.lt, journals.vu.lt
Print run copies 15